LOW-MOLECULAR WEIGHT AMINO ACID BASED SUPRAMOLECULAR METALLO-GELS FOR PHOTO AND ELECTROCHEMICAL APPLICATIONS

A Thesis Submitted to AcSIR for the Degree of
Doctor of Philosophy
in
Chemistry

By

SUBHADEEP SAHA

Research Supervisor
Dr. RAHUL BANERJEE

Physical and Materials Chemistry Division
CSIR-National Chemical Laboratory
Pune, India

February 2015

Dedicated to
My Parents

STATEMENT

I hereby declare that the matter embodied in this thesis entitled **"Low-molecular Weight Amino acid Based Supramolecular Metallo-Gels for Photo and Electrochemical Applications"** is the result of investigations carried out by me in Physical and Materials chemistry Division, National Chemical Laboratory, Pune under the supervision of Dr. Rahul Banerjee.

In keeping with the general practice of reporting scientific observations due acknowledgements have been made wherever the work described is based on the findings of other investigators.

Pune **Subhadeep Saha**

February, 2015

Certificate

This is to certify that the work incorporated in this Ph.D. thesis entitled *"Low-molecular Weight Amino acid Based Supramolecular Metallo-Gels for Photo and Electrochemical Applications"* submitted by Mr. *Subhadeep Saha* to Academy of Scientific and Innovative Research (AcSIR) in fulfillment of the requirements for the award of the Degree of *PhD*, embodies original research work under my/our supervision/guidance. I/We further certify that this work has not been submitted to any other University or Institution in part or full for the award of any degree or diploma. Research material obtained from other sources has been duly acknowledged in the thesis. Any text, illustration, table etc., used in the thesis from other sources, have been duly cited and acknowledged.

Subhadeep Saha

(Student)

Rahul Banerjee

(Supervisor)

ACKNOWLEDGEMENT

My most sincere and heartfelt thanks goes to my PhD supervisor, Dr. Rahul Banerjee. I thank him for introducing me to the wonders of scientific research. I thank him for his persistent guidance, encouragement, inspiration and support during every stage of my research work. I warmly thank him for his precious advice, analysis, criticism and discussions on my work. I would like to thank my DAC committee members Dr. Darbha Srinivas, Dr. Neelanjana Sengupta and Dr. Kumar Vanka for their constructive suggestions.

Most of the results described in this thesis would not have been obtained without a close collaboration with few laboratories. I would like to thank Dr. Sudip Roy for his support during the initial years. I would like to acknowledge the assistance of Prof. Dr. David Díaz Díaz, Institut für Organische Chemie, Universität Regensburg, Germany and IQAC-CSIC, Barcelona (Spain) for his valuable scientific discussion and suggestions throughout my PhD tenure. I owe a great deal of appreciation and gratitude to Dr. Sreekumar Kurungot for proton conductivity measurements and studies on gel materials, Dr. Asha S. K. for photoluminescence measurement and Dr S.B. Ogale for photocatalysis experiments.

I am grateful to CSIR, New Delhi for fellowship support. I thank all the non-teaching staff of CSIR NCL for their assistance on various occasions. I wish to thank all my friendly and cooperative labmates *Tamas, Pradip, Chandan, Arijit, Tanay, Sharat , Bishnu, Suman, Bikash, Divya, Mohitosh, Saibal, Arjun, Suvendu, Subash, Jayshri, Gobinda, Digambar, Manasda, Shouvik and Harshitha* for creating a cheerful and enjoyable working atmosphere in the lab. They were extremely supportive as well as helpful during my tenure. I thank project students particularly Malika, Suvendu and Akhil who helped me to reach achieve my goals. I also would like to thank my previous labmates, Chandan, Dos, Swagata, Anil, for their support.

I especially thank Prithvi Raj Pandey, Souvik Chakraborty and Dibyendu Debnath, (for tolerating my terrible ‘no’s). This journey would have been tough without them.

I thank my roommates Chinmay Nardele, Sanjay Singh Negi, Nagarajan Sankarnarayanan and Nagendra Kalva for bearing with me these years.

My stay on this campus has been pleasant with the association of all the research scholars at CSIR NCL. I am thankful to Sujitda, Debasishda, Patida, Analda, Joyashishda, Krisanuda, Shyamda, Animeshda, Parthada, Sumantrada, Garaida, Basabda, Binoyda, Analda, Saikat, Patida, Anupamda, Himadrida, Munmun, Tanaya, Sampadi, Jhumur, Chini, Achintya, Arpan Manna, Kanak, Abhik, Susanta, Anjan, Pravat, Himadri, Aryya, Prathit, Sekhar, Nagesh, Nisha, Prajitha, Senthil, Chaka, Malvi, Mrityunjoy, Vineeta, Bhawna, Praveen, Vishal, Sreekuttuan, Srinivas, Pandiraj, Bipinlal, Rajashri, Biplab Joardar, Manik Satej, Krishna Gavvala, Narsimha, Kaushal, Sushma, Nimisha, Maria, Sumana, Ghanshyam (last five shared office space with me for five years).

I would also like to thankful to my all juniors Agnimitra, Anup, Soumen (Das), Saibal Bhoumik, Shantanu, Prasenjit, Sanjeev, Jhumur, Dhanya, Atanu, Somen (Dey), Atreyee, Arunava, Shantigopal, Hridesh, Manjur, Kaushik, Subrata, Sandipan, Indradeep, Bipul, Aniruddha, Anagh, Basudev, Somsuvra, Samik, Sudip, Chayanika, Manik, Soumyajyoti, Manoj, Bappa, Saikat, Ujjwal, Sandeep, Raja, Ramkrishna, Jagadish, Akash, Biplab (Manna), Abhishek Karmakar, Manoj Sharma, Santu.

I am grateful to my school and college teachers and express my gratitude to Suman Chattopadhyay, Dr. Debasish Chakraborty, Swami Suparnananda, Dr. Arogya Varam Saha, Dr. Chandan Saha, Dr. Asish Nag, Dr. Hrishikesh Chatterjee, Prof. Amalendu Banerjee, Dr. Ramaprasad Chakraborty, Dr. Prashanta Ghosh for their encouragement in different part of my life.

Last but not least, I would like to pay high regards to my parents for their sincere encouragement and inspiration throughout my research work and lifting me uphill this phase of life. I owe everything to them. Dedicating this thesis to them is a minor recognition for their invaluable support and encouragement.

Subhadeep Saha

PREFACE

Supramolecular metallogels or co-ordination polymeric gel constitute a important subset of solid-like metal ion and bridging organic ligand structures (similar to metal–organic frameworks) which form three-dimensional networks through a trapped solvent as a result of non-covalent interactions. Although physical properties of these gels might be similar to conventional high molecular weight organic polymer gels, coordination polymer gel systems are often alienates themselves from the former often being fully reversible in the presence of external stimuli (heat, sonication, shaking) to give a solution of solvated gelators. In comparison to gels resulting from purely organic self-assembled low molecular weight gelators, metal ions incorporated into the fibrilar networks spanning the bulk solvent can impart metallogels with added functionalities. The solid/liquid nature of the gels allows external species to migrate through the gel system and interact with metals, ligands, and the solvent. These dynamic systems, taking advantage of the metal ion's coordination, the organic polydentate ligand's orientation and functionality, or a combination of these properties shows potential application in Chemosensing, catalysis, fluorescence, and drug-delivery. In my thesis, I will focus on Cu(II) and Zn(II) based low-molecular weight metallogels (LMWGs) for their application in proton conduction, controlled release and photocatalysis. Excluding introduction chapter my thesis will be divided into 5 chapters which will describe the details on synthesis of various LMWGs, their characterization and applicability in proton conduction, controlled release and photocatalysis.

Chapter 2 will address the synthesis of two Cu(II) based organogels (*viz.*CuA-Ox, CuP-Ox) utilizing oxalic acid as organic ligand. Oxalic acid has been found to be the smallest organic ligand capable of forming gel in presence of metal ion [Cu(II)]. Cu-Ox and its xerogel can exhibit proton conduction at ambient temperature which is the first report of any proton conducting metallogel (Adopted from *Chem. Eur. J.***,** 2013, **19**, 9562)

Chapter 3 depicts synthesis of a Zn(II) and valine (V) derived ligand based metallohydrogel (ZAVP). ZAVP, utilizing its supramolecular nature, exhibits self-healing response as well as response (gel-sol-gel) to a number of physical and chemical stimulus (Adopted from *Chem. Commun.*, 2014, **50**, 3004).

In Chapter 4, synthesis and properties of two similar metallohydrogels [ZNVA and ZPVA; obtained from Zn(II) and valine based ligand V] which shows unique dissolution in water (pH ≤ 7). This property has been utilized for release water soluble molecule (caffeine) entrapped in the hydrogel in presence of water and citrate buffer (Adapted from *Chem. Commun.* 2014, **50**, 7032)

In chapter 5, *in-situ* synthesis of CdS quantum dots in a metallohydrogel (ZAVA; obtained from Zn(II) and valine based ligand V) matrix has been discussed. The CdS incubated metallohydrogel exhibits tunable fluorescence depending upon the size of quantum dots. These CdS incubated metallohydrogels exhibits unique transformation to CdS loaded MOF crystal *via* an unprecedented room-temperature process.

Finally chapter 6 will describe the conclusion of the overall work presented in this thesis. The future direction of this thesis also presented in this chapter.

Subhadeep Saha

CONTENTS

List of Figures, Tables and Schemes

Figures

Table

CHAPTER 1

Supramolecular Metallogels: Synthesis, Properties and Applications

1.1. The concept behind the gel state.

Gels are commonplace items we use in our day-to-day life; for example hair gel, contact lenses, jelly etc. In general, gels are soft materials which do not flow and capable to sustain its own weight. In spite of the fact that gels are common in Nature and frequently encountered in our everyday life and in industry a precise definition of gel is still unknown. This ambiguity was indicated by Jordan-Lloyd (1.1) who in 1926 stated that "the colloidal condition, the gel, is one which is easier to recognize than to define". Since that time, scientific understanding about gels has made major improvements and nowadays scientists from various backgrounds are working on diverse types of gels. However, it remains difficult to make a consistent definition as to what composes a gel.

An important goal was achieved by Flory (1.2) who included structural criteria, such as formation of an infinite entangled network, or a three-dimensional structure, exhibiting properties such as coherence and connectedness, in the definition of a gel. A more recent definition given by Ross-Murphy (1.3) is gel is a viscoelastic solid, which, in a rheological test, exhibits a plateau in the real part of the complex modulus extending over an appreciable window of frequencies. Later on, both of these definitions were accepted and modified by Almdal *et. al.*,(1.4) who stated that a gel is a soft material exhibiting solid or solid-like character, which composed of two or more components, one of which is a liquid, present in substantial quantity. The most recent definition of gel was given by Keller (1.5): gels are fluid-containing self-sustainable dispersed systems where the non-fluidic connecting elements, such as polymer chains or large molecular assemblies are responsible for the continuity to give the retention of shape. A 3-dimensional network structure is always required to impart the mechanical strength and the networks get connected at the junctions, i.e. crosslinking points in polymer gels or contact area in molecular gels. Depending upon nature of the interaction at the cross-link points ther are

two kinds of gels; i) chemical gel (covalent bonding at crosslink junctions) and ii) physical or supramolecular gel (supramolecular bonding at crosslink junctions). In this chapter we will mainly focus on various aspects of supramolecular gels.

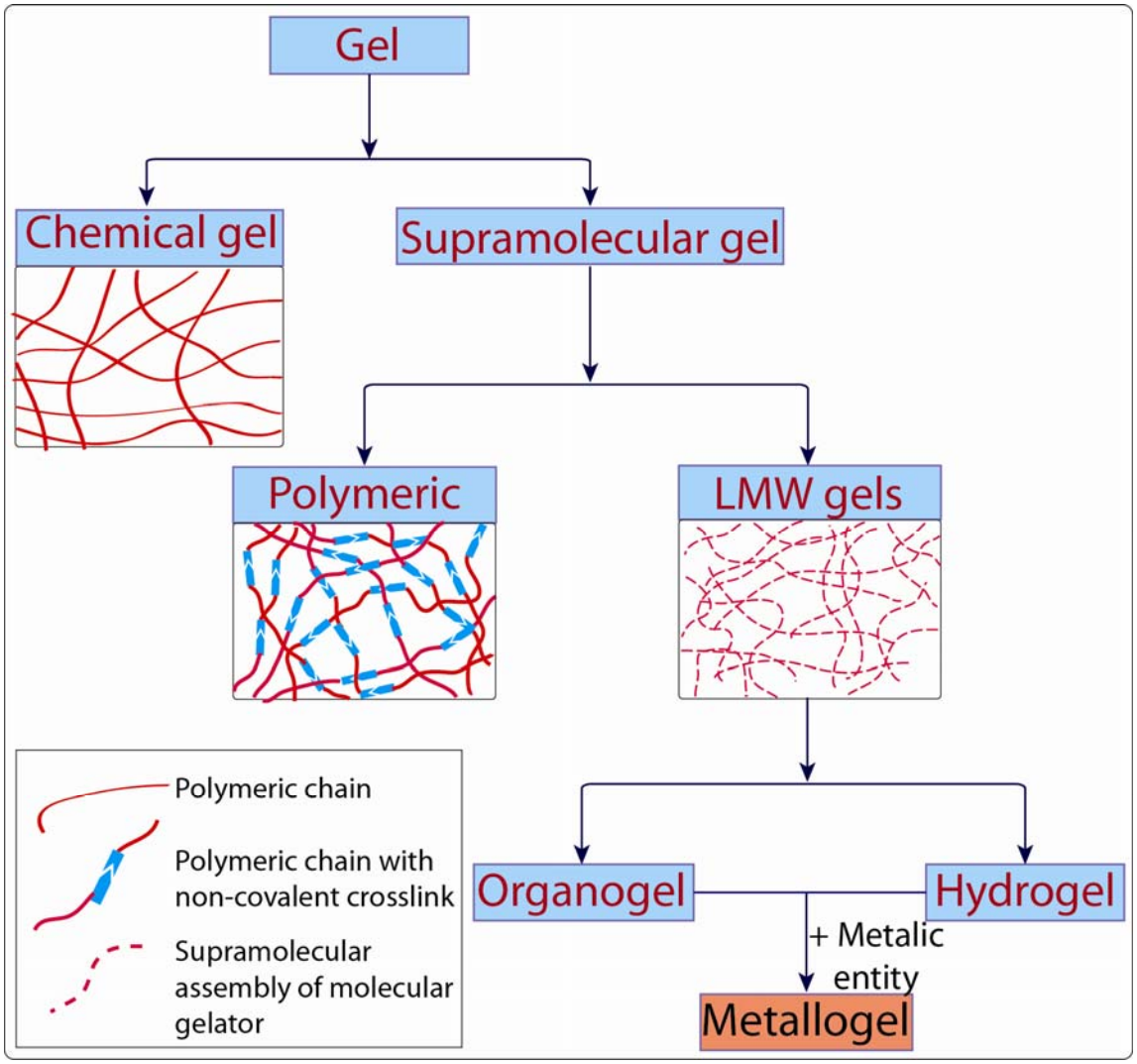

Figure 1.1. Classification of gels based on nature of the gelator.

1.1.1. Supramolecular gels.

Since chemical gels are interconnected via non-dynamic covalent bonds, they are mechanically stable and can be considered permanent on an experimental timescale. This aspect is useful for applications that require tough polymer materials, but it is detrimental if these materials needs to be further processed or recycled. Hence, the utility of chemical gels for application like encapsulation and controlled release is limited. On the contrary, supramolecular gels are responsive towards specific stimuli and a tunable form of a soft

matter. Reversible nature of supramolecular interactions in gel networks greatly facilitates their processing and recyclability. There exist a wide range of external stimuli which can dramatically affect the physical properties of the resulting gels. These stimuli include temperature variation, mechanical agitation, oxidation, change of pH value, addition of specific chemical compounds as well as light irradiation. Hence, the environmental responsiveness makes the supramolecular gels smart media for immobilizing guest molecules (drugs, proteins, etc.) and releasing them when needed. Polymeric supramolecular gels not only retain the mechanical characteristics of chemical gels, (1.6) but also de-crosslinks under presence of certain external stimuli (1.7), which significantly promotes the utility of supramolecular gels.

In recent past, several researchers have attempted to synthesize dynamic hydrogels from polymeric materials crosslinked *via* supramolecular interactions. For example, Azo (-N=N) exhibits photoisomerization in presence of UV or visible light irradiation (1.8, 1.9). α or β- cyclodextrine (CD) selectively forms an inclusion complex with the trans-isomer but not the cis-isomer as the K_a of CDs with trans-Azo is higher than that of cis-Azo.

Sol−gel transition systems have been constructed by complexation of α-CD with dodecyl side chains on the poly(sodium acrylate) backbone (1.10). The viscosity of the hydrogel of poly(sodium acrylate) modified with 5 mol % of dodecyl side chains (p(AA/ C_{12}))drastically decreases upon addition of α-CD. The viscosity of the solution with 4,4′-diazobenzoic acid (ADA) as a photoresponsive competitive guest increases with the concentration of ADA. Photoisomerization of ADA controls the association and dissociation of the dodecyl side chain with αCD, leading to photoresponsive sol−gel transitions.

Aqueous mixture of β-cyclodextrine (CD) modified poly(allylamine) with trans-Azo modified poly(acrylamide) yields supramolecular hydrogels. The K_a of trans-Azo with β-CD is larger than that of cis-Azo. Nevertheless, the cis-Azo copolymer does not form supramolecular hydrogels with β-CD copolymers in water because the host−guest interaction between β-CD and the trans-Azo group acts as a cross-linker between polymer chains (1.11).

Moreover, β-CD can form a 1:1 inclusion complex with ferrocenecarboxylic acid (FCA), but when oxidized, FCA weakly interacts with βCD. Taking the advantage of the redox-responsive complex formation, gel-to-sol transition systems was synthesized *via* complexation of β-CD with the dodecyl side chains of dodecyl-modified poly(acrylic acid) [p(AA/C_{12})] (1.12). Addition of β-CD to a hydrogel of p(AA/C_{12}) decreases the viscosity drastically to yield a sol. However, the viscosity of the sol with FCA as a redox-responsive competitive guest increases as the FCA concentration increases. After oxidation with sodium hypochlorite, the gel state changes to the sol state.

1.1.2. Low-molecular weight gels.

Low-molecular-weight gelators (LMWGs) are molecules, having molar mass of ~3000, capable of gelating organic liquids or water (1.13). These gelator molecules self-assemble in presence of organic solvents or water through certain‘‘non-covalent’’ interactions, such as hydrogen bonding, polar–polar interactions, hydrophobic interactions,electrostatic inter-actions and π-π stacking which drive the one-dimensional growth of the gelator molecules to produce nanoscale or microscale structures in the form of fibres, strands and tapes. These one dimentional extended objects entangles together to form three-dimensional networks which engulfs liquid molecules to form gels (1.14). These weak interactions can be arranged in order to their decreased strength as follows: (a) electrostatic interactions (ion– ion, ion–dipole and dipole–dipole interactions) and coordinate bonding (metal–ligand), (b) hydrogen bonding, (c) π–π stacking and (d) van der Waals forces. In addition to them, hydrophobic or solvophobic effects, as well as the fine balance of the forces amongst gelator molecules and solvent molecules, often play important role in gelation. Indeed a single weak interaction is generally much weaker than a covalent bond, however, the cooperative effect of many such interactions may lead to a supramolecular framework that is thermodynami-cally and kinetically stable under a variety of conditions (1.15). LMWGs constructed by means of a self-assembled approach are much more versatile, with tuneable functionality, than their polymeric counterpart as a result of their dynamic nature which make them molecularly defined, intelligent materials may be constructed by using the supramolecular concept (1.16). These materials are uniquely susceptible to the effects of external stimuli are of interest and play a crucial role as functional soft materials (1.17).

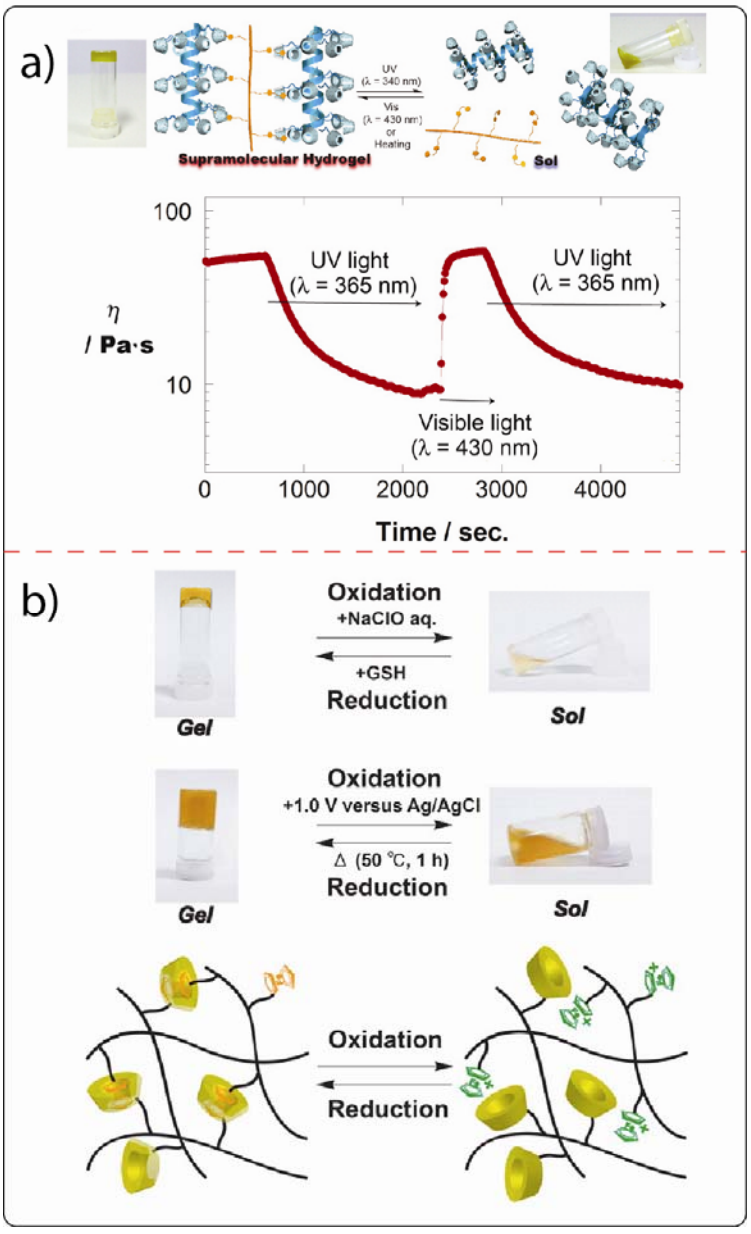

Figure 1.2. a) Schematic representation of a photoresponsive sol−gel transition material with CD-CUR and pC12Azo upon irradiating with UV light (365 nm) and visible light (430 nm) or heating at 60 °C. (b) Zero shear viscosity (η_0) change for CD-CUR/pAC_{12}Azo after repeatedly photoirradiating with UV (λ = 365 nm) and visible light (λ = 430 nm). Reproduced with permission from ref 1.41. Copyright 2010 WILEY-VCH Verlag GmbH & Co. KGaA; b) Redox-responsive sol−gel switching. Reprinted by permission from Macmillan Publishers Ltd: Nature Communications (ref 1.42), copyright 2011.

1.1.2.1. Low-molecular weight organogels (LMOGs).

Molecular entities which self-assemble in presence of particular solvents (except water) *via* supramolecular interactions are classified as low molecular weight organogels. There exists a wide range of organic small molecule (Figure 1.3) which forms gels in presence of various organic solevents.

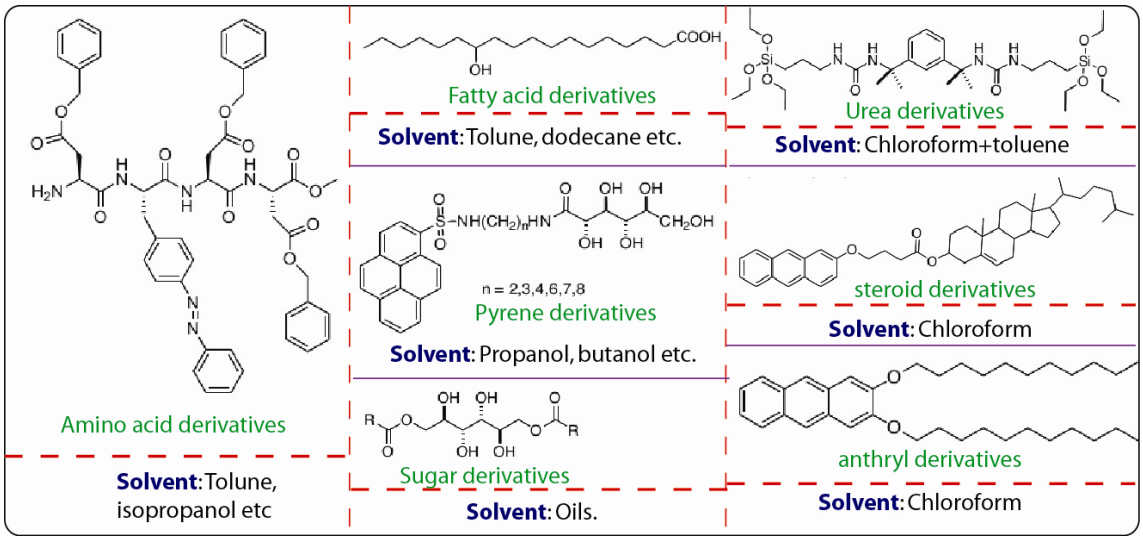

Figure 1.3. Different low molecular weight organogelator and their corresponding organic solvent.

Although LMOGs are often seems to be underarated compared to their aqueous counterpart in terms of applications, these materials are not only smart but versatile and have numerous applications.

Sugar-based molecular organogelators Figure 1.4 were developed, which turned out to be able to solidify 16 different organic solvents and oils (Figure 1.4) (1.18). Moreover, they are able to selectively gelate the oil phase from oil-water mixtures at RT. Later on, the oil can be quantitatively recovered from the gel by vacuum distillation. Hence, the gelators are not only easily synthesized, but also environmentally benign. They were found to be ideal candidates for the disposal of marine oil spills, as for starting the gelation process only an aliquot of 2.5 wt% of the gelator has to be dissolved in a hydrophilic solvent as alcohol and then added to the oil-water mixture.

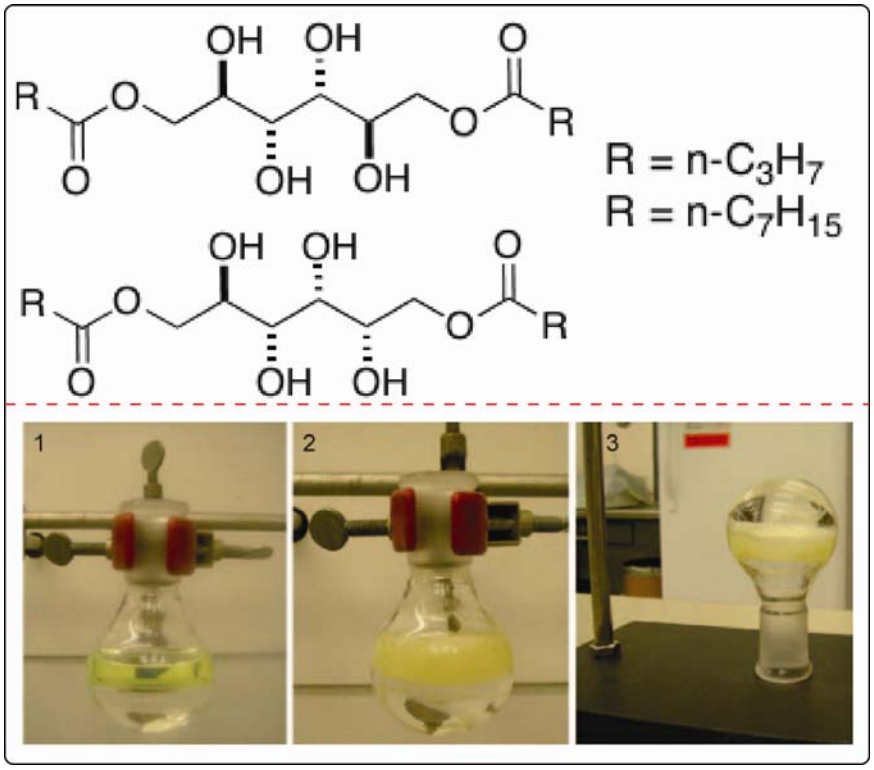

Figure 1.4. *(top)* sugar-derived organo gelators; *(bottom)* Gelation of bulk diesel in the presence of water, and its quantitative recovery throughvacuum distillation. Photographs: 1) diesel and water form a two-phase system; 2) gel forms instantaneously upon addition of gelatorby syringe; 3) Owing to the strength of the diesel gel, the flow of water stopped upon inversion of flask. Reproduced with permission from ref 1.43. Copyright 2010 WILEY-VCH Verlag GmbH & Co. KGaA.

1.1.2.2. Low-molecular weight hydrogels (LMHGs).

These are low molecular weight systems which are found to form gel in presence of water. These materials are supposed to be more promising than thein organogels counterparts as they are predominantly made up of water which makes them biocompatible in nature. LMHGs have been found to be promising materials for various fileld; e.g. sensing, nanoelectronics, biocatalysis etc. The compound shown in Figure 1.6a is a poor gelator in itself, however, it undergoes a reaction withβ-lactamase enzyme to produce a derivative that is a good gelator. β-Lactamase catalyzed hydrolysis of a β-lactam ring in penicillin-type drugs is a significant cause of bacterial drug resistance. Therefore, the formation of a gel via this biocatalytic reaction is a way to sense the presence of penicillin-resistant bacteria.

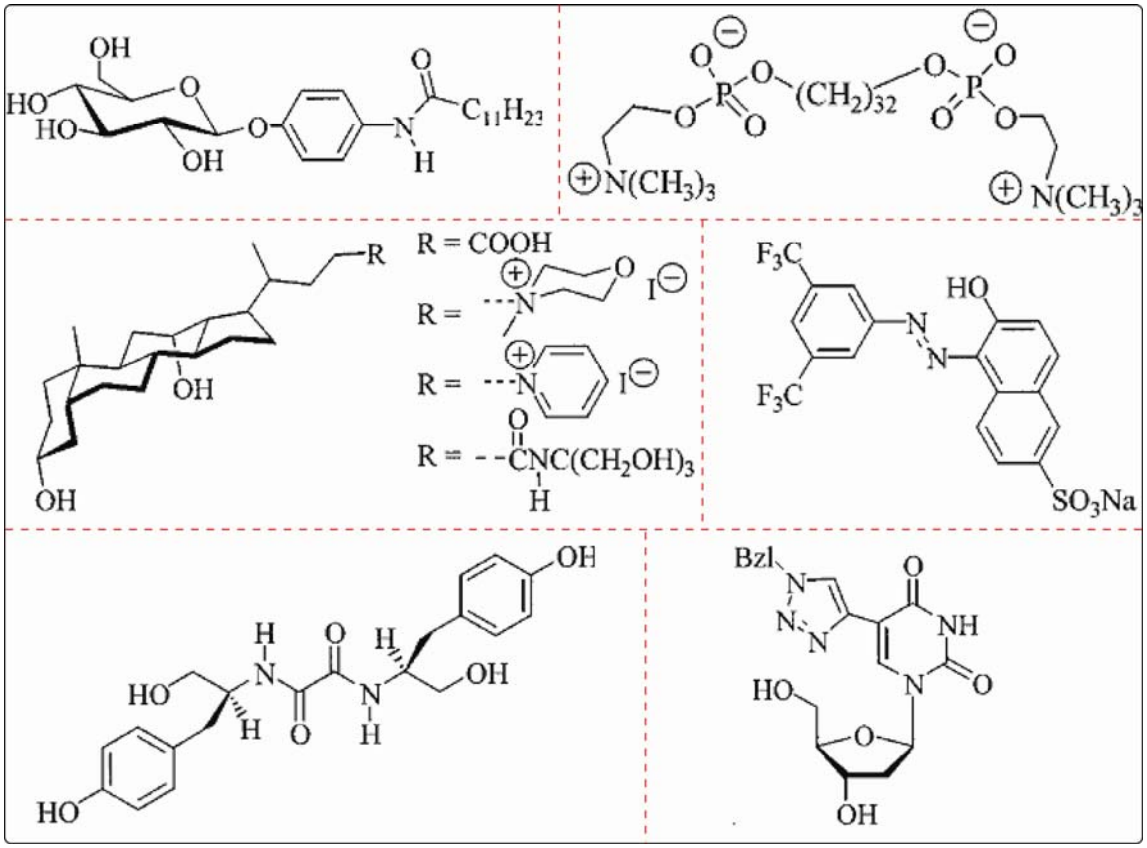

Figure 1.5. Organic molecules capable of forming gel (LMHG) in presence of water.

1.1.3. Supramolecular metallogels.

1.1.3.1. Definition of supramolecular metallogels.

Supramolecular metallogels or co-ordination polymeric gel constitute a important subset of solid-like metal ion and bridging organic ligand structures (similar to metal–organic frameworks) which form three-dimensional networks through a trapped solvent as a result of non-covalent interactions. Although physical properties of these gels might be similar to conventional high molecular weight organic polymer gels, coordination polymer gel systems are often alienates themselves from the former often being fully reversible in the presence of external stimuli (heat, sonication, shaking) to give a solution of solvated gelators. In comparison to gels resulting from purely organic self-assembled low molecular weight gelators, metal ions incorporated into the fibrilar networks spanning the bulk solvent can impart metallogels with added functionalities. The solid/liquid nature of the gels allows external species to migrate through the gel system and interact with metals, ligands, and the solvent. These dynamic systems, taking advantage of the metal ion's coordination, the

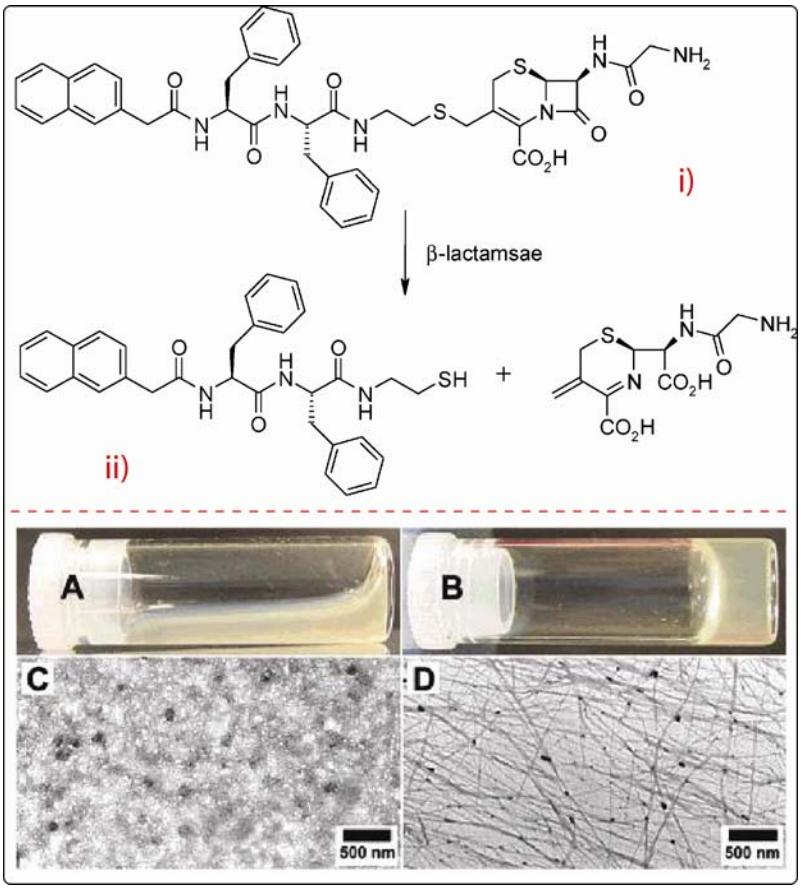

Figure 1.6. *(top)* β-Lactamase catalyzed hydrolysis of aβ-lactam ring in penicillin results in gel formation with potential applications in sensing the presence of penicillin-resistant bacteria; *(bottom)* The optical images and the transmission electron microscopy (TEM) images of (A, C) viscous solution of i) and (B, D) gel ii); Reproduced with permission from ref 1.44. Copyright 2006 WILEY-VCH Verlag GmbH & Co. KGaA.

organic polydentate ligand's orientation and functionality, or a combination of these properties shows potential application in Chemosensing, catalysis, fluorescence, and drug-delivery. Fine tuning of these systems through metal ion and ligand selection and *via* directing self-assembly with external stimuli the rational synthesis of practical systems can be envisaged.

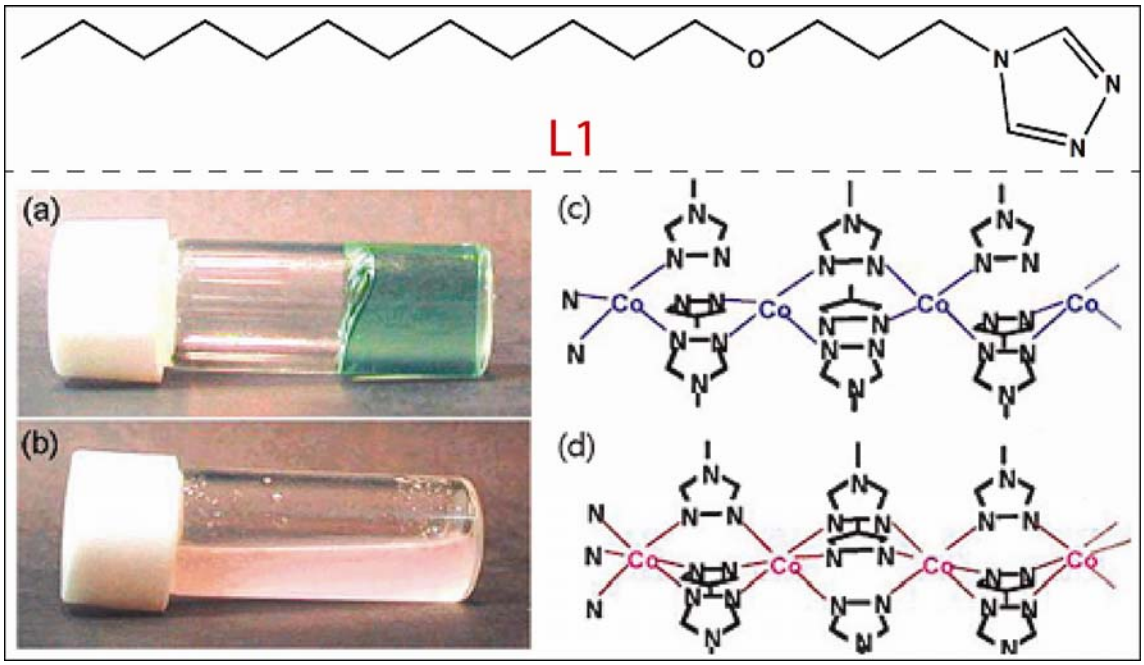

Figure 1.7. *(top)* structure of L1 ligand; *(bottom)* Pictures of $Co(L1)_3Cl_2$ in chloroform: (a) a blue gel-like phase at 25 °C; (b) a pale pink solution at 0 °C [reproduced with permission from the American Chemical Society (ref. 1.20)].

Metallogels form by means of supramolecular interactions such as co-ordination bonding, π–π stacking, hydrogen-bonds and hydrophobic interaction (1.19). Kimizuka and co-workers provided an excellent example of a metallogel reporting as the first example of thermally reversible gel networks in organic media (1.20). A lipophilic Co^{2+} complex of 4-(3-lauryloxy) propyl-1,2,4-triazole (L1) can be dissolved in chloroform to produce a blue gel (MG1; MG=Meallogel) at room temperature. Upon cooling below 25 °C the gel turns into a pale pink solution which is a consequence of a fully reversible thermochromic transition from tetrahedral Co^{2+} geometry to octahedral (Figure 1.7) (1.19).

In recent past, metallogels have been utilized for useful functional properties such as physical/chemical stimuli response, redox responsiveness, phosphorescent behaviour, catalysis and spin-crossover phenomenon (1.69). Moreover, via proper selection of the binding metal ions and organic ligands, one can affect modes of self-assembly and finely tune conditions for gelation. Similar to supramolecular chemistry, chemists have begun to rationally design ligands for metallogels having suitable coordination geometries for the incorporation of specific metals to generate scaffolds containing void spaces.

This chapter will review the applications of metallogels in sensing, drug-delivery and catalysis that have been developed over the past few years. It has been seen that pyridine, tetrazole, carboxylic acid and amino acid moieties mostly bind to metal ions to form metallogels in organic solvents or water. These metallogels are characterized by their non-discrete self-assembled fibrillar network structures. Nature of the metal ion strongly affects the structure of a metallogel. Additionally, these metallogels can selectively sense and separate specific guest molecules in environmental and biological samples. We describe metallogels that are utile in environmental and biological applications.

1.1.3.2. Catalytic metallogels.

A derivative of calix [4] arene (L1B) has been utilized as a ligand to form a metallogel using $[Pd(en)(H_2O)_2]^{2+}$ (en = ethylenediamine) as the metal complex precursor. Polymerization was stepwise monitored by ^1H NMR in DMSO-d_6.

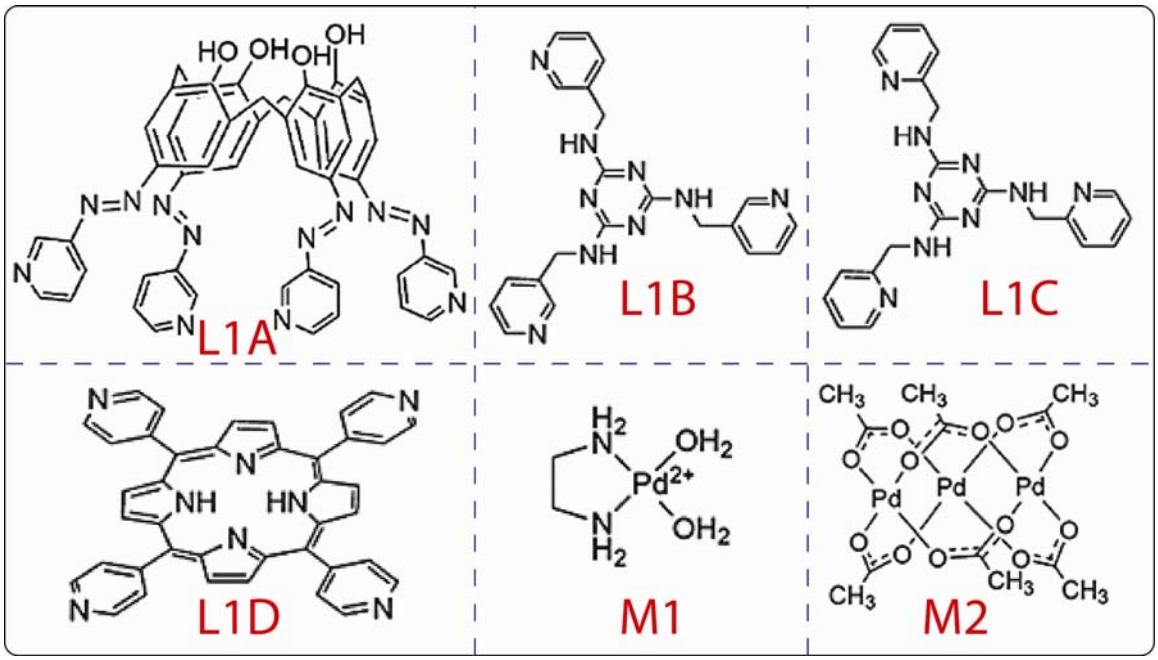

Figure 1.8. Different ligands (L1A-L1D) and Pd^{2+} precursors (M1, M2) utilized for preparation of catalytic metallogels.

The required molar ratios of Pd(II) to L1B for formation of the metallogel (MG2) were found to be from 1.8 : 1 to 2 : 1, and the concentration of the metallogelator in the gels range from 0.5 to 2 wt% (~1 mmol concentrations). Nature of gelation alters upon change in coordination complex gel precursor, e.g. substituting ethylenediamine with a 1,5-cyclooctadiene (COD) ligand. Using $Pd(COD)Cl_2$ as the metal complex precursor,

gelation happened in DMSO after 72 h, which was much longer than that of $[Pd(en)(H_2O)_2](NO_3)_2$ (4 h).

Table 1.1. The conditions used for gelation of ligands L1A-L1D in DMSO

Sr. No.	Sample	Ligand	Metal precursor	Solvent	Time (h)	Solvent/ Gelator (molar ratio)	Pd(II)/ ligand	Diameter of fibers in gel (nm)
1	Polymer	L1B	M1	DMSO	-	-	-	-
2	Polymer	L1C	M1	DMSO	-	-	-	-
3.	Oligomer	L1C	M2	DMSO	-	-	-	-
4.	Gel A	L1B	M2	DMSO	12	270	1.3-1.5	20
5.	Gel B	L1A	M2	DMSO	6	950	2.0	70-120
6.	Gel C	L1D	M1	DMSO	1680	420	1.7-2.0	10
7.	Gel D	L1A	M1	DMSO	4	1000	1.8-2.0	50

The catalytic activity of the pyridine-based calix[4]arene gel MG2 was then measured for the oxidation reaction of benzyl alcohol to benzaldehyde (Figure 1.9). Pure benzyl alcohol was added to a as-synthesized metallogel (molar ratio of catalyst to substrate is about $(1 : 10^4)$, and molecular oxygen was passed through the reaction mixture by bubbling air. Conversion of benzyl alcohol into benzaldehyde was monitored by HPLC every ten minutes over two hours and it was observed that catalysis did not affect the stability of the metallogel. Xerogel with an equal amount of catalytic metal sites were also tried under the similar reaction conditions. Catalytic turnovers of all the gels were evaluated and compared with the catalytic turnovers of 6 or 7 under similar reaction conditions. Figure 1.9 exhibits a comparison of turnovers of different catalysts after two hours of reaction. For the reactions involving $[Pd(OAc)_2]$ moieties, the turnovers maintains the order: B > A > M2 > dry A > dry B. Catalytic turnover of A was found to be twice than that of the corresponding dry gel and 1.5 times greater than that of M2 (Table 1.1); the catalytic turnover of B is twice than that of $[Pd(OAc)_2]$, three times than that of the corresponding dry gel, and four times that of similar systems (1.24) reported. Pyridine moieties was found to be inert during the oxidation reaction (1.23) as they are

part of the gel network thus eliminating the

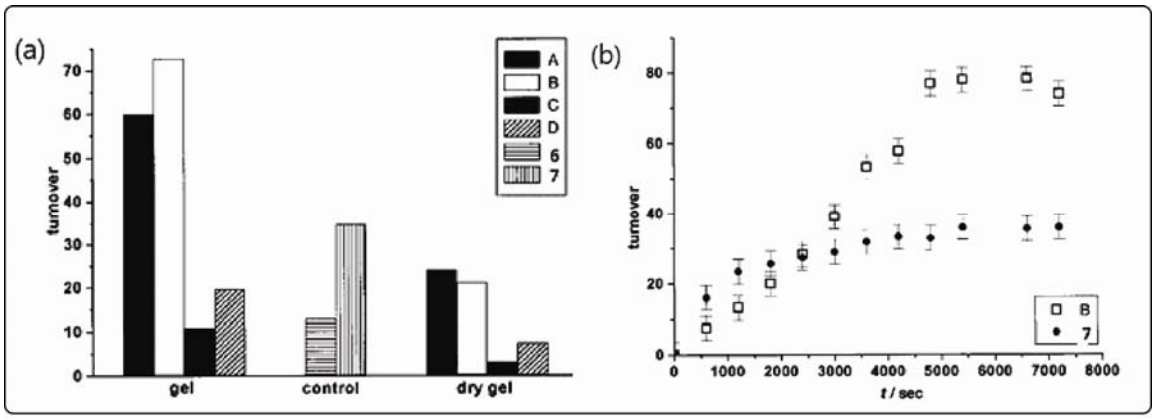

Figure 1.9. a) The catalytic turnovers (cumulative) for the oxidation of benzyl alcohol by air (1 atm) by using metallogels, their corresponding dry gels (formed by precipitating coordination polymers in acetone), and their corresponding transition-metal complexes as catalysts; (b) the catalytic turn overs versus time of gel B and compound L1B. The legends refer to Table 1 [reproduced with permission from the Wiley Verlag GmbH & Co (ref. 1.22)].

purification step of separation of pyridine from benzaldehyde (1.23). These metallogels are stable in presence of water and most organic solvents except acetone, and can catalyze the aerial oxidation of benzyl alcohol to benzaldehyde significantly utilizing their Pd^{2+} moieties as catalytic centres. These gel-based Pd^{2+} catalysts do not convet to Pd black.

1.1.3.3. pH responsive metallogels.

An amino acid based ligand N-(7-hydroxyl-4-methyl-8-coumarinyl)-glycine (L3) forms a fluorescent metallyhydrogel with Zn(II). This metallohydrogel, $[Zn(L3)(H_2O)]_n.H_2O$ (MG4), instantly forms when a basic aqueous solution of L3 reacts with $Zn(OAc)_2$ $2H_2O$. As-synthesized metallohydrogel (MG4) has been found to be pH responsive and transforms to a clear colourless solution upon acidification to a pH of 2, but it is able to reform its gel structure when the pH is raised to 8. At acidic pH values, the ligand is protonated hence disruption of in the complexation occurs which leads to destruction of the gel network. A completely different scenario has been seen upon slight modification of the ligand. Aqueous mixture of L4 and $Zn(OAc)_2$ $2H_2O$ yields a viscous liquid which doesn't form gel but produces single crystals of $[Zn(L4)(H_2O)]$ $0.5H_2O$.

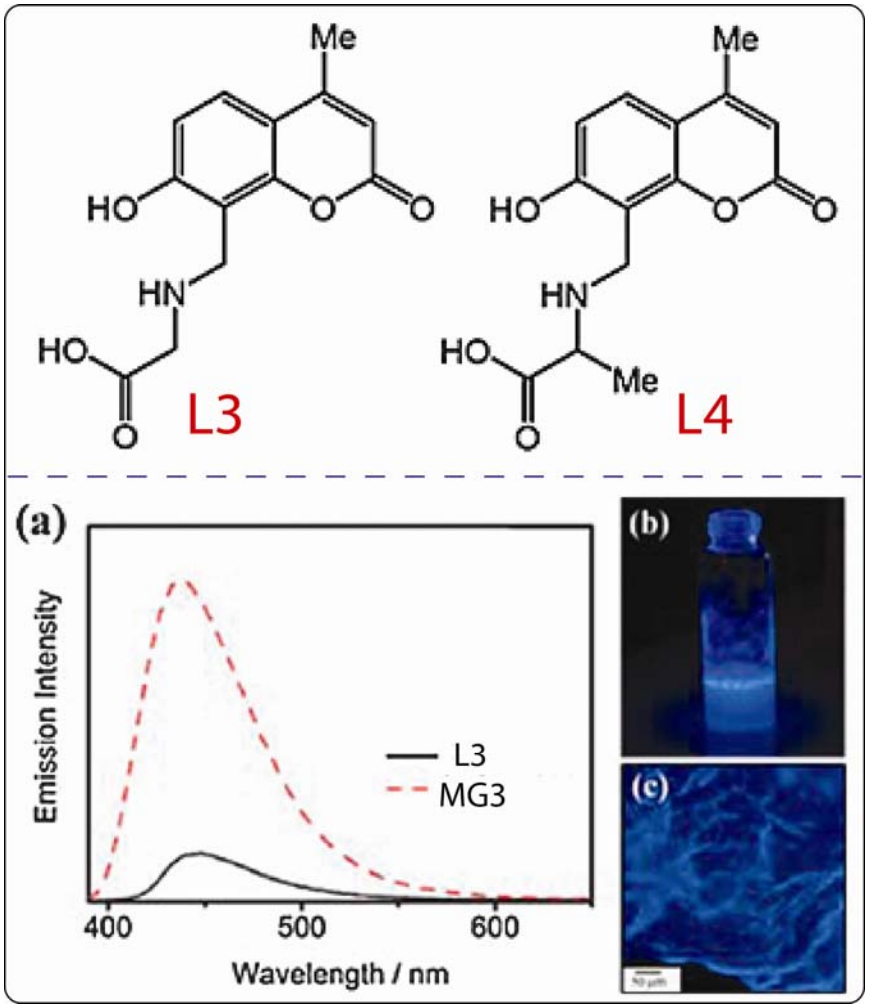

Figure 1.10. *(top)* Ligands tested for synthesis of pH sensitive metallogel; *(bottom)* (a) Emission spectra of L3 in H2O and hydrogel MG4 upon excitation at 340 nm, where the absorbance of all the samples is the same. (b) Photograph of MG3 under UV light. (c) Fluorescence micrograph of freeze-dried MG3 [reproduced with permission from the Royal Society of Chemistry (ref. 1.19)].

The SEM image of freeze-dried Zn-hydrogel (MG3) displays fibrillar network structure typical for gels. The fibers are several micrometers in length with diameters in the range of 200–500 nm. Single crystal structure of the CP crystal suggests that the 1D CPs assemble to form fibrous nanostructures, which then further entangle into a 3D network through noncovalent interactions to engulf water molecules. Fluorescence properties of the MG4 were studied which exhibits a strong blue emission with maxima at 440 nm (upon UV excitation) and a pronounced enhancement in fluorescence in comparison to solution (Figure. 1.10). A drastic drop in fluorescence is experienced when the pH of MG3 is lowered. The diossolution of the gel due to dissociation of the complex leads to

fluorescence quenching. The strong blue fluorescence of MG3 can be visualized even by the naked eye under UV light (Figure 1.10). A fluorescence micrograph of freeze-dried MG4 also shows a fibrillar structure along with a strong blue emission (Figure 1.10).

1.1.3.4. Fluorescent tetrazole-based metallogels.

Fluorescent properties of a tetrazole-based metallogel with Mg^{2+} ions have been probed in detail by Jung *et. al.* (1.25). The ligand (L5) only forms hydrogels with Mg^{2+} ions at pH = 12 (Figure 1.11). This pH sensitive hydrogel MG4 precipitates upon adjustment to acidic pH values. However, the gel phase could be restored upon adjusting the pH to a strong basic condition (pH = 12–14). The corresponding xerogel displays a fibrillar network with high aspect ratio having widths in the range 60–70 nm and thicknesses of about 3 nm (Figure 1.11). The absorption and emission spectra of sol MG5 and metallogel MG5 with were extensively studied. The maxima of UV-vis absorption band of Mg^{2+} metallogel MG4 appears at 302 nm referring to a typical π–π∗ transition (1.25). However, the π–π* absorption band of a sol of MG4 exhibits blue shift of 70 nm. The fluorescence spectra of the coordination polymer gel MG4 (λ_{ex} = 302 nm) exhibits a strong blue emission with a maximum at λ = 467 nm.

Jung and co-workers (1.26) also synthesized a fluorescent metallogel MG5 with Zn^{2+} which exhibits a strong blue emission with a maximum at λ = 475 nm in DMF/MeOH. A pronounced enhancement of fluorescence intensity is observed in gel state compared to sol MG5 (λ_{ex} = 300 nm). The photoluminescence of this Zn^{2+} metallogel MG5 can also be seen by the naked eye under UV light. The absorption and emission properties of MG5 with Zn^{2+} from DMF and DMA were found to be similar to that obtained from DMF: MeOH. On the other hand, the pure ligand L6 doesn't exhibit emission at any wavelength. Hence, the strong emission of gel L6 with Zn^{2+} originates from the self-assembled structure formed through strong supramolecular interactions and not from the monomeric ligand L6.

1.1.3.5. Chiral metallogels.

Development and discovery of chirality mediated supramolecular assemblies are proven to be significant for obtaining novel functional materials such as chiral sensing platforms. Albeit, there are plenty of reports on impact of chirality upon self-assembled systems including fibrillar networks and even supramolecular gels, to our knowledge the

formation

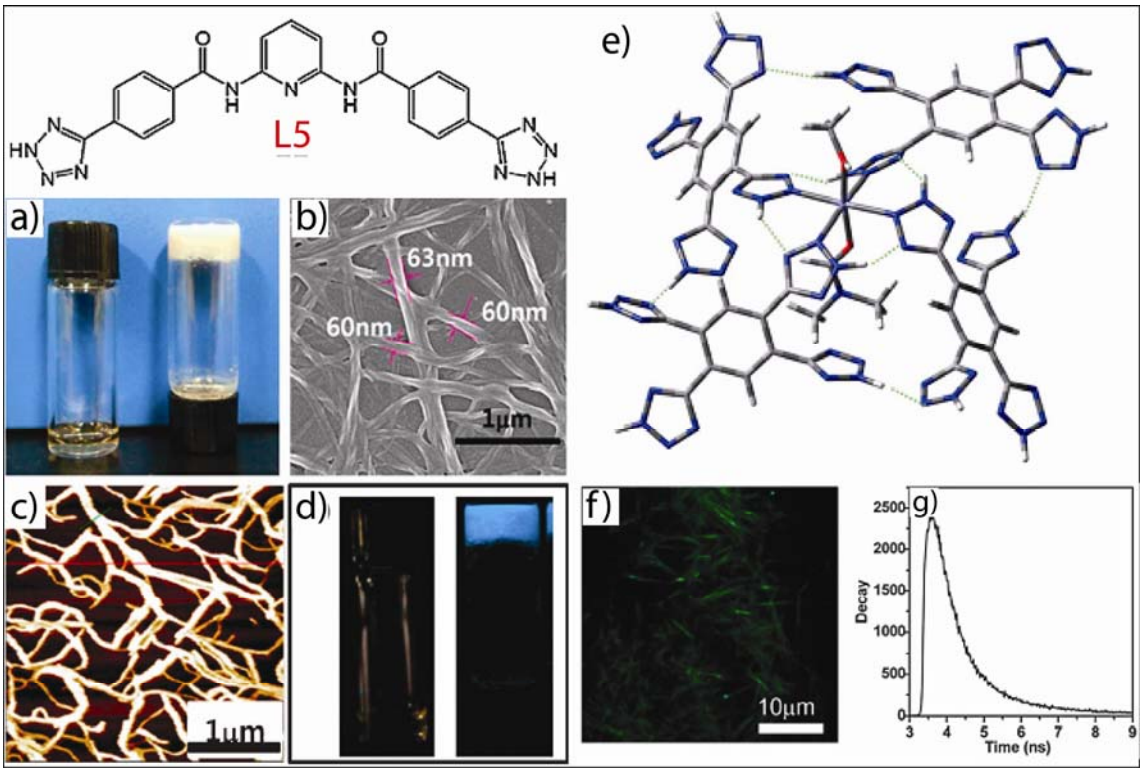

Figure 1.11. *(top)* Ligands tested for synthesis of fluorescent metallogel; *(bottom)* Photograph of sol MG4(left) and gel MG4(20 mM, right) with Mg^{2+} (80 mM, 4 equiv.). (B) SEM and (C) AFM images of gel11. (D) Photograph of sol MG4 (left) and gel MG4 (20 mM, right) with Mg^{2+} (80 mM, 4 equiv.) by irradiation with UV light; [reproduced with permission from the Royal Society of Chemistry (ref. 1.73)]; d) The B3LYP/3-21G* optimized structure of Zn^{2+} with ligand L5 [reproduced with permission from the Wiley Verlag GmbH & Co (ref. 1.74)]; e) Fluorescence image of Mg2+ metallogel L5 by time-resolved fluorescence confocal microscopy and f) its fluorescence decay [reproduced with permission from the Royal Society of Chemistry (ref. 1.25)].

of supramolecular metallogels finely controlled by ligand chirality has been hardly achieved so far. For example, Ogden *et. al.* (1.28) studied the mechanism of gelation and chiral coordination of a proline-functionalized calix[4]arene (L7) complexed with La^{3+}. Fibrous structure of the gels was confirmed by atomic force microscopy (AFM) study of the wet gels on mica. It reveals significant alteration of fibrous nature in the racemate which is consistent with changes observed in the bulk properties. Pure chiral systems were found to form elongated fibrous structures whereas the racemate appears to form connected spheroidal structures. As a result, the less stable racemic gels were found to

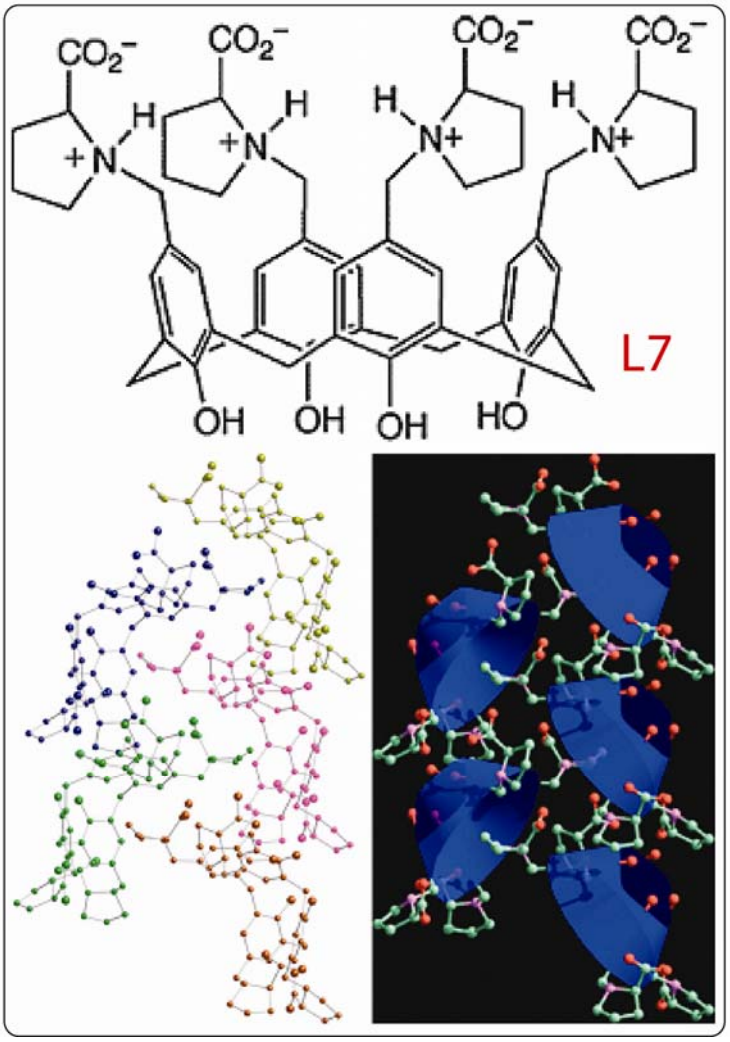

Figure 1.12. *(top)* Ligand tested for synthesis of chiral metallogel; *(bottom)* The helical packing of L7 found in the La(DL-L7) crystal structure; a ball and stick model coloured by molecule, and a schematic diagram with the calixarene backbone represented by blue ribbons [reproduced with permission from the Royal Society of Chemistry (ref. 1.38)]

collapse and crystallize over a period of days, whereas the enantiomerically pure systems remained stable for months. The X-ray structure of the racemate crystals shows intermolecular inclusion of a proline moiety into the cavity of a neighbouring calixarene resulting in the formation of a helical structure (Figure 1.12). Each helix constitutes of a single enantiomer, either the D- or L-isomer, signifying that the individual enantiomers could form comparable structures, forming the fundamental unit to create larger fibres, and fibre bundles.

1.1.3.6. Metallogels as smart materials chemosensors.

Since the gel materials contain solvent within a gel network is bound by weaker

intermolecular forces, researchers tried to exploit the fluidity of the trapped solvents and its ability to diffuse species through the fibrillar network. As introduction of a foreign chemical entity might affect the gel network as well the properties stem from the co-ordination complex in the gel network, chemosensing showed up as a potential application for metallogels.

A recent report on a Co^{2+} based metallogel shows application as a chemosensor for chlorine atom containing gases. The tetrazole-based ligand L6 immediately forms organogels (MG6) upon addition of Co^{2+} with a variety of counter anions such as ClO_4 , OAc , Cl , Br , I , and NO_3 in polar solvents such as DMF, DMA, and DMF/methanol (1 : 1 v/v) as the two solutions are mixed. These gels exhibit a red color except for the solution containing Cl (Figure 1.13). The metallogel MG6 obtained from $CoBr_2$ exhibits a spherical structure with 20–30 nm diameter particles. Uniformity of the sample and narrow diameter distribution were confirmed by transmission electron microscopy (TEM) as shown in Figure 1.13. Additionallly, TEM images of these metallogels obtained using different anions exhibit a spherical structure with 20–30 nm diameter particles. The coordination complex structure was optimized for Co^{2+} with Br by density functional theory (DFT) calculations (1.24). The co-ordination environment of Co^{2+} cation is octahedrally filled by two trans-oriented bromide anions, two trans-oriented L6, MeOH and DMF. Sensing ability of the metallogel MG6 was evaluated as a selective chemosensor for toxic gases containing chloride such as HCl, $SOCl_2$ $(COCl)_2$ and $COCl_2$ (phosgene) using UV-vis spectroscopy. $CoBr_2$ metallogel MG6 exhibit a UV-vis spectrum having an absorption band at 475 nm with a red color depicting the formation of octahedral (O_h) complexes (1.24). Presence of a small amount of $COCl_2$ (phosgene) gas causes a red shift of 195 nm in the spectrum resulting in a new band at 670 nm hence the blue coloration under UV light. This phenomenon can be explained by the replacement of bromide anions by chloride because the phosgene may decompose in the gel state (1.24), with a release of chloride anions. The absorption band at 670 nm is signature of a tetrahedral Co^{2+} complex (T_d, $^4A_2$, $^4T_1(P)$). Similarly, the fluorescence intensity of the metallogel MG6 gradually decreases upon exposure to phosgene gas. HCl, $SOCl_2$ and $(COCl)_2$ gases also induce hypsochromic shift to the emission spectrum of the metallogel MG6. For practical application of the material, a portable chemosensor

was prepared. Red coloration of a disk-type pellet of dried gel of MG6 transformed to blue within few seconds upon exposure to phosgene gas (Figure 1.13). However, upon exposure

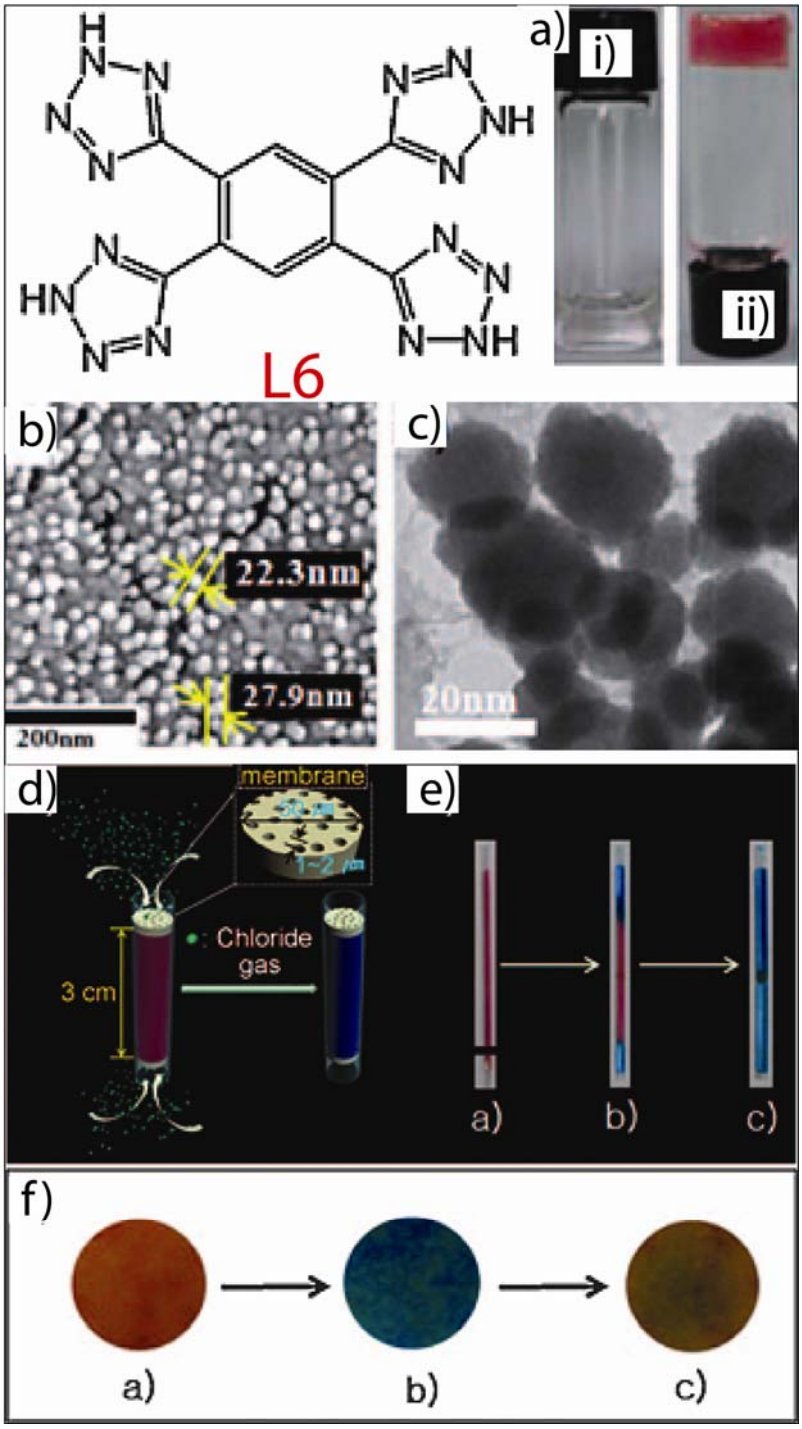

Figure 1.13. *(top left)* Ligand (L6); *(bottom)* a) Photograph of MG6 in solution (i, 20 mm) and gel MG6 (ii, 20 mm, 3.0 equivalent);b) SEM and c) TEM images of gel MG6; d) Representation of a gel MG6-coated capillary as the portable chemosensor; e) Photographs of a gel MG6-coated (20

mmol) capillary before (a),after 10 (b), and 30 s (c) of exposure to chloride gas (100 mmol); f) Photographs of disktype pellets of dried gel MG6 before (a) and after (b) exposure to phosgene gas, and after rinsing the pellet with DMF and methanol containing 100 mmol HBr [[reproduced with permission from the Wiley Verlag GmbH & Co (ref. 1.26)].

to a DMF/MeOH solution containing HBr, the blue color of the pellet reverts back to original red. It has been determined from the change in absorption and emission spectra of metallogel MG6 in presence of phosgene that the sensitivity of detection is 1-20 ppb.

1.1.3.7. Functionalized graphene-based metallogels as TNT sensor

Excellent physicochemical properties have made graphene and its derivatives versatile building blocks for carbon-based materials, thanks to their unique two- or three-dimensional (2D or 3D) structures (1.34). Recent studies have demonstrated that the self-assembly is a powerful method for construction of functional hierarchical graphene-based nanomaterials (1.78). Self-assembly of nanosized graphene to macroscopic materials helps to convey the properties of the nano regime to macroscopic obejects giving rise to numerous breakthrough applications in optoelectronics (1.30), energy-storage (1.31), biomedicine and chemosensing (1.32).

An intriguing example of this was recently reported where the formation of a metal–organic framework/azobenzoic acid-functionalized graphene oxide composite hydrogel (MOF/A-GO; MG7) has been described in the presence of Zn^{2+} and its potential application as a chemosensor for the detection of trinitrotoluene (TNT) molecules (1.32). At first, epoxy and hydroxyl groups were eradicated by reduction with $NaBH_4$. Next step involves the functionalization of chemically reduced GO (Figure 1.14) using the diazonium grafting method which allows the basal planes to become extended by azobenzoic acid groups. Red-shift in π–π^* absorption band of r-GO at 260 nm in comparison to the band of GO at 241 nm is corroborates with the partial recovery of the conjugated network. An additional absorption band appeared at 400 nm which signifies the azobenzoic acid attached onto r-GO.

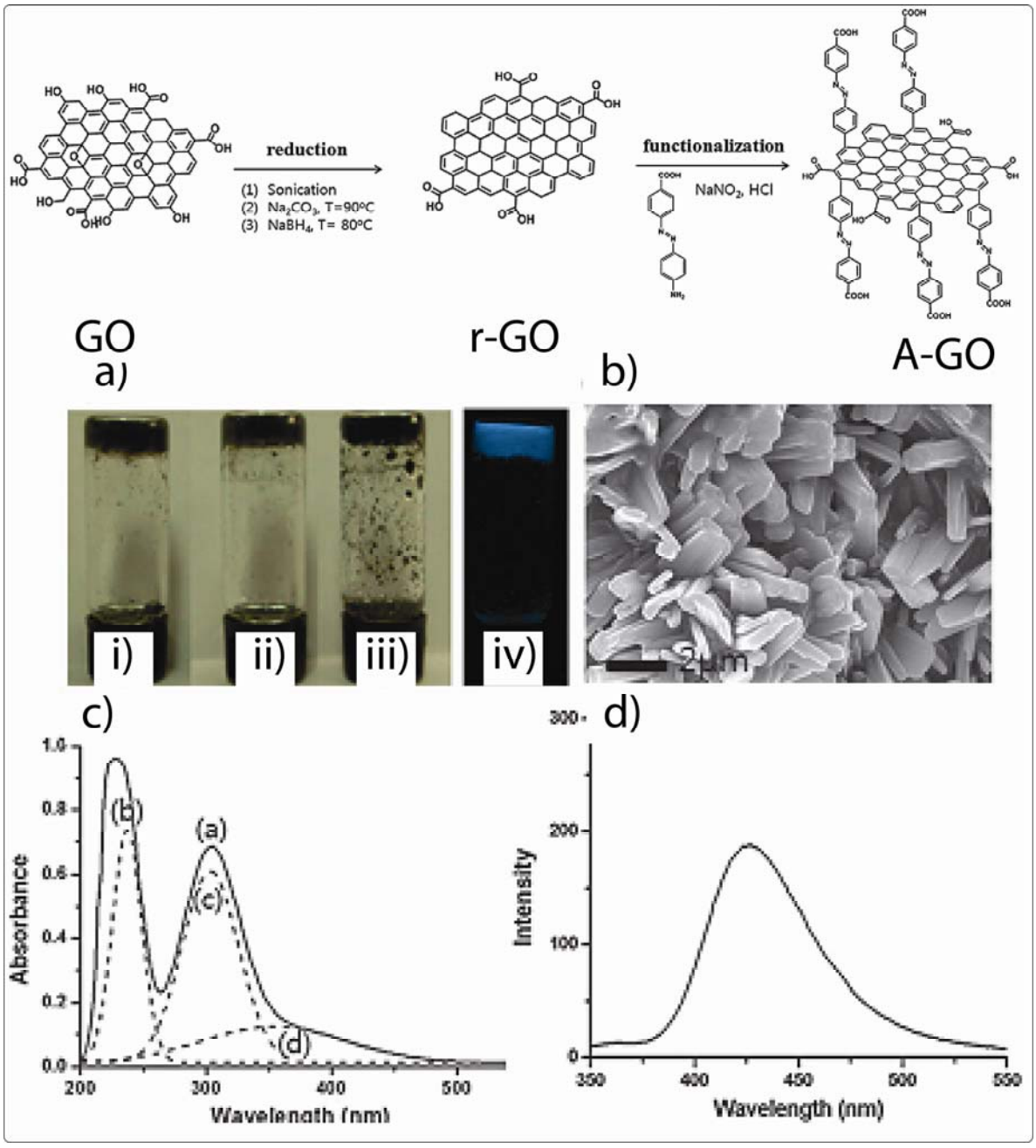

Figure 1.14. *(top)* Synthetic route for azobenzoic acid-functionalized graphene oxide (A-GO); *(bottom)* (A) Photograph of metal–organic framework/azobenzoic acid-functionalized graphene oxide composite hydrogels MG7;(a)1 : 1 : 1 (metal : ligand : graphene oxide), (b) 1 : 1 : 2, (c) 1 : 1 : 3 mole ratios, (d) (c) by irradiation with a UV lamp. (B) SEM image of metal–organic framework/ azobenzoic acid-functionalized graphene oxide composite hydrogels formed by a 1 : 1 : 3 (metal : ligand : graphene oxide) mole ratio. (C) UV-vis spectra of (a) metal–organic framework/azobenzoic acid-functionalized graphene oxide composite hydrogel MG7 (1 : 1 : 3 mole ratio), (b) reduced graphene oxide, (c) azobenzoic acid attached onto the graphene oxide, and (d) ligand L8 obtained

from (a) with curve fitting. (D) Fluorescence spectrum of metal–organic framework/azobenzoic acid-functionalized graphene oxide composite hydrogel (1 : 1 : 3 mole ratio) [reproduced with permission from the Wiley Verlag GmbH & Co (ref. 1.34)]

This system shows a potential to be utilized as chemosensor for explosives as DNT or TNT vapors. MOF/A-GO flims were made upon drop casting from water, and the films showed 70% fluorescence quenching after one minute upon exposure to saturated TNT vapour. Fluorescence intensity gets quenched by 98% upon exposure of 10 mins. This phenomenon can be attributed to the charge-transfer interactions occurring between the electron-deficient aromatic ring of TNT and the electron-rich aromatic group of L8 in MOF/ A-GO. The similar experiment has also been tried for DNT but sensing efficiency has been found to be less as in case of TNT probably due to poorer electron withdrawing nature of DNT than TNT.

1.1.3.8. Metallogels as hosts for synthesis of nanoparticles.

Steed and co-workers have recently developed an interesting strategy of making ligands for metallogels by varying the inner section of the ligand and while retaining aminopyridine

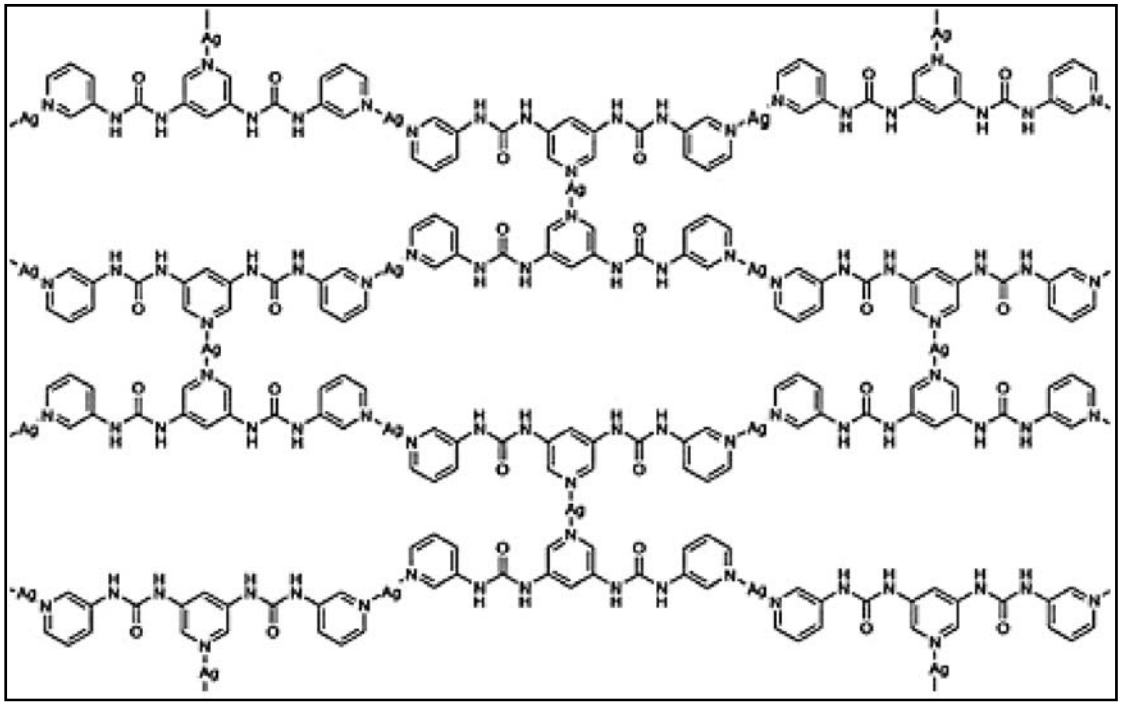

Figure 1.15. Proposed binding in a 2-dimensional sheet of the primary structure of gel fibres of L9 [reproduced with permission from the Royal Society of Chemistry (ref. 1.37)]

ends for metal coordination. Gels with varying morphologies and physical properties can

be obtained by tuning the ligand structure. Presence of both Ag+ and Cu^{2+} ions triggers the self-assembly of the ligands towards gelation, MG8 and MG9 respectively, whereas the free ligand doesn't form any gel. Recently, a series of metallogels have been prepared using pyridine coupled (diaminopyridine) bisurea products L9 in comparison to L10 (diamino benzene) analogous. It has been seen that L9-based building blocks easily produced 3D assemblies through coordination induced cross-linking (Figure 1.15) whereas, L10 assembles lacking the three dimensional structure and entanglements, which results in very weak gel structures on assembly. Bisurea derivatives form co-ordination polymeric

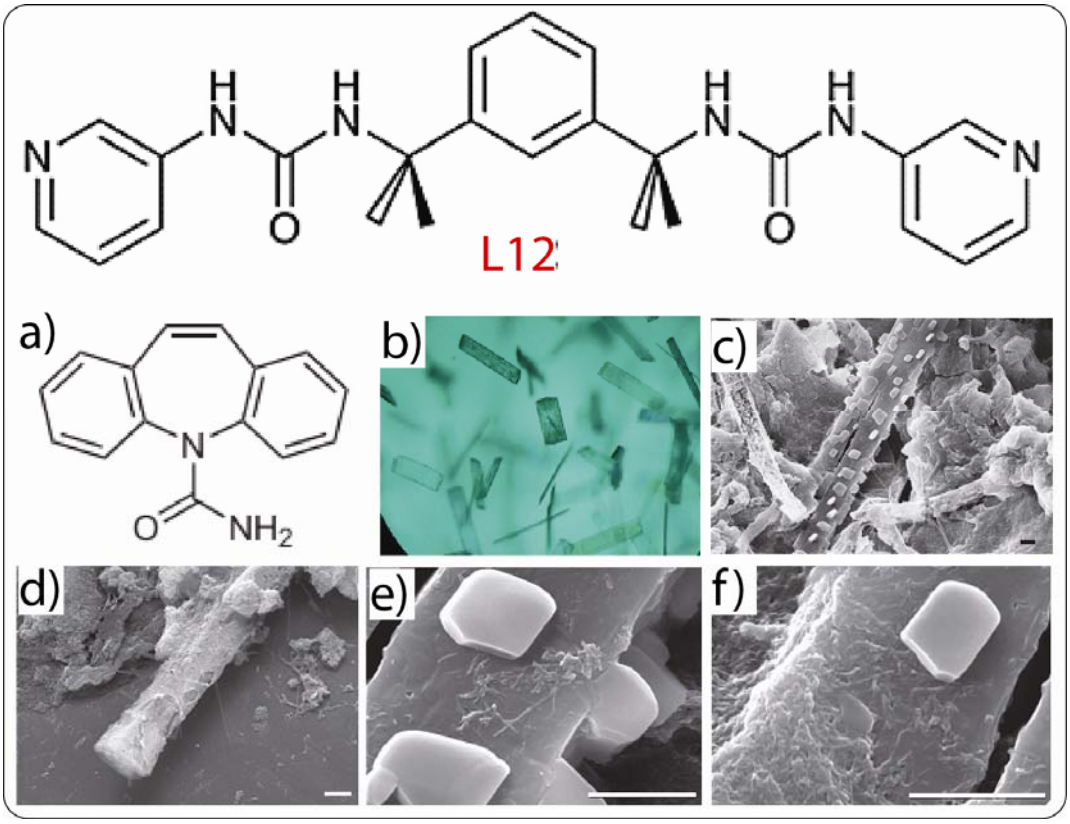

Figure 1.16. *(top)* ligand L12 which forms metallogel MG10 which acts as crystal growth matrix; a) chemical strcture of carbamazepine; b) right optical microscopy images of the carbamazepine crystals suspended in the gel matrix; c)-f) SEM images of carbamazepine crystals evolved from gel matrix. [reproduced with permission from the Nature publishing group (ref. 1.35)].

structures by complexing with silver ions to yield metallogels. The Ag+ suffers a slow reduction by the urea moiety to silver nanoparticles. This reducing ability of urea has been found to be enhanced in presence of UV irradiation (365 nm). It has also been noticed that mechanical stability of the gel increases in presence of these silver

nanopartcicles which reflects in rheological studies.

It has been reported that the preparation of silver nanoparticles by using a metallogel which have a tetrazole-based ligand L11 containing Ag^{+} ions which is catalytically active for

templating. It has been seen that the metallogels with high concentrations of the silver salt, including samples containing 3 and 4 equivalents of $AgClO_4$, showed large nanoparticles having a size distribution ranging from 1.5 to 3.5 nm. Reduction of 4-nitrophenol (4-NP) by sodium borohydride ($NaBH_4$) was presented as a model reaction in presence of Ag NP loaded gel. The reduction reaction was confirmed by disappearance of the 400 nm peak with the concomitant evolution of a new peak at 300 nm, was then attributed to 4-aminophenol (4-AP), after the catalysis.These results along with other characterization confirmed that the reaction gets catalysed due to the presence of Ag NPs distributed in the gelator matrix.

1.1.3.9. Metallogel mediated crystal growth.

Crystallization of polymorphs has a great deal of significance in pharmaceutical industry. Controlling crystal growth is of paramount importance as the in vivo dissolution rates of different crystal polymorphs vary. In recent past, Steed and co-workers have reported a pyridine bisurea ligand L12 capable of gelling methanolic solutions of Cu^{2+} halides (Figure 1.16) (1.35). Growth of the mood-stabilizing anticonvulsant carbamazepine was studied in the (Cu^{2+}-L12) metallogel (MG10) and was related to the concentration of copper halide added during the formation of the gel. Crystals of carbamazepine grows in the metallogel utilizing its stagnant crystallization-favourable matrix. It has been found that, in certain cases these metallogels was found to promote crystallization where a corresponding solution failed to do so. Formation of drug/co-crystals has not been observed which indicates effective phase separation of both of the species during reaction.

1.1.3.10. Metallogels for drug storage and delivery.

Low-molecular weight gels are emerging as a logical alternative to current polymeric gels for controlled drug-delivery. Many hydrogels made up of low molecular weight amphiphiles have been widely exploited as intelligent carriers of drug in controlled drug-delivery systems (1.84). The nature of self-assembly process plays an important role

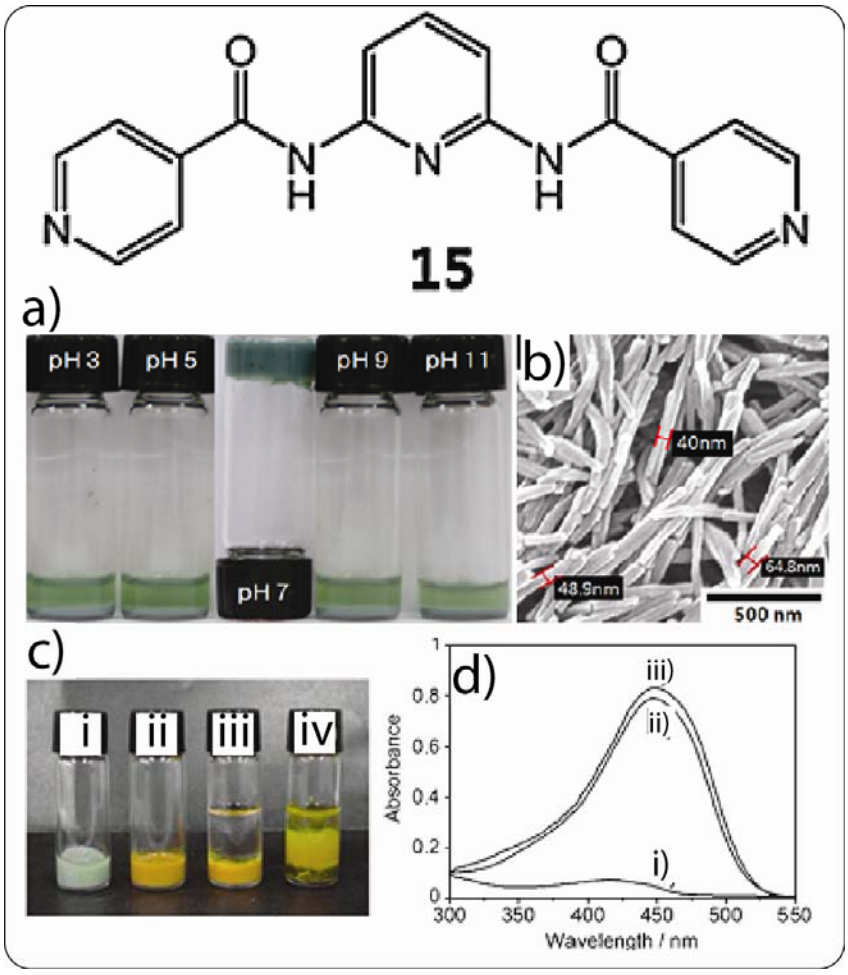

Figure 1.17. *(top)* ligand L12 which forms metallogel MG11 which acts as hosts for curcumin; *(bottom)* a) Photograph of MG11 (20 mM) in the presence of Cu^{2+} (3 equiv.) at different pH values; b) SEM image of gel MG11(20 mM) with Cu^{2+} (3 equiv.); c) Photograph of (i) hydrogel MG11 (20 mM) with Cu^{2+} (3 equiv.), (ii) hydrogel MG11 with Cu^{2+}+ curcumin (5×10^{-3}M),after (iii) 10 min and (iv) 80 min; d) UV-vis spectra of hydrogel MG11 with Cu^{2+}+ curcumin + aqueous solution (pH= 5) after (i) 10min and (ii) 80 min and (iii) curcumin solution (5×10^{-3}M). [reproduced with permission from the Royal Society of Chemistry (ref. 1.40)].

during the process of gelation in a supramolecular hydrogel. Hence, triggering the self-assembly or disassembly becomes very imporatant which is normally achieved by chemical or physical stimuli (e.g., pH, temperature, ionic strength and ultrasonic agitation). Some self-assembled molecular gels have been successfully demonstrated for delivery of regenerative medicine by several groups (1.84 and 1.85).

Recently, a pyridine-based Cu^{2+} coordination polymer hydrogel has been reported as an efficient drug delivery system. This hydrogel MG11 is pH sensitive and degrades to precipitate upon upon treatment with acid or base. However, the gel dissolved upon

acidic treatment can be restored back upon addition of suitable amount of base. The ligand L27 could also be gelated with a variety of copper salts having anions such as SO_4^{2-} , NO_3^- and Cl^- . The Cu^{2+} metallogel MG12 clearly displayed a fibrillar network. Structure of MG12 was determined by density functional theory (DFT) calculations. The optimized structure of the complex exhibited a couple of water molecules and four ligands coordinated to each Cu^{2+} ion with a probable octahedral geometry having the trans positions filled up by two water molecules.

The same group also demonstrated pH-triggered delivery of drug, curcumin, using a Cu^{2+} metallohydrogel. Curcumin was first stably entrapped in the Cu^{2+} metallogel MG12 (Figure 1.17) which is presumed to occur *via* hydrophobic or hydrogen-bond interactions. In order to monitor the degradation of the gel and the subsequent release of the drug, 1.0 ml of an aqueous solution of pH = 5 was added to the preformed gel and the system was kept at 37 °C for 80 min. At first, the added solution was colorless (Figure 1.17), which, after 80 min, solubilized the gel yellow colouration of the top solution indicated that encapsulated curcumin had been released into the solution at pH = 5 which was confirmed by the UV-Vis studies.

CHAPTER 2

Proton-conducting Metallogel from Lowest-molecular Weight assembler Ligand

2.1 Introduction:

Amongst various disciplines of supramolecular chemistry, low molecular weight gelators (supramolecular gels) have been considered to be one of the most interesting soft and smart materials due to their ability to construct polymeric structures from small molecules via non-covalent interactions. Despite the uprise of organic molecule-based gelators in the past two decades, it was only the past decade which has also seen an increasing interest in the investigation of metal complexes as supramolecular metallogelators in which at least one metallic element is incorporated into the viscoelastic (soft) gel matrix by some means. In general, this can be achieved by either physical entrapment of non-coordinating metallic elements usually during the gelation phenomenon or by utilizing unique metal-ligand interactions as the major driving force for the formation of the gel network. The discovery of new functional metallogels during the last two decades has been accompanied by a decisive development in the field of metal-organic frameworks (MOFs). In this sense, the gelling agent in metallogels are often discrete metal coordination complexes of low molecular weight (LMW) ligands or well-defined coordination polymers, which enable the formation of extended coordination networks that can immobilize large volumes of solvent by different mechanisms.The reason behind the growth of interest stems from the availability and the diversity of metal–ligand coordination that could readily influence the self-assembly process of the gel formation and thereby influences the gel properties. Early examples include alkali metal ion-responsive organogelators reported by Shinkai and co-workers (2.1, 2.2) and tris-bipyridine tripodal organogels disrupted upon addition of Fe^{2+} reported by Fages and co-workers (2.3). Also, the utilization of transition metal complexes as metallogelators has been found to exhibit interesting properties, such as optical, catalytic, and magnetic properties (2.4). An interesting fact regarding the metallogels is the organic part generally contains an aromatic ring or long alkyl chain irrespective of the metal ion present in the system. However, in a quest to find the smallest organic ligand for

metallogels, we realized that oxalic acid (MW = 90) is the smallest organic molecule which can form metallogel in presence of any metal ion (2.5) It is noteworthy that, N, N'-dimethythiourea is the smallest organic molecule which alone can gelate any solvent (CCl_4, silicone oil etc.) (2.6). Oxalic acid, has been found to gelate solvents like DMF, DEF, NMP in presence of Cu(II) acetate hydrate (CuA-Ox gel) and Cu(II) perchlorate hexahydrate (CuP-Ox) gel. Both the gels are mechanically stable and CuA-Ox gel exhibits self-standing nature.

As it is well-known that gel phase is a metastable phase, they often gets converted to thermodynamically more stable crystalline phase. CuA-Ox gels converts to a non-aquo polymorph of Cu(II) oxalate (Cu-Ox1) at 90 °C. CuP-Ox degrades to the same polymorph (Cu-Ox1) upon standing at room temperature for two months.

Proton-conducting materials are prime important component of fuel cells (2.7). The beneficial aspects of the fuel cell have prompted many researchers to look for materials that can transport protons efficiently, as the facile proton conduction appears to be at the heart of the fuel-cell technology (2.8). Recent fuel cell research focuses on the development of proton conducting materials capable of conduct protons at high temperature (>100 °C) along with high mechanical stability (2.9). Taking advantage of their high thermal stability, a large number of MOMs, especially metal–organic frameworks (MOFs), are being tested as solid electrolytes for HT-PEMFCs (2.10). However, most of these materials show carrier-assisted proton transport, viz., water at low temperature or guests like H_2SO_4, H_3PO_4, and heterocycles loaded into their pores for high temperature conductivity (2.10b, 2.10c) Moreover, being porous in nature, most of the MOF materials doesn't show promise to be utilized in real fuel cell condition as inherent porosity allows fuel cross-over through the membrane. In these circumstances, inherently proton conducting non-porous metal-organic materials will be a good alternative of porous MOFs. Hence, we had thought to test CuA-Ox gel and xerogel as proton conducting material owing to following reason; the gel network is composed of H-bonding between the Cu-Oxalate complexes (DMF is a good H-bond acceptor; $\beta = 0.69$; oxalic acid is a good H-bond donor) which is supposed to favour H-bonding. It is noteworthy that, CuA-Ox metallogel is the very first of its kind to exhibit proton conduction behaviour. As expected, CuA-Ox gel (Cu: Ox = 1.1.79) exhibits proton conductivity of 1.4×10^{-4} Scm^{-1} at ambient temperature under anhydrous conditions. We have also checked the proton conducting ability of the

CuA-Ox xerogel material and it also exhibits proton conductivity of 1.1×10^{-5} Scm^{-1} at 46 °C under anhydrous conditions. The drop in conductivity in the case of xerogel can be attributed by the absence of DMF and water molecules which assisted proton conductivity in case of wet CuA-Ox gel.

2.2 Results and discussion:

2.2.1 Synthesis of proton-conducting metallogel:

Contrary to conventional heating-cooling protocols, the gelation phenomenon that we describe here takes place efficiently at room temperature (RT). A transient colloidal suspension forms immediately upon mixing the stock solutions of the two components, which begin to evolve towards a gel phase within seconds. The use of $Cu(ClO_4)_2 \cdot 6H_2O$ afforded complete and homogeneous gelation (namely, CuP-Ox gel) within seconds without additional stirring, whereas in the case of $Cu(OAc)_2 \cdot H_2O$ complete gelation (namely, CuA-Ox gel) was achieved within 6 h after 10 min sonication. The gel nature and mechanical robustness of the so obtained materials was first confirmed by the absence of flow upon inversion of the test tube, (Figure 2.1) and subsequently by oscillatory rheological characterization (*vide infra*). The CuA-Ox gel is self-standing in nature for instance, high-scale synthesis as well as molding and cutting some bulk materials into a desired shape without major losses of fluid (Figure 1).

2.2.2 Gelation ability:

Formation of CuA-Ox gel has been found to be dependent on the metal salt and the ligand. Hydration water molecules of the components were found unnecessary for the gelation phenomenon. Thus, gelation ability and gelation time remains the same for the bicomponent systems [$Cu(OAc)_2 \cdot H_2O$ + oxalic acid dihydrate] and [$Cu(OAc)_2$ anhydrous + oxalic acid anhydrous]. However, the use of hydrated Cu(II) salts such as $Cu(OAc)_2 \cdot H_2O$ allowed the preparation of more concentrated stock solutions than those using the anhydrous salts. This could be used for instance to accelerate remarkably the gelation kinetics (ca. 16-fold) while affording metallogels with comparable mechanical stabilities. The gelation ability of the gelator system (i.e., Cu(II) salt + oxalic acid) was evaluated in different solvents. The results showed that stable metallogels could be prepared in polar aprotic solvents such as DMF, DEF, DMAC and NMP, whereas partial gelation was observed in acetone, THF and CH_3CN (Table 1). In terms of Kamlet-Taft parameters, all these solvents are characterized by virtually null H-bond donor ability (i.e., $\alpha \sim 0–0.2$), medium H-bond acceptor ability

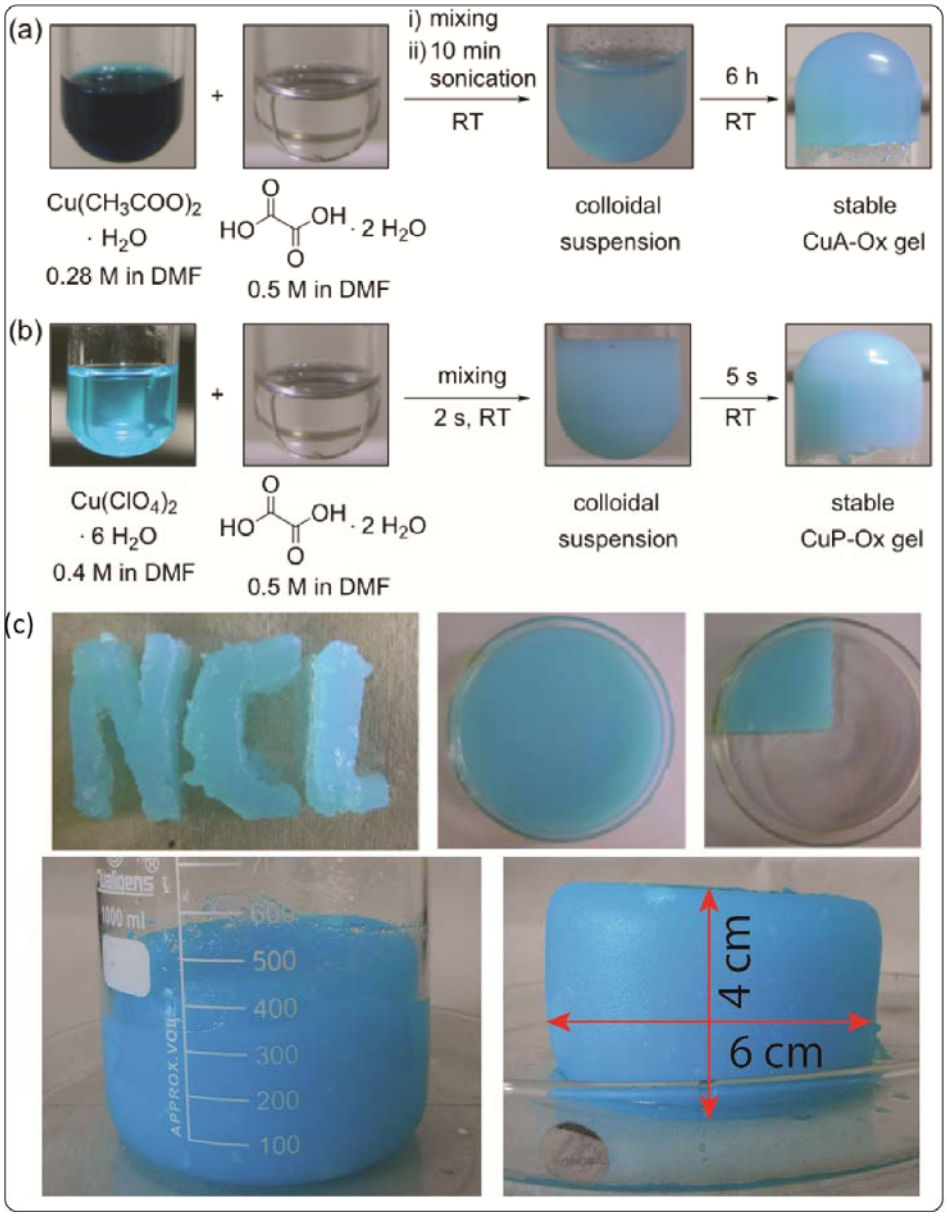

Figure 2.1 Synthesis of (a) CuA-Ox gel and (b) CuP-Ox gel upon mixing stock solutions of the corresponding Cu(II) salt and oxalic acid in DMF at optimized concentrations. A transient light-blue colloidal solution precedes in each case the formation of the stable and homogeneous metallogels.(c) CuA-Ox gel synthesized at high scale (ca. 500 g weight); (b) the same gel showing its characteristic self-standing nature. [Reprinted with permission from (2.5). Copyright 2013 WILEY-VCH Verlag GmbH & Co. KGaA]

(i.e., $\beta \sim 0.4–0.7$) and medium/high polarizabilities (i.e., $\pi^* \sim 0.6–0.9$). The

Table 2.1. Gelation ability in various solvents[i] of the bicomponent systems [$Cu(OAc)_2 \cdot H_2O$ or $Cu(ClO_4)_2 \cdot H_2O$ + oxalic acid dihydrate].[a]

Entry	Solvent[b]	Phase[c]	Molar conc.[d]	Gelation time[e]	Gel-phase color[f]	Kamlet-Taft solvent pararmeters		
						α	β	π*
1	H_2O	S	0.2–0.5	–	–	1.17	0.47	1.09
2	DMF	G	0.39	5–6 h	Blue	0.00	0.69	0.88
3	DEF	G	0.32	5–6 h	Blue	[g]	[g]	[g]
4	DMAC	G	0.47	5–6 h	Blue	0.00	0.76	0.88
5	NMP	G	0.54	5–6 h	Blue	[g]	[g]	[g]
6	Acetone	PG	0.2–0.5	< 10 s	Blue	0.08	0.43	0.71
7	THF	PG	0.2–0.5	< 10 s	Blue	0.00	0.55	0.58
8	CH_3CN	PG	0.2–0.5	< 10 s	Blue	0.19	0.40	0.75
9	MeOH	P	0.2–0.5	–	–	0.98	0.66	0.60
10	EtOH	P	0.2–0.5	–	–	0.86	0.75	0.54
11	*i*-PrOH	P	0.2–0.5	–	–	0.76	0.84	0.48
12	*n*-Hexane	I	0.2–0.5	–	–	0.00	0.00	-0.04
13	Et_2O	I	0.2–0.5	–	–	0.00	0.47	0.27
14	EtOAc	I	0.2–0.5	–	–	0.00	0.45	0.55
15	CH_2Cl_2	I	0.2–0.5	–	–	0.13	0.10	0.82
16	$CHCl_3$	I	0.2–0.5	–	–	0.20	0.10	0.58
17	Benzene	I	0.2–0.5	–	–	0.00	0.10	0.59
18	Toluene	I	0.2–0.5	–	–	0.19	0.40	0.75
19	DMF/H_2O	P	0.2–0.5	–	–	[g]	[g]	[g]

[a] Gelation tests were performed as described in the Experimental Section: $Cu(OAc)_2 \cdot H_2O$ or $Cu(ClO_4)_2 \cdot H_2O$ (0.28 mmol) + oxalic acid dihydrate (0.5 mmol), total DMF volume = 2 mL. When sonication was used, the final temperature of the ultrasonic bath was 27 ± 1 ºC. [b] Solvent abbreviations: DMF = *N*,*N*-dimethylformamide; DEF = *N*,*N*-diethylformamide; DMAC = *N*,*N*-dimethylacetamide; NMP = 1-methyl-2-pyrrolidone; THF = tetrahydrofuran. [c] Abbreviations: S = solution; G = stable gel; PG = partial gel; I = insoluble; P = precipitates. The amount of non-gelled solvent in the cases of partial gels was ca. 15–20% of the total initial volume. [d] Optimized molar concentration (mol/L) of the gelator system (i.e., [metal salt + ligand]) or range of concentrations used forgelation tests. [e] Time required for complete gelation at given concentration. [f] All gels were completely opaque indicating the formation of aggregates smaller than the visible wavelength range. [g] Unknown value.

simultaneous coexistence of these parameters defines optimal liquid phases to achieve stable gels, thus excluding polar protic (high α), non-polar (low β and/or π*), or other polar aprotic solvents with low β values (e.g., CH_2Cl_2, EtOAc). Such correlations have been confirmed experimentally (Table 2.1), providing critical information to rationalize plausible gelation mechanisms. A series of experiments were also carried

Table 2.2. Representative influence of the metal counteranion on the gelation ability of the bicomponent system.[a]

Entry	Metal salt	[Metal salt][b]	[Ligand][c]	Vol. DMF[d]	Phase[e]	Picture
1	$Cu(OAc)_2 \cdot H_2O$	0.14 M	0.25 M	1 mL	G (blue opaque)	
2	$Cu(ClO_4)_2 \cdot 6H_2O$	0.2 M	0.25 M	1 mL	G (blue opaque)	
3	$CuSO_4$	0.2 M	0.5 M	1 mL	P (blue opaque)	
4	$CuCl_2$	0.2 M	0.5 M	1 mL	S (yellow turbid)	
5	$Cu(NO_3)_2 \cdot xH_2O$	0.2 M	0.5 M	1 mL	WG[f] (blue opaque)	

[a] Gelation tests were performed as described in the Experimental Section.[b] Molar concentration of metal salt (mol/L). [c] Molar concentration of oxalic acid ligand (mol/L).[d] Total volume of solvent. [e] Abbreviations: G = stable gel; P = precipitates; S = solution; WG = weak gel. Aspect of the phase is indicated in brackets for each case. [f] Amorphous precipitates obtained within 12 h at RT.

out in order to confirm the influence of both the metal ion and the counteranion on the gelation process as it has been observed with other metallogels (Table 2.2 and 2.3). According to the hard-soft acid-base (HSAB) theory, oxalate (a medium field ligand, stronger than acetate and halides but weaker than water) interacts preferably with hard-to-borderline metal ions such as Cu^{2+}. Indeed, the use of either soft (e.g., Ag^{+}, Cd^{2+}) or hard metal ions (e.g., Fe^{3+}, Ca^{2+}, Cr^{3+}, Mn^{2+}) with hard counteranions (e.g., SO_4^{2-}, Cl^{-}, NO_3^{-}, OH^{-}) prevented the formation of steady gels upon reaction with oxalic acid in DMF or other solvent systems. However, other borderline metal ions such as Co^{2+}, Zn^{2+} or Ni^{2+} resulted also inefficient in terms of gelation.

Table 2.3. Gelation tests using urea and *N*,*N*-dimethylurea as alternative ligands.[a]

Entry	Ligand	[Ligand][b]	Metal salt	[Metal salt][e]	Vol.[f]	Result[g]	Pic[h]
1	Urea	0.5 M	$Cu(OAc)_2 \cdot H_2O$	0.28 M	200 μL	C	(a)
2	*N*,*N*-Dimethylurea	0.5 M	$Cu(OAc)_2 \cdot H_2O$	0.28 M	200 μL	S	(b)
3	*N*,*N*-Dimethylurea	Saturated	$Cu(OAc)_2 \cdot H_2O$	0.28 M	200 μL	C	(c)
4	Urea	0.5 M	$Cu(ClO_4)_2 \cdot 6H_2O$	0.4 M	200 μL	S	–
5	*N*,*N*-Dimethylurea	0.5 M	$Cu(ClO_4)_2 \cdot 6H_2O$	0.4 M	200 μL	S	–
6	*N*,*N*-Dimethylurea	Saturated	$Cu(ClO_4)_2 \cdot 6H_2O$	0.4 M	200 μL	S	–
7	*N*,*N*-Dimethylurea	0.57 M[c]	–	–	200 μL	WG	(d)
8	*N*,*N*-Dimethylurea	0.57 M[d]	–	–	200 μL	GP	(e)

[a] Solvent used for the preparation of stock solutions (entries 1□9) = DMF. [b] Concentration of ligand (stock solution). [c] Control experiment: Solvent = CCl_4.[Error! Bookmark not defined.] [d] Control experiment: Solvent = silicone oil.[Error! Bookmark not defined.] [e] Concentration of metal salt (stock solution). [f] Volume used of each stock solution (i.e., total volume = 400 μL). [g] Abbreviations: S = solution without any visible change over time; C = crystallization within few hours (remaining solution was colorless); WG = weak gel (upon "heating-cooling" cycle); GP = gelatinous precipitates (upon "heating-cooling" cycle). [h] Digital pictures of the vials:

Moreover, the exchange of oxalic acid by other potential coordinating assemblers such as pyruvic acid, succinic acid, benzene 1,4-dicarboxylic acid, isonicotinic acid,

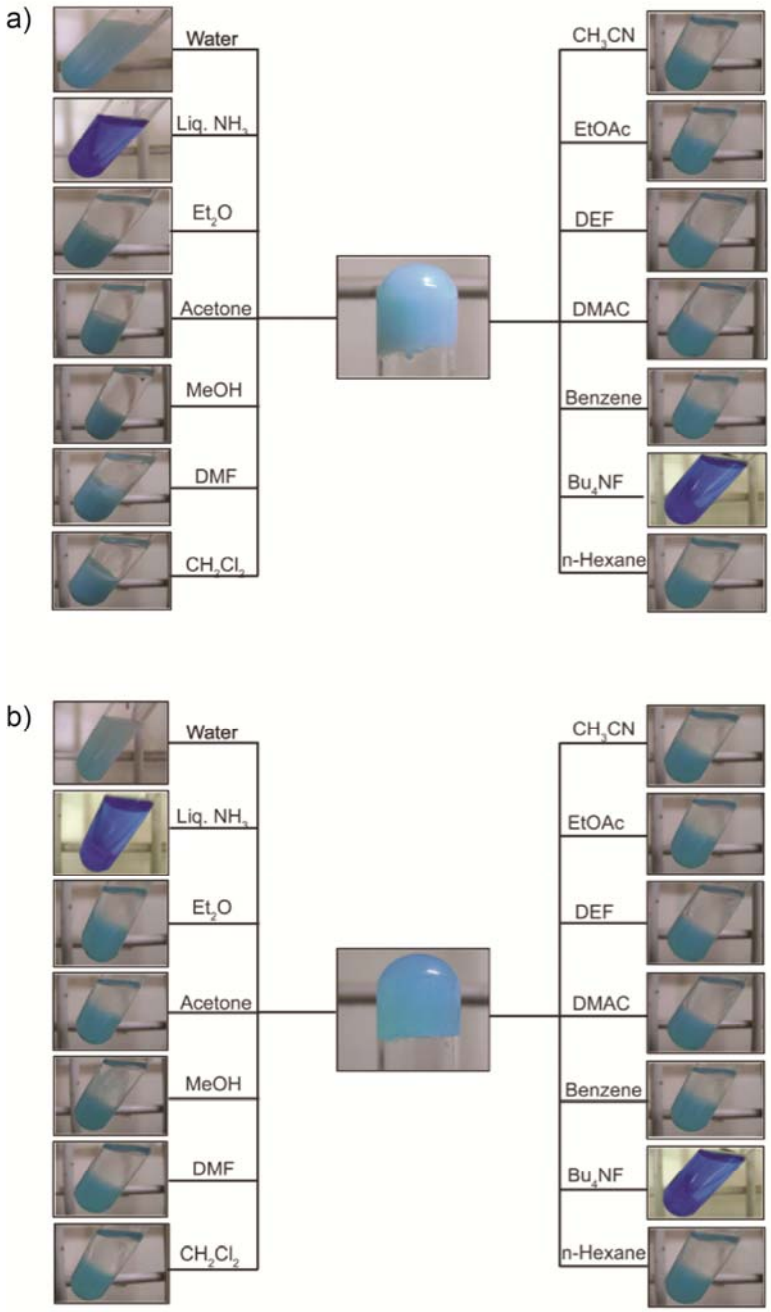

Figure 2.2. Metallogels (i.e., (a) CuP-Ox gel, (b) CuA-Ox gel) made in DMF remained stable in the presence of additional solvents and upon shaking for 5 h at 70 rpm. ICP measurements revealed no leaching of metal ions to the new organic phase. Gradual precipitation of the gels was found in the presence of water, and complete dissolution in the presence of liquor ammonia and tetrabutylammonium fluoride. [Reprinted with permission from (2.5). Copyright 2013 WILEY-VCH Verlag GmbH & Co. KGaA]

urea, 1,3-dimethylurea, or 1,3-diaminourea, did not yield any steady gel (Table 2.3). Consequently, oxalic acid represents the smallest ligand (M_w = 90.03 g mol^{-1}) capable

of forming stable supramolecular metallogel networks through specific interactions.

2.2.3 Response towards chemical stimuli:

In terms of stability, both CuA-Ox and CuP-Ox bulk gels remains visually intact either under vigorous sonication or in the presence of additional organic solvents including polar protic, polar aprotic and non-polar solvents (Figure 2.2). Only addition of water or liquor ammonia caused precipitation or dissolution of the gels, respectively. Disruption of gels in presence of water can be attributed to the hydrolysis of the gelator (Cu-oxalate complex) as it consisted of a borderline acid and hard base. In presence of ammonia, the gels form soluble Cu(II) tetramine complex. Similar to some other metallogels, a chemical response to fluoride anions was also observed leading to gradual dissolution of the gels (Figure 2.2).

2.2.4 Thermal Stability:

Regarding thermal stability, thermogravimetric analysis (TGA) of the samples showed clear degradation of the materials in two major stages. The first weight loss (ca. 4%) occurs in the region below 120 ºC, which was attributed to solvent evaporation in good agreement with the estimated value. A further weight loss was observed at ca. 300 ºC, which was ascribed to degradation of the coordination polymer by comparison to the TGA curves of the xerogels obtained by freeze-drying the corresponding gels (Figure 2.3).

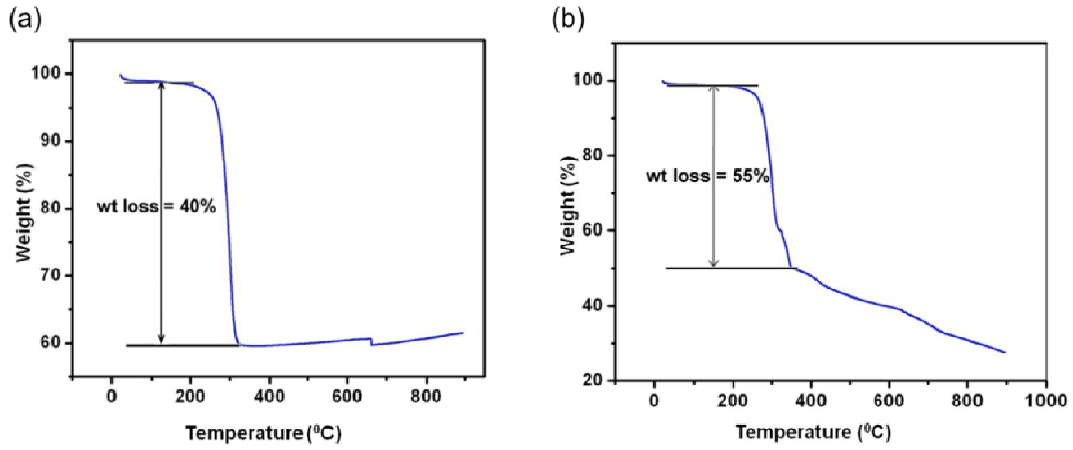

Figure 2.3. TGA traces of (a) CuA-Ox and (b) CuP-Ox xerogels showing stability of the structures up to 300 ºC. Collapse of the networks was evident above this temperature. The final decomposition product is likely CuO. Initial weight loss in the case of CuP-Ox was attributed to residual solvent molecules in this material.

2.2.5 Morphological study and porous nature:

In order to obtain insights about the microstructure of the metallogels, we took transmission electron microscopy (TEM) and scanning electron microscopy (SEM) images (Figure 2.4). The interwined nanofibrilar morphology of the corresponding xerogels was evident in the TEM photographs (Figure 2.4). In general, most of the fibers presented uniform widths in the range of 20–45 nm and lengths on the micron scale. In particular, CuA-Ox gels are found to be extraordinarily stable over time at a macroscopic level when stored at RT (i.e., no visual degradation of the CuA-Ox gel was observed after more than 1 year). Microscopically, only in the case of CuP-Ox gel a supramolecular living process can be observed by an increment of the degree of

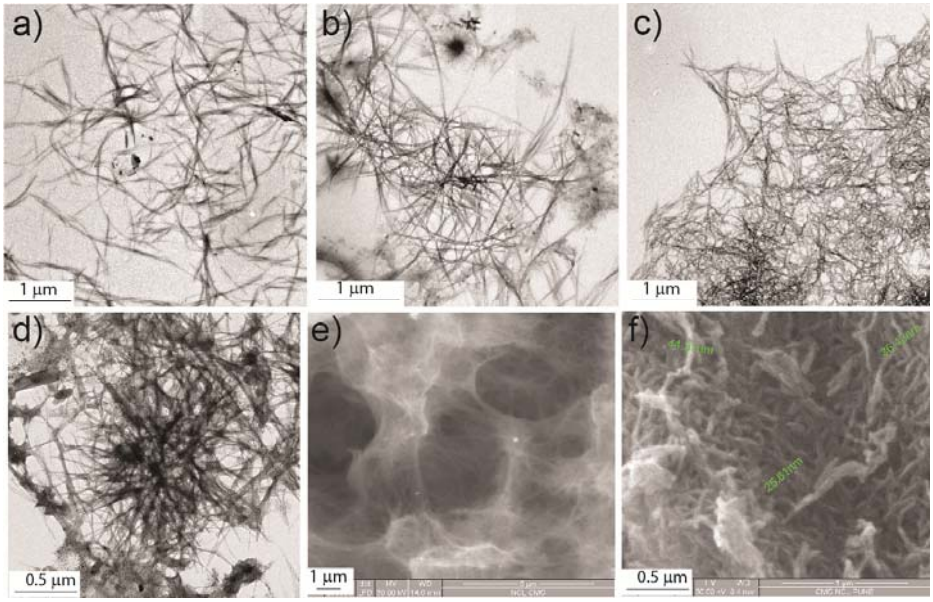

Figure 2.4. TEM images of (a) freshly prepared CuP-Ox gel (10 min old); (b) CuP-Ox gel aged for 1 month; (c) CuP-Ox gel aged for 2 months (showing increase in crosslinking density upon aging); (d) freshly prepared CuA-Ox gel. SEM images of (e) CuP-OX xerogel and (f) CuA-Ox xerogel.

fiber entanglement upon aging.

On the other hand, a complementary high aspect ratio fibrilar morphology can also be observed in the SEM micrographs (Figure 2.4e and 2.4f). However, in contrast to CuA-Ox, CuP-Ox xerogel shows a permanent porosity that can further be confirmed by BET surface area analysis. In agreement, Atomic force microscopy (AFM; Figure 2.5) micrographs also reveals the aggregation of individual fibers forming fibrilar bunches with average heights in the range of ca. 20–160 nm and apparent diameters of ca. 80–250 nm (Figure 2.5).

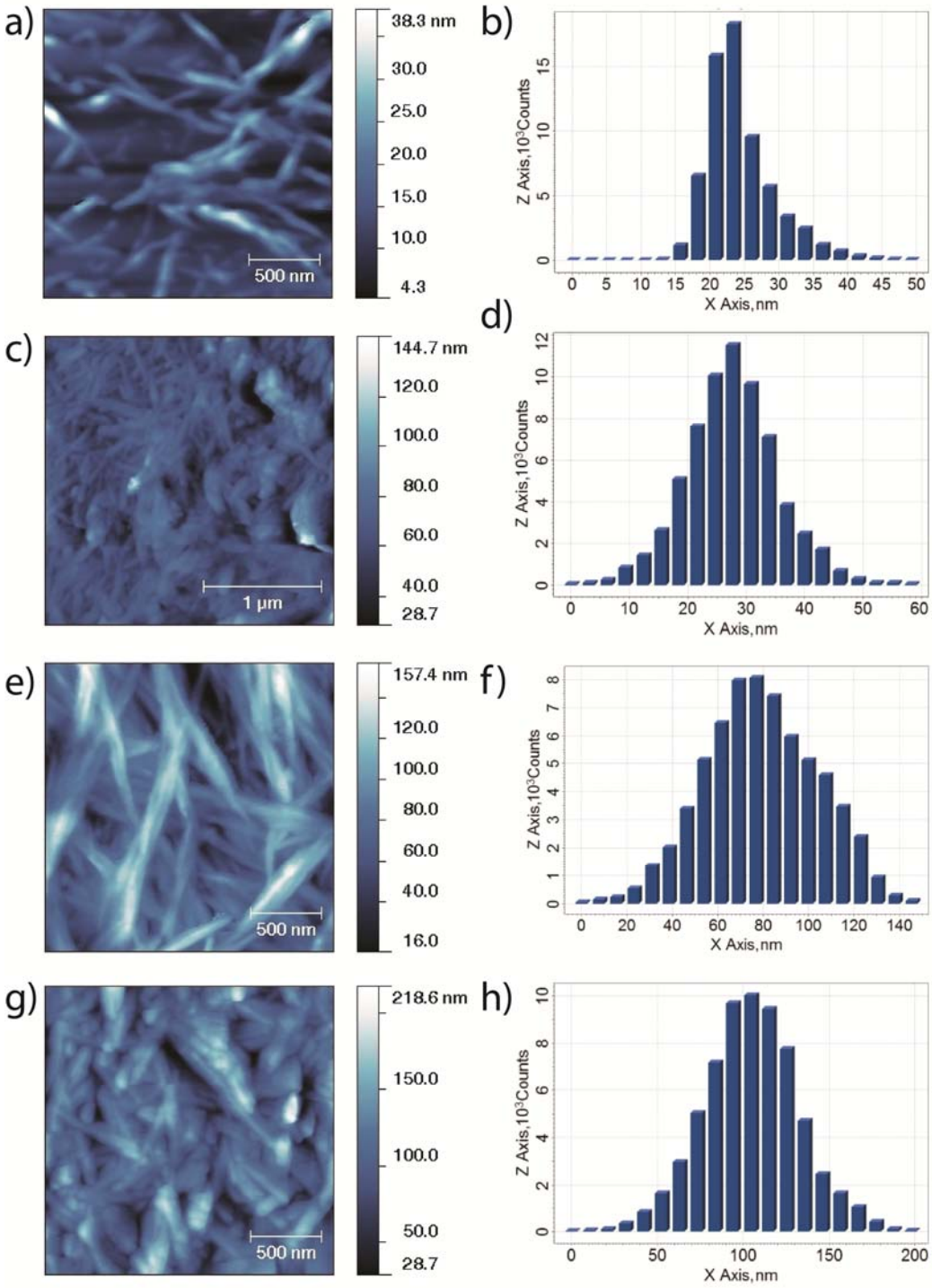

Figure 2.5. AFM images from different zones of the sample and settings: a-b) CuA-Ox gel; c-d) CuA-Ox xerogel; e-f) CuP-Ox gel; g-h) CuP-Ox xerogel.

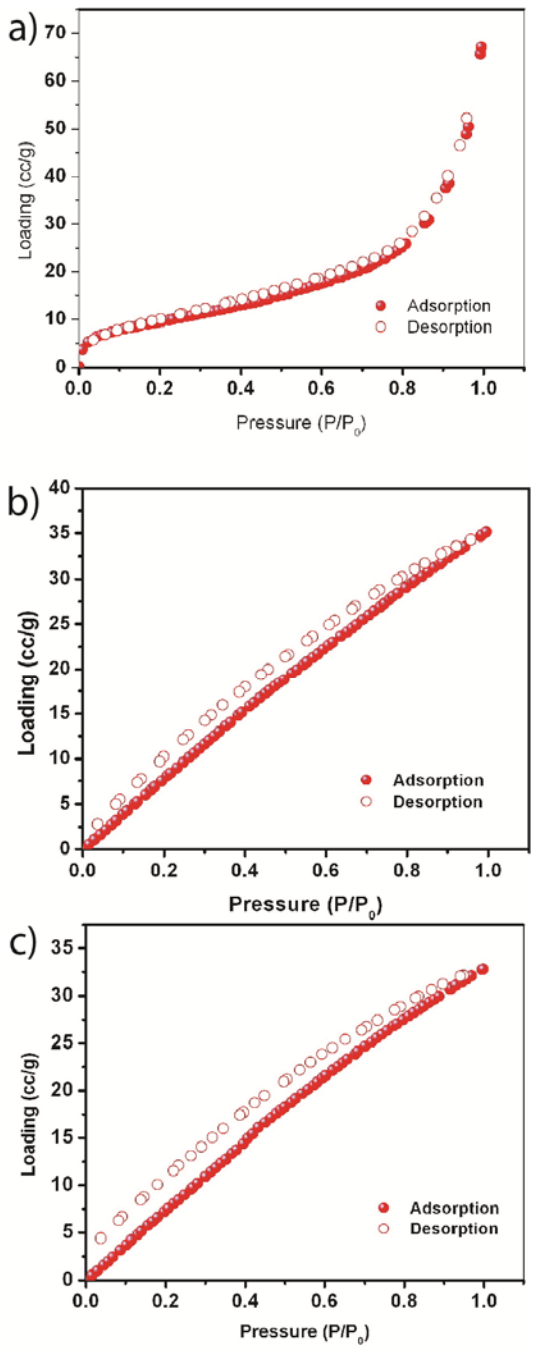

Figure 2.6. Gas adsorption properties: (a) N_2 adsorption isotherms of CuP-Ox xerogel recorded at -196 °C and below 1 atm (surface area = 35.437 m^2 g^{-1}; pore size = 4.31 nm);(b) CO_2adsorption behavior CuP-Ox xerogel at 273 K and 1 atm; (c) CO_2 adsorption behavior CuP-Ox xerogel at 25 °C and 1 atm. Filled and open circles represent adsorption and desorption data, respectively.

In agreement with SEM images, CuA-Ox xerogel appears to be practically non-porous to N_2 (uptake 20 cc/g), whereas CuP-Ox xerogel shows type-I N_2 adsorption and CO_2 uptake of 33 cc g^{-1} at RT and 1 atm through a surface area of 67 m^2 g^{-1}

(Figure 2.6).

2.2.6 Crystalline nature of the gels:

In order to explore the exact nature of the coordination complex, presumably formed *in situ* upon mixing the two stock solutions (i.e., metal salt and ligand), powder X-ray diffraction (PXRD) patterns of the gels (i.e., CuA-Ox and CuP-Ox gels) and the corresponding xerogels have been compared to that of the commercially available Cu(II) oxalate hemihydrate (Figure 2.7). As expected, PXRD of the bulk gels differs from that of the xerogels due to substantial scattering of the X-ray beam by the large amount of solvent trapped in the interstices of the gel network (Figure 2.7a and 2.7b). However, PXRD patterns of the xerogels was found to be some extent similar with the pattern of the commercially available Cu(II) oxalate hemihydrate, although this was unable to induce gelation by its own. On the other hand, the crystalline nature of CuP-Ox gel decreased in comparison to its xerogel, whereas the poorly crystalline CuA-Ox gel becomes crystalline upon freeze-drying. Furthermore, the increment of the entanglement of CuP-Ox gel observed by TEM was parallel to a gradual increment of the crystallinity of the material upon aging. This could be confirmed by the evolution of the PXRD pattern in function of the aging time. Such slow evolution from a poorly crystalline metastable gel can be illustrated on the basis of the Ostwald rule of stages, which anticipates the crystallization due to the transition to a more stable phase governed by irreversible thermodynamics.

2.2.7 Mechanical Properties:

The ultimate confirmation of the gel nature of the materials was obtained from the mechanical response in dynamic rheological experiments (Figure 2.8). Thus, both CuA-Ox and CuP-Ox gels exhibits an average storage modulus (G') ca. one order of magnitude higher than the loss modulus (G'') within the linear viscoelastic regime (pulsation (ω) = 1 rad s^{-1}; strain = 0.1%) as determined by dynamic frequency (DFS, range = 0.1–100 rad s^{-1}), strain (DSS, range = 0.1–100%) and time sweep (DTS) experiments. In this regard, the brittle nature of the metallogels was confirmed by their

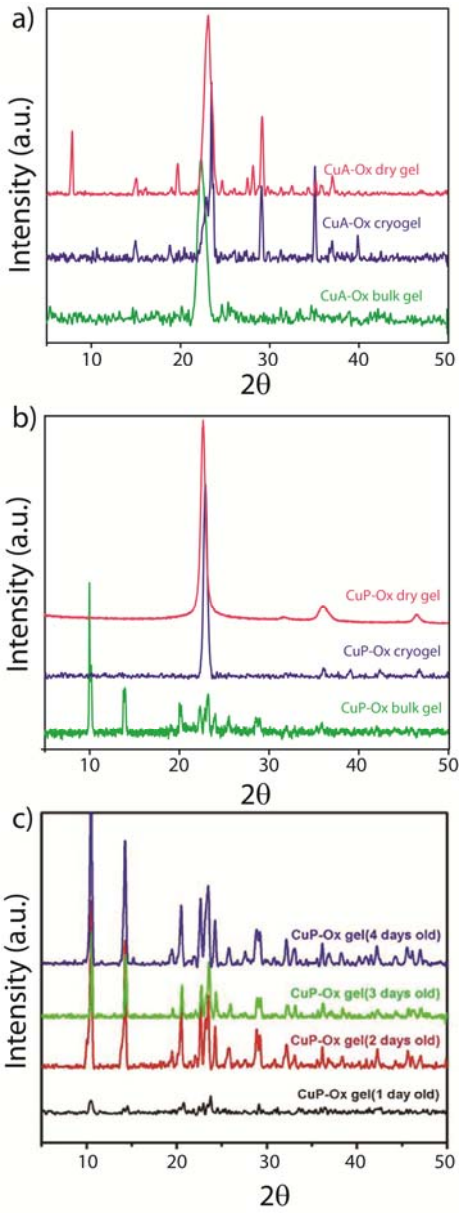

Figure 2.7. Comparative PXRD pattern of (a) CuP-Ox gel, (b) CuA-Ox gel, their corresponding xerogels and Cu(II) oxalate hemihydrate, (c) time dependent PXRD pattern of CuP-Ox showing increase of crystallinity upon aging.

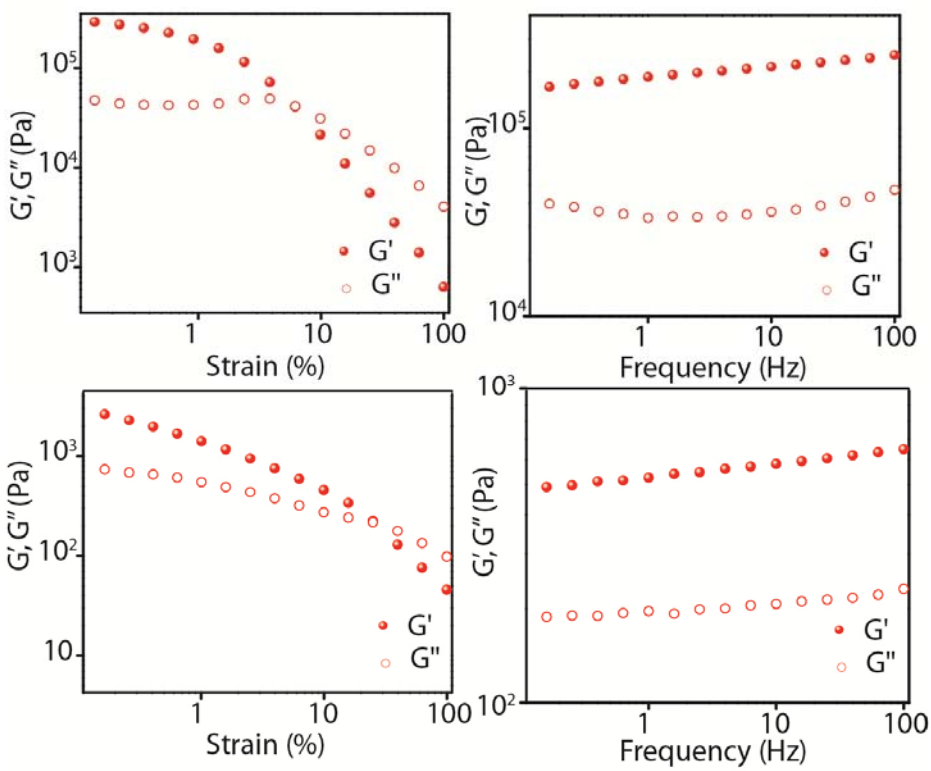

Figure 2.8. a), c) are strain sweep plots for CuA-Ox and CuP-Ox gel and b),d) denotes frequency sweep plot for CuA-Ox and CuP-Ox gel.

fracture at strain (deformation) below 1%. In each case, the storage modulus presents a perceptible albeit low dependence on the frequency (i.e., $G' \sim \omega^{0.047\text{-}0.061}$; tan $\delta \sim$ 0.09–0.13), which is characteristic of viscoelastic fibrillar networks. As expected, a sample of CuP-Ox gel aged for one month showed a 3-fold increment in G' compared to as-synthesized sample (in contrast, G' of CuA-Ox gel remained constant), which corroborates to the increase in the crosslink density observed by TEM. The slow logarithmic growth of G' monitored over time depicts the slow kinetics of the aging process. Interestingly, a self-healing response (at micro-level) of the material to large straining has also been confirmed through a rheological loop test.

2.2.8. Crytalline nanofibres of Cu-oxalate gel and gel to crystal transformation:

Gelation is often known as a hindered crystallization process. As a matter of fact, blue block-shaped crystals of Cu(II) oxalate (Cu-Ox1) spontaneously produced upon aging

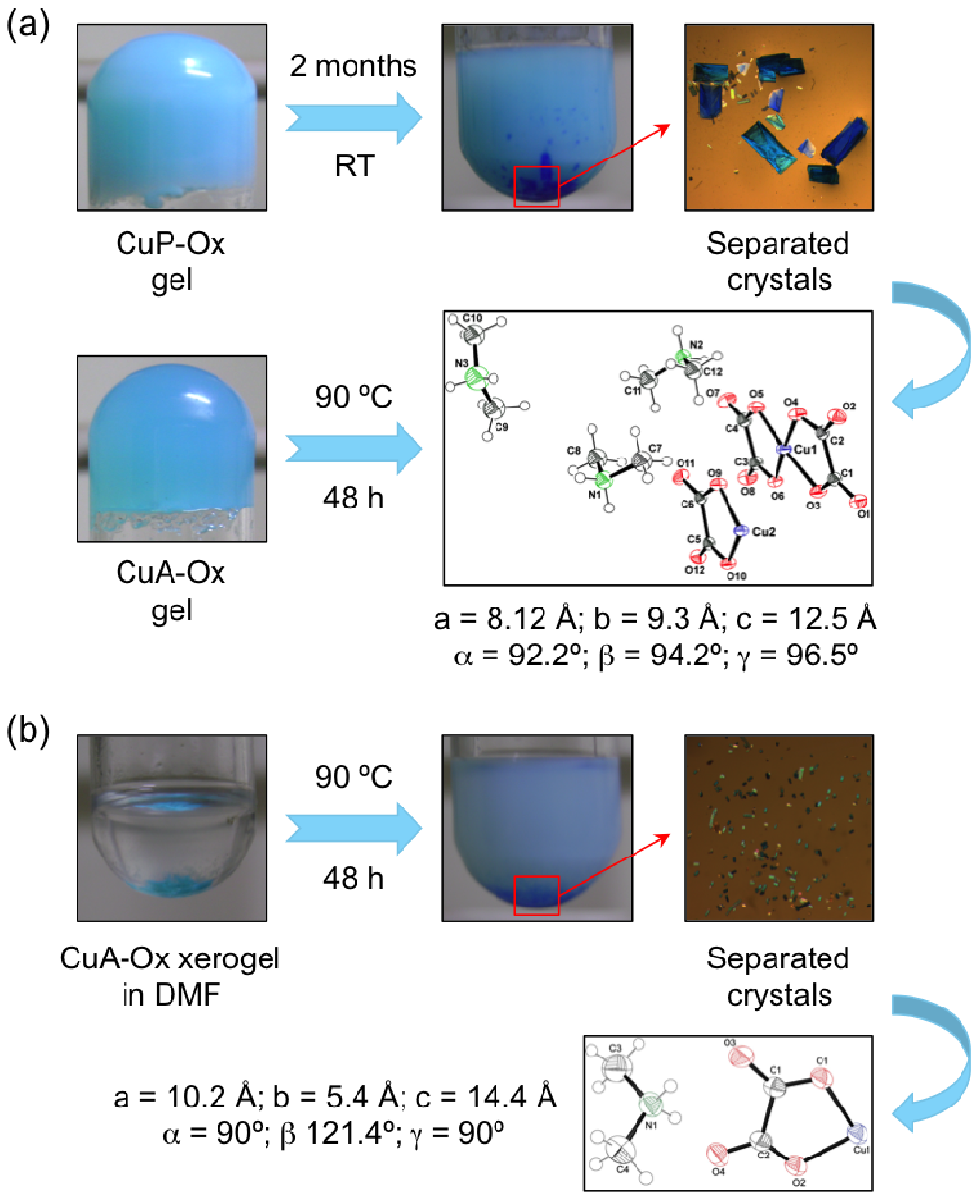

Figure 2.9. Formation of blue block-shaped Cu-Ox polymorphs from (a) CuP-Ox or CuA-Ox gels, (b) CuA-Ox xerogel. [Reprinted with permission from (2.5). Copyright 2013 WILEY-VCH Verlag GmbH & Co. KGaA]

the CuP-Ox gel for two months at RT. The growth of crystals accompanies by a gradual collapse of the gel matrix, indicating the disruption of weak attractive interactions between Cu-Ox particles (Figure 2.8). The existence of such weak forces allows both the observed microscopic self-healing process and the formation of thermodynamically favored Cu-Ox1 through a critical mass effect reached by nucleation.[11] This constitutes an uncommon phenomenon where metallogels generates

to crystalline metal-organic materials via self-destruction in absence of any external stimulus[12] at RT. Similarly, Cu-Ox1 crystals can also be obtained by heating CuA-Ox gel at 90 ºC for 10 h. XRD studies reveals that the asymmetric unit of Cu-Ox1 (space group *C2/c*) comprises of one Cu(II) centre, one oxalate and one dimethylammonium cation. Each metal centre is linked to four oxygen atoms from two oxalate anions in a square planar fashion, whereas the non-coordinated oxygen atoms are H-bonded with dimethylammonium cations. Surprisingly, a structurally different Cu(II) oxalate (Cu-Ox2) phase was obtained by resuspending CuA-Ox xerogel in DMF and heating the mixture at 90 ºC for 48 h (Figure 2.9). Despite the similar PXRD and FTIR patterns of CuA-Ox xerogel and Cu(II) oxalate hemihydrate, this new polymorph Cu-Ox2, cannot be produced from the latter under the above-mentioned conditions. In contrast to Cu-Ox1, the asymmetric unit of Cu-Ox2 (space group *P-1*) contains two metal centers, three oxalate anions and three dimethylammonium cations involved in H-bonding.[13] In this case, the first Cu(II) centre is connected to five oxygen atoms of three oxalate anions in a square-pyramidal fashion, whereas the second metallic centre is connected again to four oxygen atoms from two oxalate anions in a square-planar geometry (Figure 2.9). As far as we know, Cu-Ox1 and Cu-Ox2 represent the only two examples of Cu(II) oxalate non-aquo complexes reported so far. In addition, although the growth of crystals within gel matrix is a well known approach to obtain unique polymorphs in function of the characteristics of the matrices (e.g., solvent, gelator structure) (2.14), the formation of two different polymorphs from a supramolecular gel and its corresponding xerogel is an unprecedented phenomenon.

2.2.9. Proton conductivity:

Precedents of proton-conducting materials based on polymer gels (2.15) and crystalline metal-organic materials (e.g. MOFs; 2.16) motivated us to investigate proton transport in our materials. The prime reasons behind choosing CuA-Ox gel material for proton conductivity are the following; i) DMF (the gelling solvent) is a good H-bond acceptor and ii) oxalic acid is a good H-bond donor, hence the gel network is predominantly formed via H-bonding between the gelator complex. Contrary to most LMW metallogels, the remarkable mechanical and temporal stability of our oxalic acid-based metallogels allowed us to conduct this study accurately at different temperatures. As far as we are aware, proton conductivity (σ) in molecular

gels has not yet been demonstrated.

2.2.9.1 Methods and plots

Proton conductivity was measured in Solartron instrument. CuA-Ox gel was grown inside a hollow Teflon® cylinder having two stainless steel stoppers at both ends, affording a gel column of 13 mm diameter × 5 mm thickness. Xerogel samples of CuA-Ox were pelletized (of 0.6 mm and 1.25 mm thickness, with 6.5 mm diameter) and then subjected to analysis for proton conduction.

The resistances were calculated from the semicircle of the Nyquist plots. The activation energy values were obtained from the slope by least square fitting of the straight line. If the data points are (x_1,y_1), (x_2,y_2), ..., (x_n,y_n) where x is the independent variable and y is the dependent variable. The fitting curve $f(x)$ has the deviation (error) d from each data point, i.e., $d_1 = y_1 - f(x_1)$, $d_2 = y_2 - f(x_2)$,..., $d_n = y_n - f(x_n)$. According to the method of least squares, the best fitting curve has the properties:

$$\Pi = d_1^2 + d_2^2 + \ldots + d_n^2 = \sum_{i=1}^{n} d_i^2 = \sum_{i=1}^{n} [y_i - f(x_i)]^2 = \text{a minimum}$$

N.B. From the semicircle we got the resistance **R** (Ohm). Now, from diameter **r** (mm) and thickness A (mm) proton conductivity (σ) value can be calculated by the following equation,

$$\sigma = A / (R \times \pi r^2) \ \text{Scm}^{-1}$$

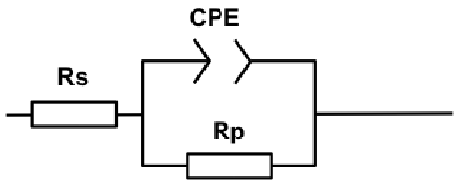

Figure 2.10. Three-component model used for impedance measurements, consisting of a resistor (R_s) connected in series with a circuit formed by a resistor (R_p) and a constant phase element (CPE) in parallel.

For high-temperature proton conductivity measurements, the pellets were inserted within a glass chamber (2.11c and 2.11f), which was encircled with a controlled

heating coil attached with an automated temperature controller. The heat flow within the temperature controller was controlled by a dimerstat accordingly. The temperature of the chamber was measured by an infrared temperature sensor attachment, having a

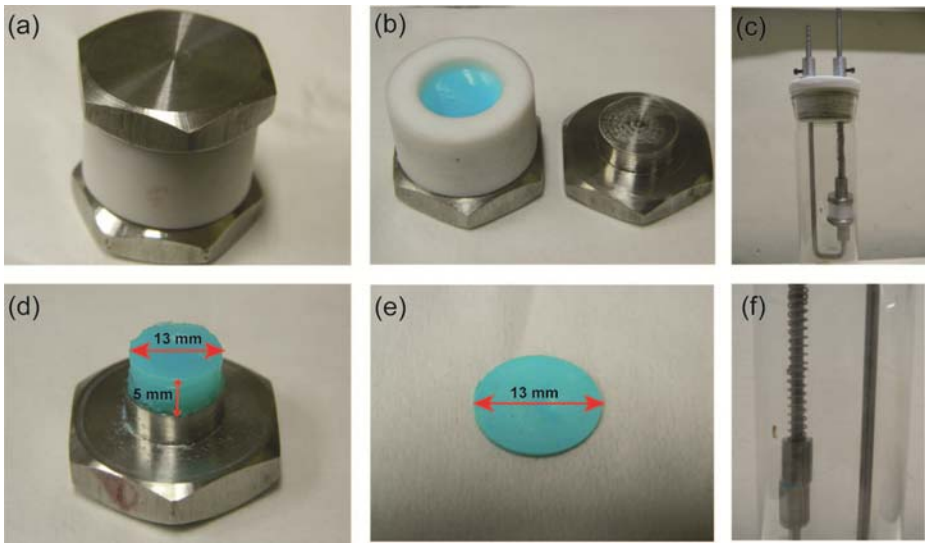

Figure 2.11. (a) Teflon® cylinder with stainless steel stopper for measurement of proton conductivity of gel; (b) CuA-Ox gel (metal:ligand = 1:1.79) grown inside the Teflon® cylinder; (c) gel containing Teflon® cylinder pressed between stainless steel electrodes placed inside glass chamber;(d) CuA-Ox gel column having 13 mm diameter and 5 mm thickness; (e) CuA-Ox xerogel (metal:ligand = 1:1.79) pellet having diameter 13 mm and 0.413 mm thickness; (f) CuA-Ox xerogel pellet sandwiched between two stainless steel electrode placed inside a glass chamber.

sensing accuracy of ±0.5 °C. The pellets were inserted within a humidification chamber for low-temperature proton conductivity measurements which was encircled with a water circulation coil attached with a chiller integrated with an automated temperature controller. The heat flow within the chamber was controlled by the chiller accordingly. The temperature of the chamber was measured by an infrared temperature sensor attachment, having a sensing accuracy of ±0.5 °C.

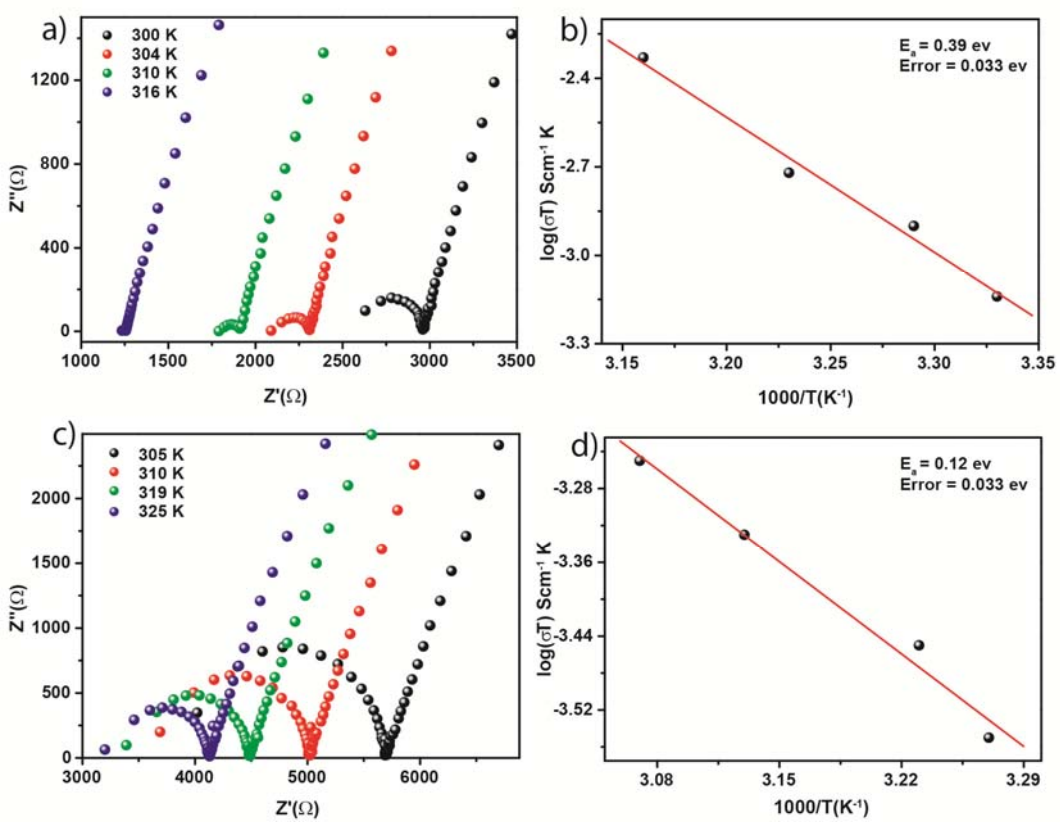

Figure 2.12. a) Comparative Nyquist plots and b) Arrhenius plots of CuA-Ox gel (Cu:Ox = 1:1.79); Comparative Nyquist plots and b) Arrhenius plots of CuA-Ox gel (Cu:Ox = 1:1).

Resistance data derived from impedance measurements have been fit into a three-component model consisting of a resistor (R_s) connected in series with a circuit formed by a resistor (R_p) and a constant phase element (CPE) in parallel (Figure 2.10). Adequate fitting of the Nyquist semicircle at all temperatures validates this model. In this way, the σ-value of the CuA-Ox gel (Cu: Ox = 1: 1.79) membrane at 27 ºC under dehumidified conditions was 1.4×10^{-4} S cm^{-1} (Figure 2.12). Such conductive behavior could be unequivocally ascribed to ionic transport (i.e., H^+ ions), as the metallogel did not show any significant electrical conductance.

It is to be noted that, MOF materials, which can be considered to some extent as crystalline counterpart of some metallogels, rarely conduct protons under anhydrous

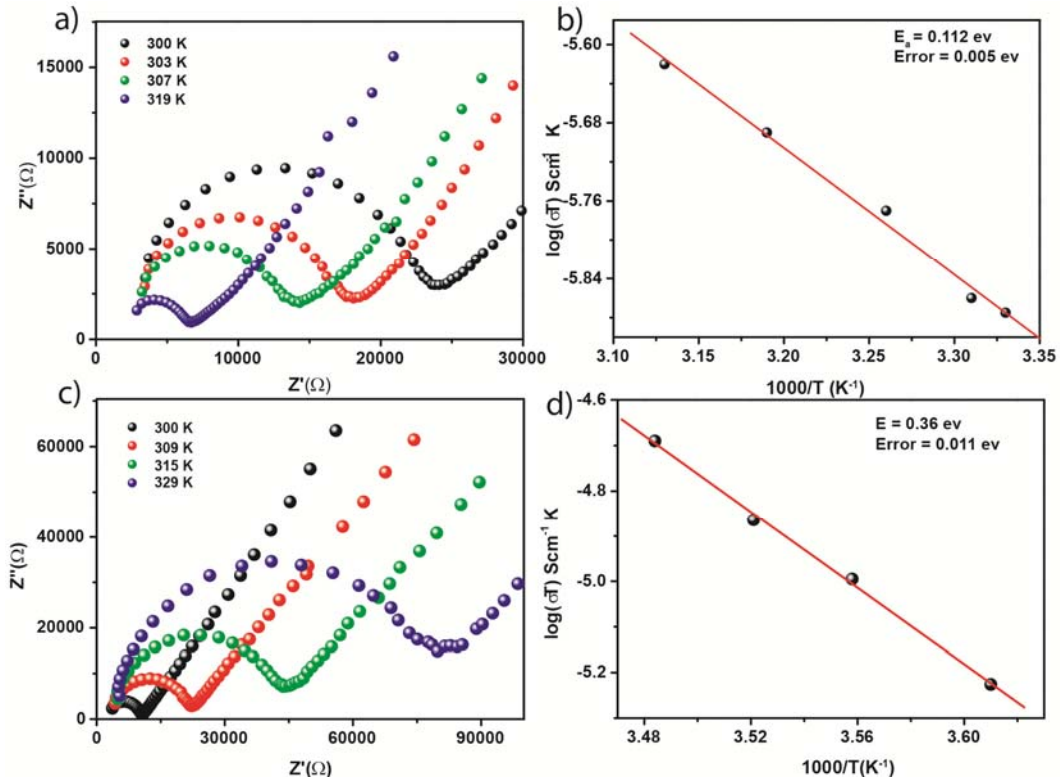

Figure 2.13. a) Comparative Nyquist plots and b) Arrhenius plots of CuA-Ox xerogel (Cu:Ox = 1:1.79); Comparative Nyquist plots and b) Arrhenius plots of CuA-Ox xerogel (Cu:Ox = 1:1)

.

conditions and, sometimes, requires loading of small molecules to assist proton transport.[16a] The conductivity data fits well with the Arrhenius equation, revealing a transport activation energy (E_a) of 0.39 ± 0.033 eV (Figure 2.12b). As expected, σ-value of CuA-Ox gel increases with increasing temperature as the resistance decreases. A reduction of proton conductivity was observed for the gel prepared without excess of oxalic acid (molar ratio of components = 1:1; σ (27 ºC) = 8.1×10^{-5} S cm^{-1}; E_a = 0.12 ± 0.033 eV) (Figure 2.12d). Such reduction was even more prominent for the corresponding xerogels (due to the absence of DMF molecules acting as transfer vehicle), and negligible values were obtained with commercial Cu (II) oxalate hemihydrate. In the best case, proton conductivity was observed up to 72 ºC. The E_a values calculated for xerogel samples are comparable to that of the lithium doped MOF material described as a electrolyte solid superconductor by Long and co-workers.[16b]To the best of our knowledge, this value corresponds to one of the lowest proton transport activation barrier for any metal-organic material reported so far.

Mechanistically, the above results corroborates with a Grotthuss-type transport in these porous materials. As mentioned earlier, species such as unreacted oxalic acid, ammonium ions and acetic acid could contribute to the formation of additional H-bonded networks, which would facilitate the proton transfer.[16c]

Table 2.4: Representative proton conductivity (σ) and activation energy (E_a) values of CuA-Ox materials.

Entry	Molar ratio (metal:ligand)	Phase	Temperature (ºC)	Temperature (K)	σ (S cm^{-1})	E_a (eV)
1	1:1.79	Gel	27	300	1.43×10^{-4}	0.39 ± 0.03
2	1:1.79	Gel	43	316	3.0×10^{-4}	0.39 ± 0.03
3	1:1.79	Xerogel	27	300	9.4×10^{-6}	0.112 ± 0.005
4	1:1.79	Xerogel	46	319	1.1×10^{-5}	0.112 ± 0.005
5	1:1	Gel	32	305	9.4×10^{-5}	0.12 ± 0.033
6	1:1	Gel	52	325	1.2×10^{-4}	0.12 ± 0.033
7	1:1	Xerogel	27	300	6.4×10^{-6}	0.36 ± 0.011
8	1:1	Xerogel	56	329	4.4×10^{-6}	0.36 ± 0.011

2.3. Conclusion:

In summary, we have synthesized new modular, stimuli-responsive, and multifunctional metallogels (i.e., CuA-Ox and CuP-Ox gels) based on the combination of two commercially available and inexpensive components: A Cu(II) salt and oxalic acid as the only bridging ligand. The gelation process occurs at RT upon mixing stock solutions of each component prepared under optimized concentrations, while the facile and economic procedure allows the preparation of the metallogels at multigram scale. The overall stability of this type of materials represents a complex equilibrium between thermal stability of the coordination aggregates, electrostatic interactions involving also the counteranions, degree of crosslinking and solvation-related interactions. Major novelties of this investigation

include (a) introduction of oxalic acid as the lowest molecular weight organic ligand that is able to form stable metallogels, (b) growth of different Cu(II) oxalate non-aquo polymorphs from one metallogel and its corresponding xerogel, which illustrates an unprecedented xerogel-to-crystal phase transition and (c) first demonstration of proton conductivity in molecular gels with lowest activation energy among metal-organic materials and. The described results open new perspectives on bootom-up approach of high temperature proton conducting metal-organic material and inorganic crystal engineering.

2.4. Experimental Procedures:

2.4.1. Materials.

Unless otherwise noted, oxalic acid, inorganic salts and solvents were purchased from commercial suppliers and used without further purification.

2.4.2. Typical synthesis of CuA-Ox gel:

Preparation of stock solutions:

$Cu(OAc)_2 \cdot H_2O$ (0.28 g, 1.40 mmol) was dissolved in dry DMF (5 mL) at RT affording 0.28 M deep green solution (Sol-1). Oxalic acid dihydrate (0.32 g, 2.54 mmol) was dissolved in dry DMF (5 mL) at RT affording 0.5 M transparent solution (Sol-2). Preparation of CuA-Ox gel: 1 mL of Sol-1 was added rapidly at RT over 1 mL of Sol-2 placed into a glass test tube (10 cm length × 1 cm diameter, 1 mm wall thickness), forming immediately an bluish–green partial inhomogeneous gel. The mixture was shaken vigorously and subsequently sonicated during 10 min at RT to form a blue homogeneous colloidal suspension, which evolved to a stable gel within 6 h under undisturbed conditions. The gel remained stable after 1 year.

2.4.3. Typical synthesis of CuP-Ox gel:

Preparation of stock solutions:

$Cu(ClO_4)_2 \cdot 6H_2O$ (0.74 g, 1.98 mmol) was dissolved in dry DMF (5 mL) at RT affording 0.4 M light blue solution (Sol-3). Solution of oxalic acid dihydrate was prepared as described above (Sol-2). Preparation of CuP-Ox gel: 1 mL of Sol-3 was added rapidly at RT over 1 mL of Sol-2 placed into a glass vial (10 cm length × 1 cm

diameter, 1 mm wall thickness), and the mixture shaken vigorously to form a blue homogeneous colloidal suspension, which evolved to a stable gel within 5 s. Disruption of the gel and initial crystallization was observed after 3 months.

NOTES:

a) The above general experimental procedures were also used to prepare metallogels at different molar ratios of the two components. The order of addition (e.g., oxalic acid over Cu(II) solution or vice versa) was found irrelevant in terms of gel properties.

b) The production cost (lab scale) of the bulk gels was estimated in less than 0.5 EUR / g of gel. It is worth to mention that naturally occurring oxalic acid and metal oxalates (e.g., hydrated copper oxalate) are harmless for the environment.

c) Although the metallogels could be prepared using a molar ratio 1:1 of the two components, optimized ratios provided the maximum temporal stability of the metallogels.

d) If necessary, the fast gelation kinetics could be decreased by reducing the mixing temperature. For instance, CuP-Ox gel was not formed when the stock solutions were mixed at -47 ºC. Gel started to form gradually when the mixture was allowed to warm to RT.

2.4.4. Preparation of xerogels:

Freeze-dried gel materials were obtained as following: 10 mL of the corresponding metallogel was homogeneously frozen in a liquid nitrogen bath (ca. -78 ºC), and subsequently evaporated to dryness at -168 ºC under a 10^{-4} bar vacuum overnight using a freeze dryer. In the case of lyophilized CuP-Ox material, it was necessary to complete the drying using blotting paper at 36 ºC. Furthermore, air-dried xerogel samples could be obtained by soaking 5 mL of the corresponding metallogel with filter paper (i.e., Whatman® 40). The resulting paste-type material was then spread on a glass slide and kept at RT for 1 day.

2.4.5. Instruments and analyses:

2.4.5.1. PXRD, FT-IR, TGA and DSC studies.

Powder X-ray diffraction patterns were recorded at RT using a Phillips PANalytical X'PERT PRO instrument using iron-filtered Cu Kα radiation (λ=1.5406 Å) in the *2θ* range of 5–50° with a step size of 0.02° and a time of 0.3 second per step. FT-IR spectra of precursor materials, gels and xerogels (ca. 1 mg) were taken on a Bruker Optics ALPHA-E spectrometer with a universal Zn-Se ATR (attenuated total reflection) accessory in the 4000–600 cm^{-1} region or using a Diamond ATR (Golden Gate). TGA data were obtained with a TG50 analyzer (Mettler-Toledo) or a SDT Q600 TG-DTA analyzer under N_2 atmosphere at a heating rate of 10 ºC min^{-1} within a temperature range of 20-800 °C. DSC measurements were performed on a TA Q10 differential scanning calorimeter at a heating rate of 10 ºC min^{-1} under N_2.Endothermic/exothermic processes were in good agreement with TGA derivatives.

2.4.5.2. MALDI-TOF and EPR spectroscopy:

MALDI-TOF spectra were recorded on an ABSCIEX 5800 MALDI TOF/TOF (USA) spectrometer. The samples were prepared by dispersion of the gels in DMF and dropcasting on dry dithranol matrix. EPR spectra were recorded on a Bruker EMX X-band spectrometer at 100 kHz field modulation.

2.4.5.3. Electron microscopy an AFM studies:

TEM images were recorded using FEI Tecnai G2 F20 X-TWIN transmission electron microscope at an accelerating voltage of 200 kV. The specimens were prepared by dropcasting a gel sample presuspended in ethyl acetate (ca. 10^{-3} M) on copper grids TEM Window (TED PELLA, INC. 200 mesh).

The material was further dried under vacuum for 12 h prior imaging. SEM images were obtained with a FEI, QUANTA 200 3D scanning electron microscope with tungsten filament as electron source operated at 10 kV. The xerogel samples were sprinkled on conductive carbon tape and sputtered with Au (nano-sized film) prior to imaging with a SCD 040 Balzers Union.

2.4.5.4. AFM characterization was carried out on both gel and xerogel samples deposited on mica substrate (Aname, Cat. # 71855-15) as following:

Gel samples were cast onto the mica substrate under ambient conditions, and then dried at 55 °C for 1 h before analysis. Xerogel specimens were first suspended in acetone (p.a.), from which a drop was placed onto the mica substrate and dried on air for 1 day before analysis. The AFM measurements were performed with a Ntegra Aura, NT-MDT instrument equipped with an Universal measuring head and 100 mKm scanner, and using NSG01/TiN tips from NT-MDT (characteristics of the tips -*AFM «Golden» Silicon Probes*-: single crystal silicon, N-type, 0.01-0.025 Ω-cm, TiN coating, reflective side of Au, antimony doped cantilever, drive resonant frequency = 87-230 kHz, drive amplitude = 0.10□0.14 mV, force constant = 1.45-15.1 N/m). Due to the soft nature of the samples, semicontact mode (Tapping mode) was used in order to avoid undesired damage or deformation. Images (1 μm^2, 2 μm^2, 4 μm^2 or 10 μm^2) were further processed using Gwyddion open source software (http://gwyddion.net/). Direct deposition of the xerogel material onto In substrates provided low-resolution images in comparison to the deposition of the acetone suspension onto the mica substrate and subsequent evaporation.b).

2.4.5.5. Gas adsorption experiments:

60 mg of CuP-Ox dry gel was first dried under a dynamic vacuum (1.33×10^{-6} bar) at RT overnight. Low-pressure volumetric gas adsorption measurements were performed at -196 ºC K for N_2, maintained by a liquid-nitrogen bath, with pressures ranging from 0 to 1.01 bar on a Quantachrome Quadrasorb automatic volumetric instrument. CO_2 adsorption measurements were made at 25 ºC under same pressure range.

2.4.5.6. Rheological studies:

Rheology was performed using a TA-ARES rheometer equipped with a force rebalance transducer. The measurements were carried out thrice and average values represented. A Couette geometry was used for the measurement with cup and bob diameters of 27 and 25 mm, respectively, and height of 38 mm. Dynamic strain sweep (DSS) measurements were initially performed to estimate the smallest strains at which reasonable torque values (ca. ten times the resolution limit of the transducer) could be

obtained. The linear viscoelastic region (LVR) of the gels was determined by increasing amplitude of deformation from 0.1% to 100% at 1 rad s^{-1}. Subsequently, dynamic frequency sweep (DFS) measurements were performed as a function of ageing time (frequency range = 10^{-2}–10^{2} rad s^{-1}; strain = 1%). Zerotime position was set after a pre-shearing process (i.e., shear 10º, time 50.28 s) of the specimen in order to obtain a well-defined initial state. The brittle nature of the metallogels was confirmed by their fracture at strain (deformation) below 1%. In each case, the storage modulus presented a perceptible albeit low dependence on the frequency, which is characteristic of viscoelastic fibrilar networks. Both CuA-Ox and CuP-Ox gels were characterized by an average storage modulus (G') ca. one order of magnitude higher than the loss modulus (G'') within the linear viscoelastic regime (pulsation (w) = 1 rad s^{-1}; strain = 0.1%).

2.4.5.7. Proton conductivity measurements:

Proton conductivities were measured using Solartron 1287 Electrochemical Interface with 1255B frequency response analyzer via quasi-four-probe method in the frequency range 1 Hz to 1 MHz with input voltage amplitude of 30 mV under inert condition (N_2 atmosphere). To measure open circuit voltage (OCV) a membrane electrode assembly (MEA) was prepared using the following process: The material (i.e., gel containing Teflon cylinder in case of gel, and pellet in case of xerogel) was pressed between two stainless steel electrodes. The stainless steel rods were then attached onto both sides of the electrodes, and the MEA was set in two holes punched at a Teflon® sheet as a gasket (ESI, Figure S22). For high-temperature proton conductivity measurements, the pellets/Teflon cylinders were inserted within a glass chamber (dry and N_2 filled), which was encircled with a controlled heating coil attached with an automated temperature controller. The heat flow within the temperature controller was controlled by a dimerstat accordingly. The temperature of the chamber was measured by an infrared temperature sensor attachment, having a sensing accuracy of ± 0.5 °C. For low-temperature proton conductivity measurements, the pellets were inserted within a glass chamber (dry and N_2 filled), which was encircled with a water circulation rubber pipe attached with a chiller integrated with an automated temperature controller. The heat flow within the chamber was controlled by the chiller accordingly. The temperature of the chamber was measured

by an infrared temperature sensor having a sensing accuracy of ± 0.5 °C.

2.4.6 X-ray Crystallography

2.4.6.1 General Data Collection and Refinement Procedures:

Data were collected on a Super Nova Dual source X-ray Diffractometer system (Agilent Technologies) equipped with a CCD area detector and operated at 250 W (50 kV, 0.8 mA) to generate Mo Kα radiation (λ = 0.71073 Å) and Cu Kα radiation (λ = 1.54178 Å). The crystal reported in this paper was mounted on Nylon CryoLoops (Hampton Research) with Paraton-N (Hampton Research). Initial scans of each specimen were performed to obtain preliminary unit cell parameters and to assess the mosaicity (breadth of spots between frames) of the crystal to select the required frame width for data collection. CrysAlis^{Pro} [2.17] program software suite to carry out was used overlapping φ and ω scans at detector (2θ settings (2θ = 28). Following data collection, reflections were sampled from all regions of the Ewald sphere to redetermine unit cell parameters for data integration. In no data collection was evidence for crystal decay encountered. Following exhaustive review of collected frames the resolution of the dataset was judged. Data were integrated using CrysAlis^{Pro} software with a narrow frame algorithm. Data were subsequently corrected for absorption by the program SCALE3 ABSPACK [2.18] scaling algorithm.

These structures were solved by direct method and refined using the SHELXTL 97 software suite. Atoms were located from iterative examination of difference F-maps following least squares refinements of the earlier models. Final model was refined anisotropically (if the number of data permitted) until full convergence was achieved. Hydrogen atoms were placed in calculated positions (C-H = 0.93 Å) and included as riding atoms with isotropic displacement parameters 1.2-1.5 times Ueq of the attached C atoms. Data were collected at 100(2) K for the Cu-Oxalate complexes presented in this paper. This lower temperature was considered to be optimal for obtaining the best data. The structure was examined using the Addsym subroutine of PLATON [2.19] to assure that no additional symmetry could be applied to the models. The ellipsoids in ORTEP diagrams are displayed at the 50% probability level unless noted otherwise.

Crystallographic data (excluding structure factors) for the structures are reported in this paper have been deposited in CCDC as deposition No. CCDC 897214-897215. Copies of the data can be obtained, free of charge, on application to the CCDC, 12 Union Road, Cambridge CB2 lEZ, U.K. [fax: þ 44 (1223) 336 033; e-mail: deposit@ccdc.cam.ac.uk].

2.4.6.2. Experimental and Refinement Details for Cu-Ox1:

A blue plate like crystal of **Cu-Ox1** was placed in 0.7 mm diameter nylon CryoLoops (Hampton Research) with Paraton-N (Hampton Research). The loop was mounted on a Super Nova Dual source X-ray Diffractometer system (Agilent Technologies) equipped with a CCD area detector and operated at 250 W power (50 kV, 0.8 mA) to generate Mo Kα radiation (λ = 0.71073 Å) at 100(2) K in a liquid N_2 cooled stream of nitrogen. A total of 15548 reflections were collected of which 7034 were unique. The range of θ was from 3.29 to 29.15. Analysis of the data showed negligible decay during collection. The structure was solved in the triclinic *P-1* space group, with Z = 4, using direct methods. All non-hydrogen atoms were refined anisotropically with hydrogen atoms generated as spheres riding the coordinates of their parent atoms. we have repeatedly collected the single crystal XRD data of In-IA-2D-1 at different temperature (90, 120, 150K). Final full matrix least-squares refinement on F^2 converged to $R_1 = 0.0415$ ($F > 2\sigma F$) and $wR_2 = 0.1048$ (all data) with GOF = 1.074.

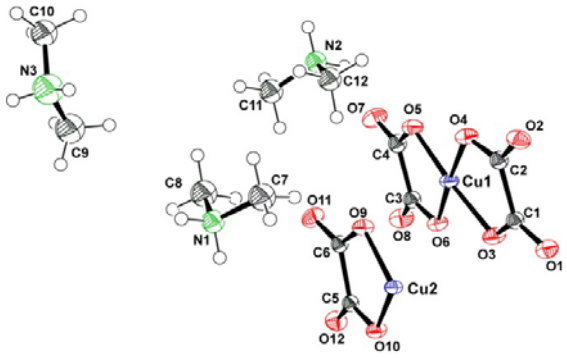

2.4.6.3. Experimental and Refinement Details for Cu-Ox1:

A blue plate like crystal of **Cu-Ox2** was placed in 0.7 mm diameter nylon CryoLoops (Hampton Research) with Paraton-N (Hampton Research). The loop was mounted on a Super Nova Dual source X-ray Diffractometer system (Agilent Technologies) equipped with a CCD area detector and operated at 250 W power (50 kV, 0.8 mA) to generate Mo Kα radiation (λ = 0.71073 Å) at 100(2) K in a liquid N_2 cooled stream of nitrogen. A total of 15548 reflections were collected of which 7034 were unique. The range of θ was from 3.29 to 29.15. Analysis of the data showed negligible decay during collection. The structure was solved in the monoclinic *C2/c* space group, with Z = 4, using direct methods. All non-hydrogen atoms were refined anisotropically with hydrogen atoms generated as spheres riding the coordinates of their parent atoms. we have repeatedly collected the single crystal XRD data of In-IA-2D-1 at different temperature (90, 120, 150K). Final full matrix least-squares refinement on F^2 converged to R_1 = 0.0308 ($F > 2\sigma F$) and wR_2 = 0.0793 (all data) with GOF = 1.099. [CCDC 897215].

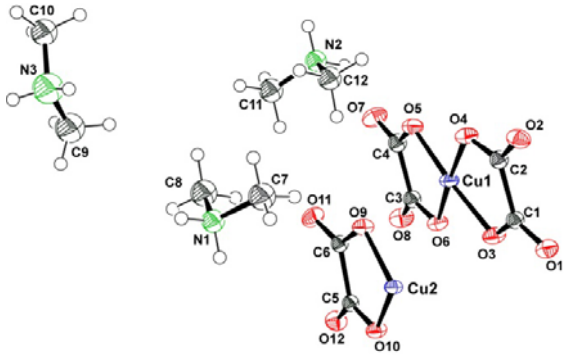

NOTE: The results of this chapter have already been published in ***Chem. Eur. J.***, 2013, 19, 9562 – 9568. with the title: "*Proton-Conducting Supramolecular Metallogels from the Lowest Molecular Weight Assembler Ligand: A Quote for Simplicity.*" These publications were the results from the group of Dr. Rahul Banerjee and his students Subhadeep Saha from CSIR National Chemical Laboratory, Pune, India. Majority of the work is contributed by Subhadeep with the help of the instrumental facilities of CSIR National Chemical Laboratory.

CHAPTER 3

Amino Acid-based Multiresponsive Low-Molecular-Weight Metallo-hydrogels with Load-bearing and Rapid Self-healing Ability

3.1 Introduction:

The ability of autonomic self-repairment to restore a damaged function is one of the most intriguing and important properties of any material which have diverse applications in various fields (3.1). Over the past few decades, this feature has inspired researchers to develop self-healable synthetic materials, mostly polymeric materials, to reduce replacement costs which improve their lifetime (3.2). In general, these materials are based on either irreversible (e.g., encapsulation of repairing agents) or reversible approaches (e.g., dynamic covalent bonds, non-covalent bonds) (3.2a). Among materials with potential self-healing ability, viscoelastic (soft) materials such as hydrogels are very promising for biomedical applications due to their biocompatibility and similar mechanical properties to those of natural tissues (3.2d). The existence of cooperative dynamic interactions in supramolecular hydrogels (3.3) offers interesting possibilities to promote self-healing mechanisms without requirement of external stimuli. Harada *et. al.* synthesized a transparent supramolecular hydrogel, which forms quickly upon mixing poly(acrylic acid) (pAA) containing β-CD as a host polymer with pAA possessing ferrocene as a guest polymer (3.4). This system could induce a reversible sol–gel phase transition in presence of a suitable redox stimulus in the gel, and furthermore, re-adhesion between broken surfaces could be also controlled by the stimulus. Sureshan and co-workers reported two sugar-based super-gelators which gel oils and hydrocarbon solvents to give self-standing and transparent gels with self-healing properties (3.5). Recently, Huang *et. al.* reported a number of molecular gels with self-healing properties formed through host–guest interactions between crown ether and its guest group.

In this chapter, we report (3.6) a very rare free-standing, moldable and load-bearing supramolecular metallohydrogel synthesized at room temperature from a low-molecular-weight (LMW) amino acid-based ligand [V = L-3-methyl-2-(pyridine-4-yl-methylamino)-butanoic acid) and sodium perchlorate as ligand systems (VP,

respectively)] in the presence of Zn(II) salts. The ligand co-ordinates with the Zn(II) ion to form a complex (*vide infra*) which self-assembles *via* H-bonding to form 1D fibre which entangles to form the gel network. The presence of dynamic supramolecular bonding enables the gel to show unique gel-sol reversibility in presence of a number of physical and chemical stimuli.

3.2 Results and discussion:

3.2.1 Synthesis of ZAVP metallohydrogel:

Figure 3.1 illustrates the synthesis of ZAVP gel which forms upon mixing the aqueous solutions of the two components (0.5 ml each), *viz.* zinc acetate dihydrate (ZA, 0.2 M) and ligand system L-VP (derived from L-valine; 0.4 M), which turns into a gel (CGC=84 gL^{-1}) within a few seconds at room temperature. Physical mixture of pure V and sodium perchlorate (P) also has the potential of forming gels.

3.2.2 Gelation ability:

Contrary to typical heating-cooling protocol, gelation phenomenon discussed here takes place efficiently at room temperature (25-30 °C). This combination of metal salt (ZA) and ligand (VP) cannot afford gelation in most of the protic and aprotic solvents (Table 3.1 lists the solvents that have been tried for gelation) but water. This feature can be attributed to H-bond donor (3.6) (N_{amine}-H...O_{Water}) and acceptor (O_{Water}-H...$N_{Pyridine}$) nature of the gelator complex (Figure 3.3). The organic part (VP) of the gelator contains an amine functionality in protonated form ($–NH_3^+$) which acts as a H-bond donor by accepting lone pair of electrons from electronegative element (*e.g.* oxygen of water) via its electron deficient proton to form H-bonding (3.7). It (VP) also contains a pyridine functionality which can act as H-bond acceptor. Hence, for a efficient gelation to take place, a solvent like water is required which is capable of acting as both H-bond donor (α = 1.17) as well as acceptor (β = 0.47) (3.8). This leads to an assembly of water molecule and the gelator complex which results in the formation of gel network. The ligand VP yields precipitates with most of the other metal salts [*e.g.* common salts of Ca(II), Mg(II), Al(III), Fe(III/II), Co(II/III), Ni(II) etc.].

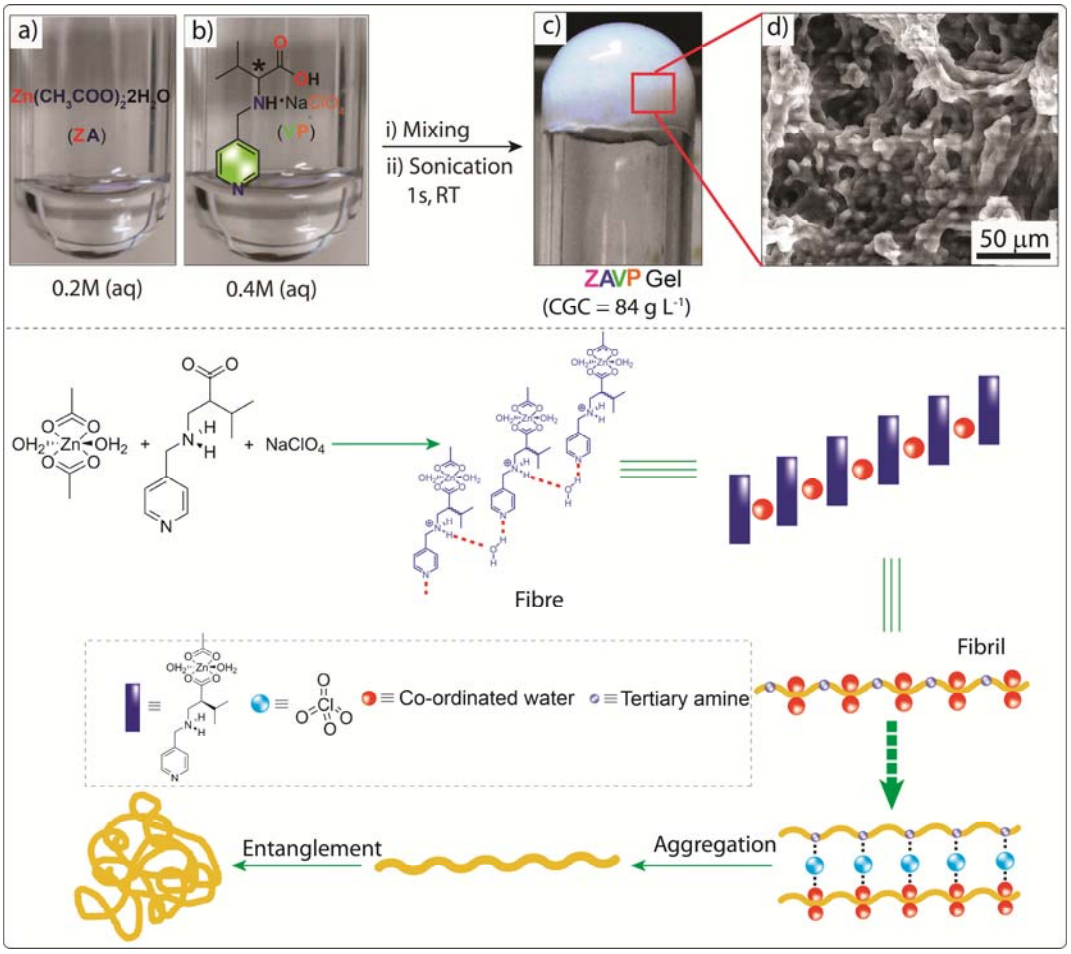

Figure 3.1 (*top*)Synthesis of ZAVP (a-c) at the CGC. Total volume of each solution = 0.5 mL. d) SEM-images of the corresponding xerogel; (*bottom*) Probable structure of the gelator and the possible self-assembly process leading to the formation of gel network.

The critical gelation concentration (CGC) for ZAVP hydrogel was found to be 84 gL^{-1}. ZAVP hydrogel is thermoreversible and the gel-to-sol transition temperatures (T_{gel}) has been established to be 61 ± 2 ºC. Complete sol-to-gel transition occurs within 20 min

upon spontaneous cooling the corresponding isotropic solutions. As often observed with other chiral gelators (3.9), the enantiomeric purity of the ligand has been found to play a key role on the formation of stable gels. The most stable gels can be obtained while using enantiomerically pure ligands, although complete gelation could be observed when the enantiomeric excess (ee) was 85% ≤ ee ≤ 100%. In contrast, only

Table 3.1. Solvents tested for gelation:

S.No.	Solvent	Phase	Gelation time	Gel-phase color	Kamlet-Taft solvent pararmeters		
					α	β	γ
1	H_2O	G	~30 s	White	1.17	0.47	1.09
2	DMF	P	–	–	0.00	0.69	0.88
3	DEF	P	–	–	–	–	–
4	DMAC	P	–	–	0.00	0.76	0.88
5	NMF	P	–	–	–	–	–
6	Acetone	S	–	–	0.08	0.43	0.71
7	THF	S	–	–	0.00	0.55	0.58
8	CH_3CN	S	–	–	0.19	0.40	0.75
9	MeOH	S	–	–	0.98	0.66	0.60
10	EtOH	S	–	–	0.86	0.75	0.54
11	*i*-PrOH	S	–	–	0.76	0.84	0.48
12	*n*-Hexane	I	–	–	0.00	0.00	-0.04
13	Et_2O	I	–	–	0.00	0.47	0.27
14	EtOAc	I	–	–	0.00	0.45	0.55
15	CH_2Cl_2	I	–	–	0.13	0.10	0.82
16	$CHCl_3$	I	–	–	0.20	0.10	0.58
17	Benzene	I	–	–	0.00	0.10	0.59
18	Toluene	I	–	–	0.19	0.40	0.75
19	DMF/H_2O	S	–	–	–	–	–

[Solvent abbreviations: DMF = *N*,*N*-dimethylformamide; DEF = *N*,*N*-diethylformamide; DMAC = *N*,*N*-dimethylacetamide; NMP = 1-methyl-2-pyrrolidone; THF = tetrahydrofuran. Abbreviations: S = solution; G = stable gel; I = insoluble; P = precipitates; PG = Partial gel.]

partial gelation can be achieved in the range 60-80% ee, and no gelation has been observed when the ee was < 60% (Figure 3.2). Moreover, if two ZAVP gel blocks made up of ligands of opposite chirality are kept in contact to each other, both the blocks disrupts to sol. The use of ligands containing K^+ instead of Na^+ ions yields hydrogels with similar properties suggesting a minor role of these ions on the gelation phenomenon. Interestingly, the results of a large screening indicates that the gelation is specific regarding the presence of Zn(II) salts as coordinating metal.

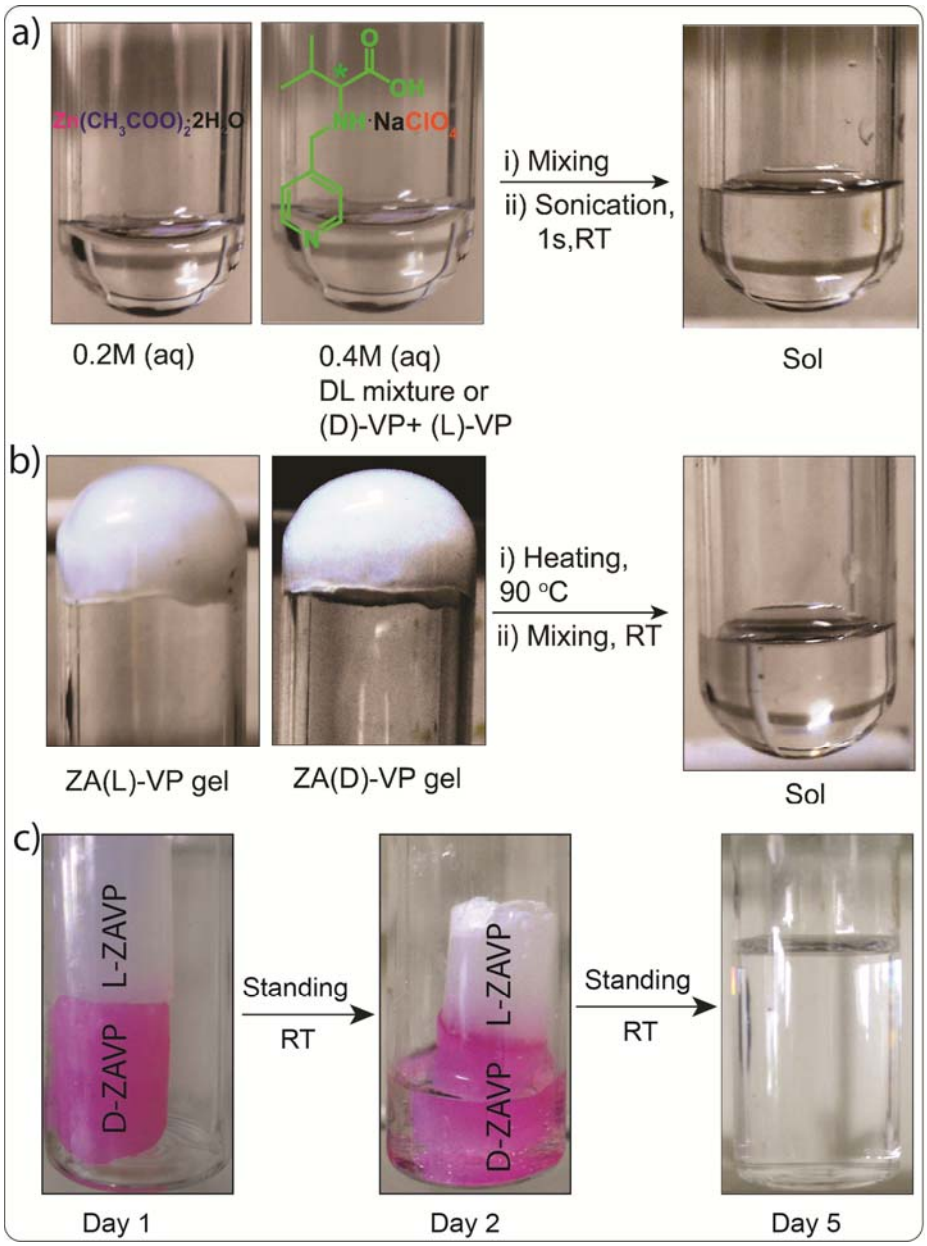

Figure 3.2. a) Formation of sol phase by reaction DL mixture (1:1) of VP ligand and zinc acetate in water.; b) Formation of sol *via* reaction of L and D-ZAVP sols (obtained by heating the gels to 90 °C); c) destruction of self-standing gels kept in contact to each other [L-ZAVP (made from L-VP) and D-ZAVP (made from D-ZAVP)] to sol phase.

3.2.3 Morphological study:

Insights into the morphology of the ZAVP hydrogel were obtained by recording SEM/FESEM and ESEM images of the corresponding xerogel (prepared by freeze-drying) and native gel phase, respectively, which exhibits a high-aspect ratio fibrillar network as a consequence of a highly anisotropic growth process (Figure 3.1 and 3.4). Most of the fibers are of relatively uniform diameters in the range of 20-80

nm and lengths on the micrometer scale.

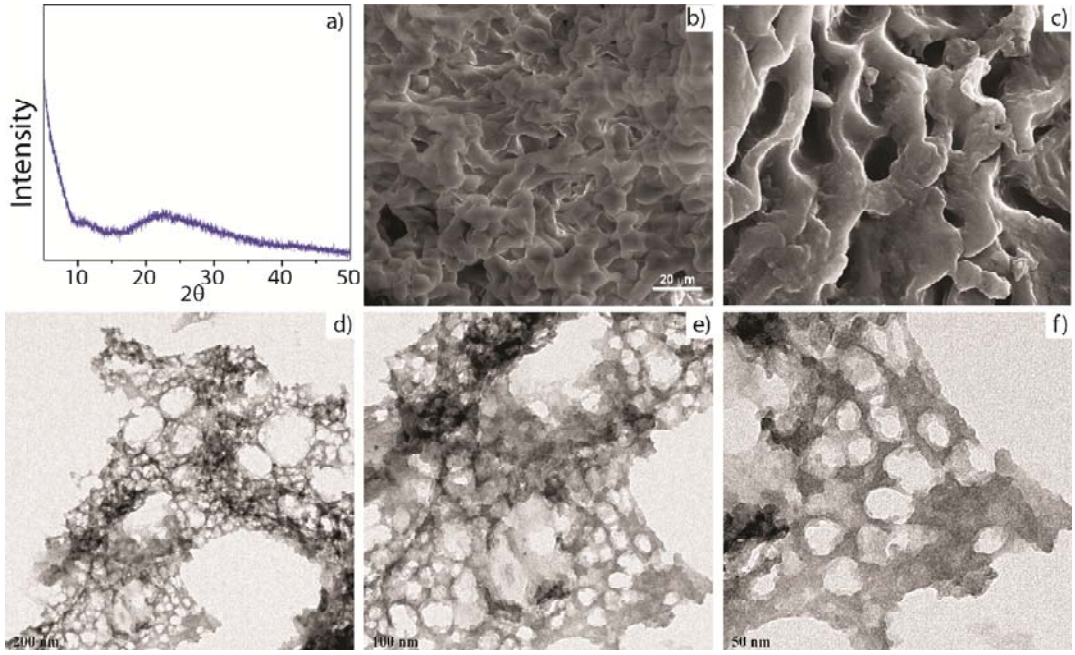

Figure 3.3. a) PXRD indicates amorphous nature and b) ESEM, c) FESEM, d), e) and f) TEM images of ZAVP xerogel illustrates its fibrillar nature.

3.2.4 Mechanical properties:

The Viscoelastic nature of ZAVP hydrogel has been confirmed by oscillatory rheological measurements (Figure 3.5). Within the linear viscoelastic regime, established by dynamic frequency and strain sweep experiments (DFS and DSS, respectively), the average storage modulus ($G' > 10^5$ Pa) is found to be one order of magnitude higher than the loss modulus (G') and constant over the entire range of frequencies (0.1-10 Hz) (Figure 3.5). Reproducible and relatively constant dissipation factors ($\tan \delta = G''/G' \approx 0.1$) during DFS indicated a good tolerance of the hydrogels to external forces. Further dynamic time sweep (DTS) measurements (Figure 3.5) at 0.1% strain and 1 Hz frequency confirmed the mechanical stability of the hydrogels at RT within the linear regime. It is noteworthy that, ZAVP hydrogel also displayed a rapid thixotropic response against the mechanical stress caused by large-amplitude oscillations at room temperature. Figure 3.5d shows a loop test involving consecutive cycles of low-high strain separated by enough time which warrants complete gel-to-sol ($G' < G''$) and sol-to-gel ($G' > G''$) transitions while minimizing inertial effects between the steps. These results depicts that the original mechanical properties of the gel were fully recovered within 3 ± 1 min after termination of the large stress. This process is reproducible for at least 15 cycles without appreciable reduction in the

average magnitude of *G′* and *G″* (Figure 3.5).

This thixotropic behaviour was also macroscopically observed within ca. 4 min after a shaking-resting cycle applied to the test tube containing the 'just synthesized' ZAVP

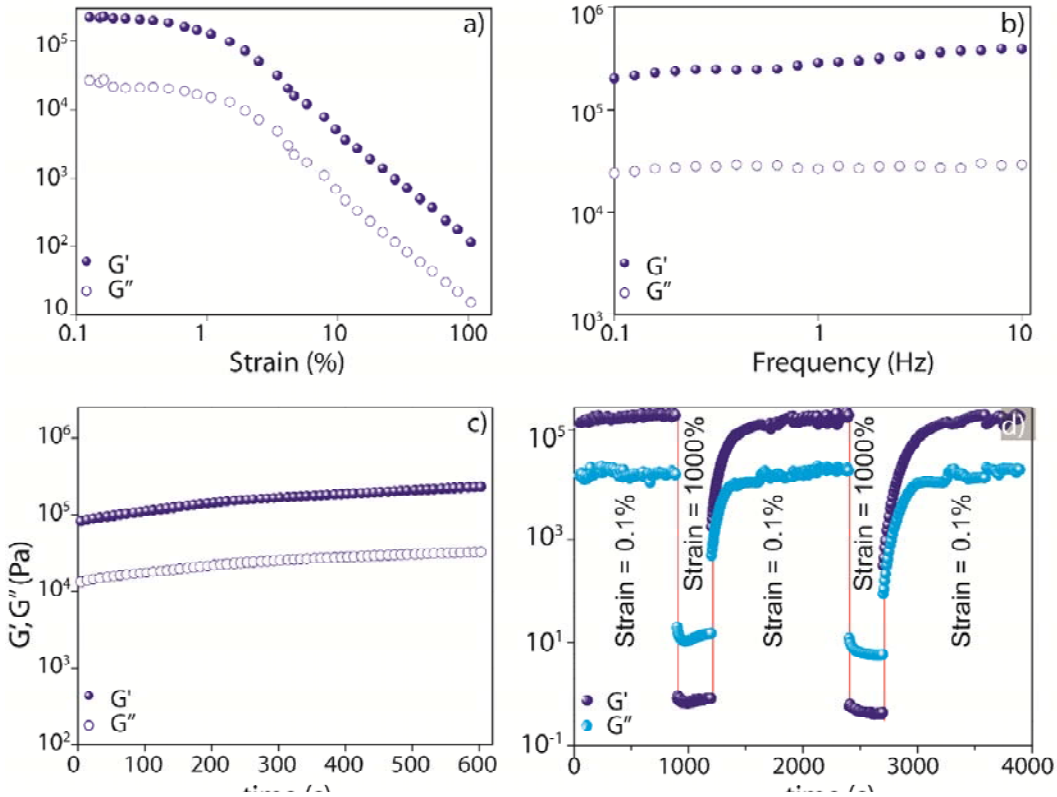

Figure 3.4. Oscillatory rheology of ZAVP hydrogel prepared at the CGC: a)DSS experiment at constant frequency of 1 Hz, b) DFS experiment at strain = 0.1%, c) DTS experiment at constant strain at 0.1% and frequency constant at 1 Hz c) b) Thixotropy-loop test via continuous step-strain measurements at 0.1 Hz frequency.

hydrogel (the phase which has not achieved its self-standing nature). The shear thinning property of this gel has also been observed in microscale and bulk forms.

3.2.5 Response towards external stimuli:

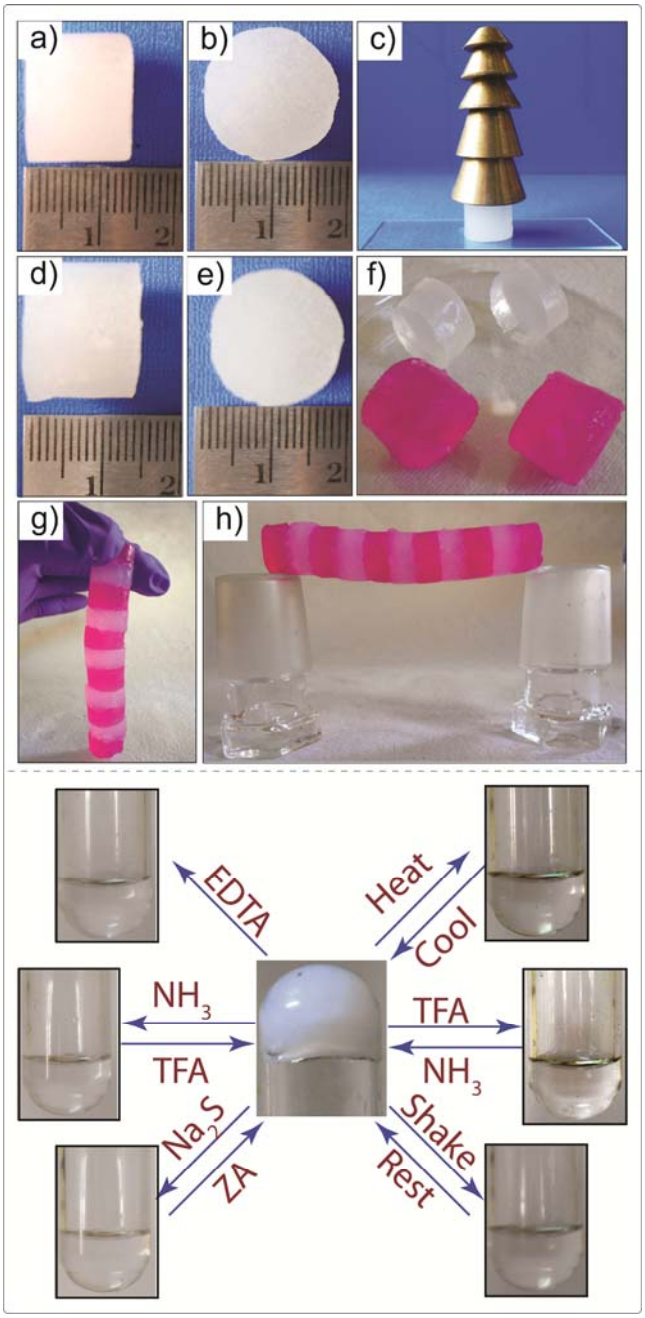

Figure 3.5. ***(****Left****)*** Pictures of a), b) freshly prepared hydrogel cylinder of 1.4 cm thickness and 1.6 cm diameter; c) 2 g mass bearing a load up to 90 g (total weight of 5 truncated brass cones); d) and e) maintaining its shape after load is released. f) Moldable and shape-persistent hydrogel blocks cut from a larger cylinder. Pink objects correspond to hydrogel pieces upon doping with Rose Bengal dye. g-h) Bridge constructed by fusing 11 hydrogel blocks together, Light pink coloration of undoped gel blocks is due to the rapid diffusion of the dye through the hydrogel network; ***(****right****)*** Thermal, mechanical, pH, and chemical stimuli-triggered gel–to-sol transitions of ZAVP hydrogel. ZA = Zinc acetate dihydrate.

Besides the described response to thermal and mechanical stimuli inducing gel-to-sol

transitions, ZAVP hydrogel also exhibits a rapid pH and chemoresponse (Figure 3.6). The hydrogel, with an intrinsic pH of ca. 6.5, turns into a clear solution within seconds upon addition of 1 M TFA solution. The gel phase is easily restorable upon addition of an equivalent amount (to the amount of TFA) of ammonia to the previous solution. Presence of excess proton in the system protonates the free pyridinic N (which takes part in H-bonding by donating its lone pair electron density) which leads to the disruption of H-bonded gel network. It should be noted that, hydrogelation with other pyridine-containing gelators at low pH has been previously described as an unfavorable process (3.9). Surprisingly, gel-to-sol transition can also be achieved by adding a 4-fold excess of ammonia (4 M) with respect to the concentration of Zn(II) in the gel phase. Similar to the previous case, subsequent addition of 4 M TFA solution causes the inverse sol-to-gel process. This particular phenomenon takes place due to the reversible formation of Zn(II)-tetramine complex in the presence of ammonia. Under the same principle of dynamic non-covalent metal-complexation, the addition of solid crystalline EDTA or Na_2S (equimolar to the amount of Zn(II) present in gel) on top of the gel causes complete dissolution or formation of white precipitate (ZnS), respectively, in quantitative yields within 30 min. Separation of the solid ZnS and addition of equimolar amount of zinc acetate to the remaining solutions restores the gel phase within a few minutes. No difference in properties has been observed in the properties of the gels obtained through the multiresponsive map depicted in Figure 3.6.

3.2.6 Self-healing nature:

In addition to the reversible (*gel-sol-gel*) response towards external stimuli, ZAVP hydrogel also exhibited rapid self-healing in air at room temperature without use of any kind of healing agent. In recent past, a number of metallogels with self-healing properties have been reported. Nevertheless, many of these examples are either organogels (3.10) or based on (1) formation of metal coordination polymers (3.11),

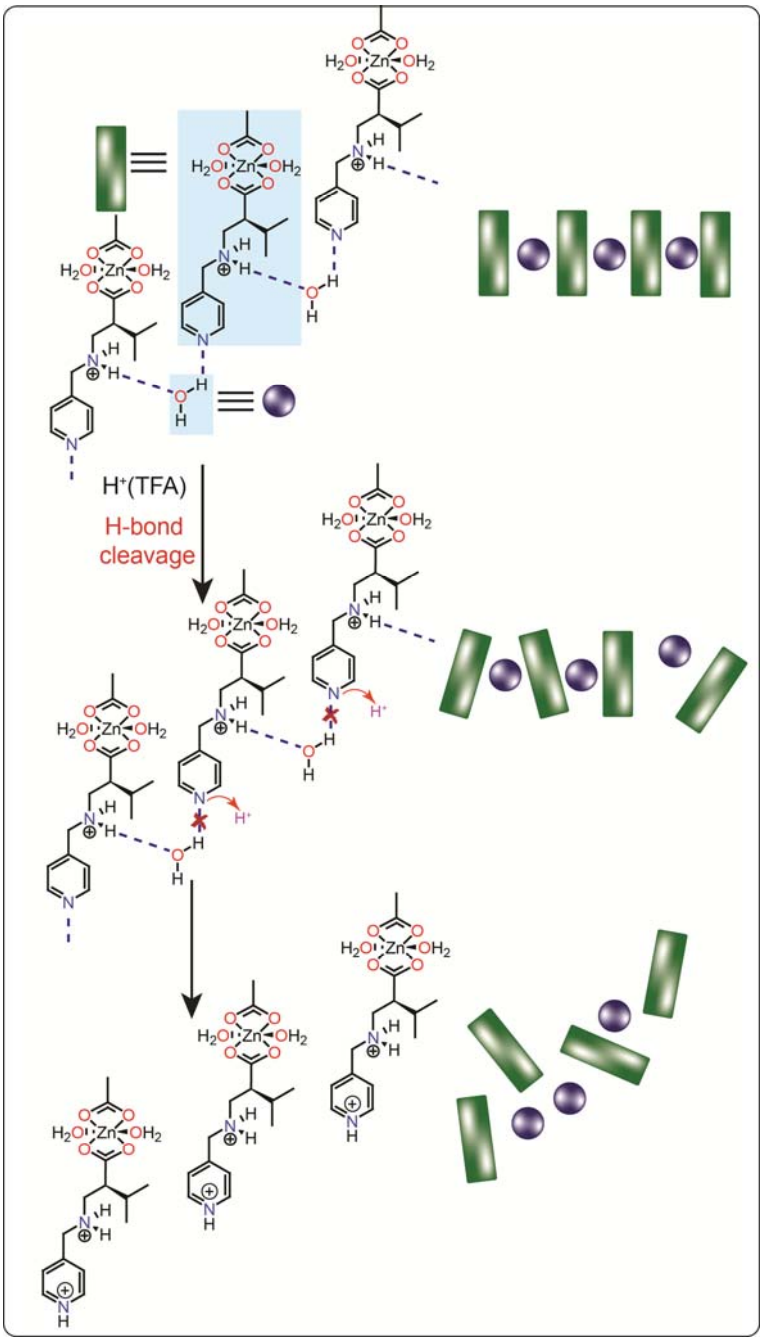

Figure 3.6. Plausible Dissolution mechanism in presence of TFA.

(2) utilization of of ligand-containing polymers for metal complexation (3.12), or (3) host-guest polymer interactions (3.13). To the best of our knowledge, this is the second example of low molecular weight metallohydrogel which shows autonomic self-healing ability (3.14). Figure 3.7 describes the self-healing ability of the supramolecular ZAVP hydrogel in a conventional 'gel block fusion' experiment. ZAVP hydrogel was first synthesized inside a hollow glass cylinder, and further cut

into smaller pieces (Figures 3.7). To our surprise, the gel body was able to support (regardless of time) up to 60-fold its own weight without causing any visible change on its dimensions, shape and consistence (Figure 3.7a-e). Such high load-bearing strength has been found a very rare property for LMW gels (3.14). When different gel blocks were placed in direct contact along the cut surfaces, they were recombined within 3 h at room temperature without the need of any external stimuli. To check the strength of healed portions, we constructed a 30 cm long bridge upon connecting 11 hydrogel blocks, which could be held vertically and horizontally (Figures 3.7 f-h). The experiment was made alternating dye-doped (i.e., Rose Bengal) and undoped gel blocks for the sake of clarity.

3.3. Conclusion.

We have described the facile preparation of new non-polymeric supramolecular metallohydrogels by combining two stock solutions of an amino acid-based ligand (i.e.,L-3-methyl-2-(pyridine-4-yl-methylamino)-butanoic acid) and a Zn(II)salt. These hydrogels displayed unique multiresponsive gel-to-sol and sol-to-gel transitions, as well as remarkable moldable, load-bearing, andautonomic self-healing behavior at room temperature**.**

3.4. Experimental section.

3.3.1. Preparation of amino acid based ligands: The ligand system VP was prepared following a modified literature procedure. To an aqueous solution (8 ml) of L-valine (1g, 8.5 mmol) and Na_2CO_3 (0.46 g, 4.25 mmol), 4-pyridinecarboxaldehyde (0.92 g, 8.5 mmol) in MeOH (5 mL) was added slowly. The solution was stirred for 3 h and cooled in an ice bath. $NaBH_4$ (0.38 g, 10.2 mmol) was added to the solution slowly. The mixture was stirred for 12 h, and 30% perchloric acid (for the ligand L-VP)/ 50% acetic acid (for the ligand L-VA) was used to neutralize the basic (pH~12) reaction mixture and adjust the pH to 7.1-7.2. As a result, in the reaction mixture sodium perchlorate/ sodium acetate (for perchloric acid and acetic acid, respectively) gets generated which eventually plays a very important role in the gelation process. The solution was stirred further for 1 h and then evaporated to dryness. The solid was extracted in hot and dry EtOH, and the filtrate was evaporated to get a white powder. L-VP has been prepared using same procedure. Yield (L-VP): 1.4 g, 70% yield. Yield (L-VA): 1.25g, 65%. The ligand has been crystallized from the aqueous solution the

both. L-VA and L-VP. Crystals were collected and utilized for its characterization. IR (KBr, cm^{-1}):ν_{OH},3421; ν_{as}(CO2), 1562; ν_s(CO2), 1409.^{1}H NMR (D_2O, ppm): -CH_3(1.21, d, 3H), -CH_3 (1.35, d, 3H), -CH (3.20, m, 1H), -HN-CH (3.65, m, 1H), -CH2 (3.82, dd, 2H), py-H (7.34, d, 2H), py-H (8.38, d, 2H).

NOTE: The results of this chapter have already been published ***Chem Commun.***, **2014,** 50, 3004-3006. with the title: "*Amino Acid-based Multiresponsive Low-Molecular-Weight Metallo-hydrogels with Load-bearing and Rapid Self-healing Ability"*. These publications were the results from the group of Dr. Rahul Banerjee and his student Subhadeep Saha from CSIR National Chemical Laboratory, Pune, India. Majority of the work is contributed by Subhadeep with the help of the instrumental facilities of CSIR National Chemical Laboratory.

CHAPTER 4

Dissolvable Metallohydrogels for Controlled Release: Evidence of a Kinetic Supramolecular Gel Phase Intermediate

4.1 Introduction:

Self-assembled supramolecular hydrogels have attracted great attention during the past decades because of promising high-tech applications in very various fields such as biomedicine, nanoelectronics and catalysis (4.1). These colloidal materials can be formed *via* self-assembly of either by low- or high-molecular-weight hydrogelators by means of non-covalent interactions (e.g., π–π stacking, Van der Waals forces, hydrogen bonds, hydrophobic interactions) (4.2). Within these materials, metallohydrogels (4.3) make an important subclass where at least one metallic element has been incorporated by some means into the gel network.

In this chapter, synthesis of two unique, amino acid based LMW metallohydrogels (*viz.* ZNVA and ZPVA; Figure 4.1), which displayed an unprecedented (*opaque gel*)-to-(*transparent gel*) transition for this type of gels, has been described. Moreover, the equilibrated gels exhibit a unique time-dependent dissolution in both water and acidic aqueous solutions (pH ≤ 7), which could be used for the controlled release of entrapped molecules. Figure 4.1 exhibits the spontaneous formation of metallohydrogels, namely ZNVA and ZPVA, upon mixing of two aqueous solutions containing amino acid (L-valine) based ligand [i.e., L-3-methyl-2-(pyridine-4-yl-methylamino)-butanoic acid)] with sodium acetate as ligand systems (**VA**) and Zn(II)-based salts [i.e., zinc nitrate hexahydrate = **ZN** and zinc perchlorate hexahydrate = **ZP**], respectively. In a previous work, we have discussed about a similar metallohydrogel made up of zinc (II) acetate and VA. This hydrogel was found to be self-healing in nature. In addition to that, it also exhibits reversible gel-sol-gel transition in presence of a number of different physical and chemical stimuli. These ligands were easily synthesized by minor modification of a previously reported procedure (4.4). These hydrogels becomes opaque white in color

immediately after formation but loses the opacity over time becoming transparent after standing one week at RT without formation of solution phase intermediate. To the best of our knowledge, the changes in the optical properties of gel-based materials reported so far involve either temperature-stimulated transitions (4.5) or translucent/transparent-to-opaque transitions as a consequence of domain

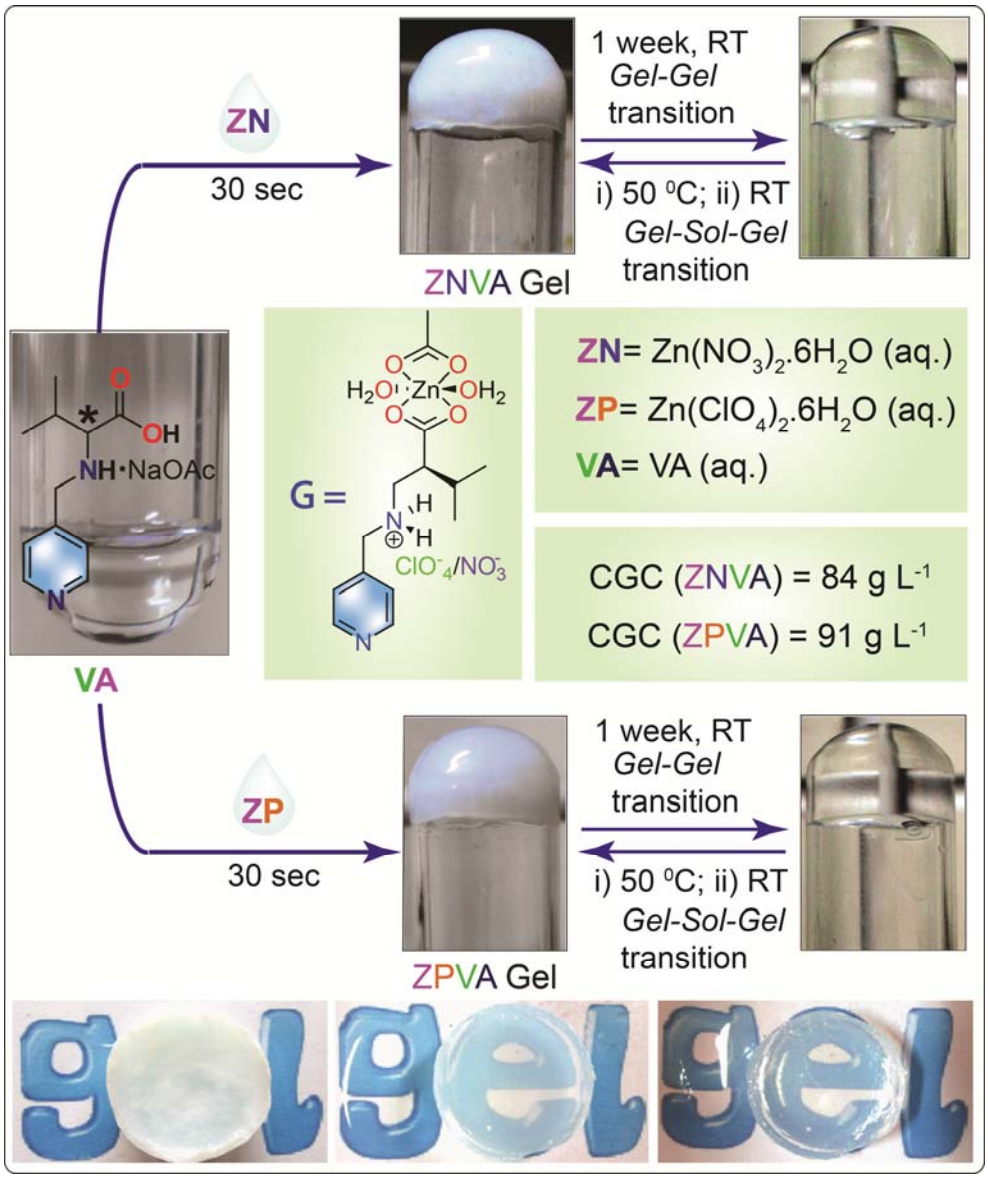

Figure 4.1. *(top)* Synthesis of ZNVA and ZPVA hydrogels at CGC. Total volume of each solution = 0.5 mL. Inset: Plausible structure of the fundamental unit (G) of the gel fiber deduced from MALDI-TOF spectroscopy; *(bottom)* Opaque to transparent conversion of ZNVA hydrogel with time.

Table 4.1. Solvents tested for gelation:

S.No.	Solvent	Phase	Gelation time	Gel-phase color	Kamlet-Taft solvent pararmeters		
					α	β	γ
1	H_2O	G	~30 s	White	1.17	0.47	1.09
2	DMF	P	–	–	0.00	0.69	0.88
3	DEF	P	–	–	–	–	–
4	DMAC	P	–	–	0.00	0.76	0.88
5	NMF	P	–	–	–	–	–
6	Acetone	S	–	–	0.08	0.43	0.71
7	THF	S	–	–	0.00	0.55	0.58
8	CH_3CN	S	–	–	0.19	0.40	0.75
9	MeOH	S	–	–	0.98	0.66	0.60
10	EtOH	S	–	–	0.86	0.75	0.54
11	*i*-PrOH	S	–	–	0.76	0.84	0.48
12	*n*-Hexane	I	–	–	0.00	0.00	-0.04
13	Et_2O	I	–	–	0.00	0.47	0.27
14	EtOAc	I	–	–	0.00	0.45	0.55
15	CH_2Cl_2	I	–	–	0.13	0.10	0.82
16	$CHCl_3$	I	–	–	0.20	0.10	0.58
17	Benzene	I	–	–	0.00	0.10	0.59
18	Toluene	I	–	–	0.19	0.40	0.75
19	DMF/H_2O	S	–	–	–	–	–

[Solvent abbreviations: DMF = *N*,*N*-dimethylformamide; DEF = *N*,*N*-diethylformamide; DMAC = *N*,*N*-dimethylacetamide; NMP = 1-methyl-2-pyrrolidone; THF = tetrahydrofuran. Abbreviations: S = solution; G = stable gel; I = insoluble; P = precipitates; PG = Partial gel.]

aggregation to sizes that start to scatter light (e.g., via crosslinking). However, in our case, the *gel*-to-*gel* transition occurs naturally from an opaque phase to a transparent phase.The original opaque gel phase can be restored upon a heating/cooling treatment on the transparent gel through the corresponding solution phase. The so-obtained opaque gel exhibitsthe same thermal, morphological and mechanical properties than the original opaque gel obtained at RT, and hence it also underwent evolution towards the transparent material upon ageing. The entire cycle can be repeated multiple times without any appreciable change in the obtained materials after each cycle. This phenomenon indicates a reversible transformation in the structure of the supramolecular aggregate in the

presence of water.

4.2. Results and Discussions:

4.2.1. Optimization of stock solution and preparation of hydrogels.

Figure 1 illustrates the synthesis of ZNVA and ZPVA hydrogels which forms upon mixing the aqueous solutions of the two components (0.5 mL each), *viz.* zinc nitrate hexahdrate (ZN, 0.2 M; for ZNVA)/ zinc perchlorate hexahdrate (ZP, 0.2 M; for ZPVA) and ligand system L-VA (0.4 M), which turns into a gel within a few seconds at room temperature.

4.2.2. Gelation ability.

The metallohydrogels discussed in this chapter (ZNVA and ZPVA) (4.6), are similar to previously reported ZAVP hydrogel (4.4a) where the metal ion precursor was zinc acetate (ZA) and (pyridine-4-yl-methylamino)-butanoic acid) with sodium perchlorate (VP) was used as ligand system. ZAVP hydrogel shows self-healing and multiresponsive nature but it is difficult to dissolve it in water under ambient conditions. The minimum gelation concentration (MGC) for opaque ZNVA and ZPVA hydrogel has been found to be 84 g L^{-1} and 91 g L^{-1}, respectively. The hydrogels are thermoreversible in nature and the *gel*-to-*sol* transition temperatures (T_{gel}) were 49 ± 1 ºC and 58 ± 1 ºC for ZNVA and ZPVA, respectively. However, it is noteworthy that, the transparent ZNVA and ZPVA exhibit a lower *gel-to-sol* transition temperature (41 ± 1 ºC and 45 ± 1 ºC, respectively). Complete *sol*-to-*gel* transitions takes place while cooling the corresponding isotropic solutions for 15 minutes. Interestingly, the results obtained from a large screening of metal ions establish that the gelation was specific in the presence of Zn(II) salts as coordinating metal. The contribution of the counter-anion is, however, less critical and similar gel could be obtained by using acetate instead of nitrate and perchlorate. In this chapter, we focus on the detailed study of the ZNVA and ZPVA as model systems.

4.2.3. Mechanical Properties.

The viscoelastic nature of the hydrogels has been established by oscillatory rheological measurements (Figure 4.2). The average storage modulus ($G' > 10^5$ Pa) of as-synthesized gels (6 h after synthesis) has been found to be one order of magnitude higher than the loss modulus (G'') and constant over the entire range of frequencies (0.1-10 Hz) (Figure 4.2).

Reproducible and relatively unchanged dissipation factors (tan $\delta = G''/G' \approx 0.1$) during DFS indicates a good tolerance of the hydrogels to external forces. Furthermore, dynamic time sweep (DTS) measurements at RT (Figure 4.2) at 0.1% strain and 1 Hz frequency confirmed the temporal stability of the hydrogels. These values of mechanical properties remained intact up to 4 days of synthesis of the hydrogels. But, to our surprise, mechanical strength of both the hydrogels deteriorated as they becomes transparent with time. Storage modulus of both of these gels de-escalates (10^4 Pa < G' < 10^5 Pa) with insignificant change in viscous moduli. Brittle nature of the transparent hydrogels can be attributed to their early fracture at strain (deformation) below 10% compared to their opaque counterparts (> 10%) (Figure 4.3). Hence, oscillatory rheological measurements suggest that transparent gel possess a lower mechanical strength than the precursor opaque gel.

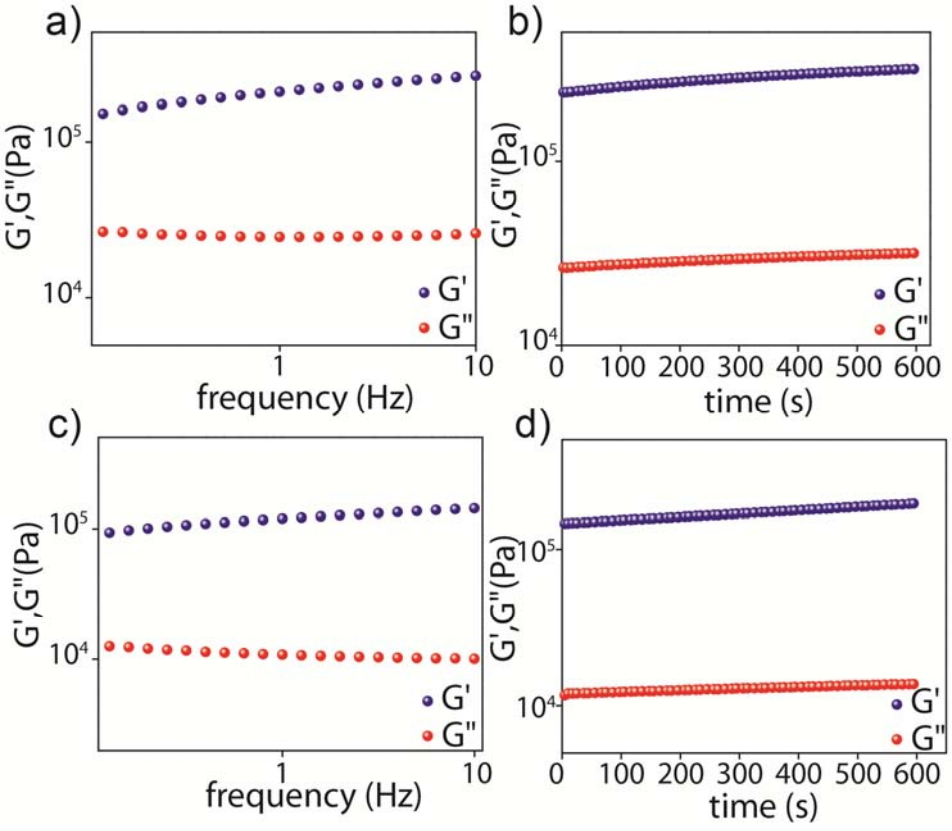

Figure 4.2. Oscillatory rheology of ZNVA and ZPVA hydrogels prepared at the CGC: Dynamic frequency sweep (DFS) experiment at constant strain of 0.1% of a) ZNVA and c) ZPVA hydrogel. b) and d) shows dynamic time sweep measurement at constant frequency of 1 Hz and constant strain of 0.1%.

4.2.4. Morphological properties.

Electron microscopy imaging of the corresponding xerogels proves the presence of nanostructured networks in each case with apparent differences in the crosslink densities (Figure 4.4). TEM images (Figure 4.4) obtained from opaque and transparent gel materials also support the hypothesis based upon the rheological measurements. Initial fibrillar supramolecular aggregates detoriates to smaller and thinner aggregates with time as the gel goes to transparent phase from opaque phase. So, the achievement of a stable transparent gel over time indicates the formation of new aggregates that are shorter in dimension than the visible wavelength region, which is in good agreement with the observed decrement in the storage modulus of the material, albeit the overall network may be more ordered.

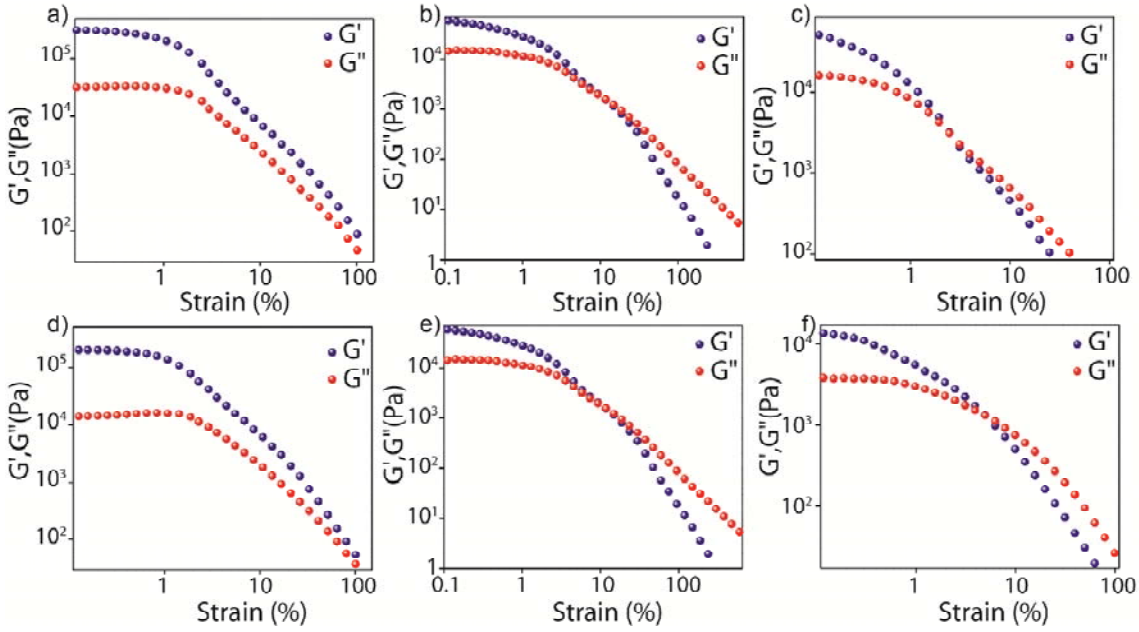

Figure 4.3. Oscillatory rheology of ZNVA and ZPVA hydrogels prepared at the CGC: DSS experiment at constant frequency of 1 Hz of a) of 6 h old, b) 3 days old and c) 7 days old ZNVA gel and c) 6 h old, b) 3 days old and c) 7 days old ZPVA gel.

4.2.5. Thermal Stability.

Difference in thermal stability (Figure 4.5 and b) of the corresponding xerogels also support the gradual weakening of the hydrogels during their journey from opaque to transparent state. Similar pattern of the plots indicates the basic structure of the gel network remains similar in both opaque and transparent state which can also be

illustrated by the PXRD and the IR spectra (Figure 4.5 c-f). But deviation in the patterns (Figure 4.5 and b) arise ~110°C which is indicative of a subtle loss of mass from the gelator self-assembly which eventually reflects in a considerable difference in leftover mass (~6-7%) at the end of the experiment (800 °C).

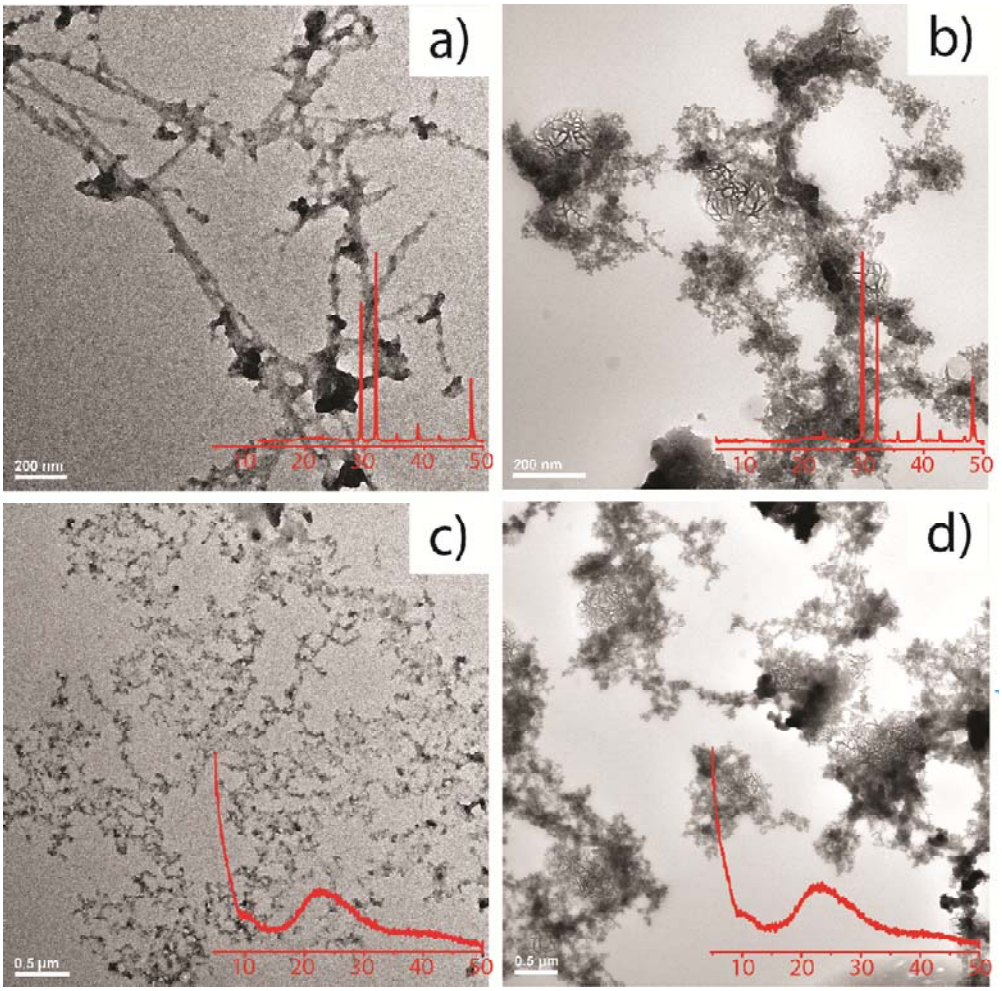

Figure 4.4. TEM image of (a) opaque and (b) transparent ZNVA hydrogels; TEM image of (c) opaque and (d) transparent ZPVA hydrogels; *(inset)* PXRD patterns of the corresponding xerogel materials.

4.2.6. Multiresponsive nature.

ZNVA and ZPVA shows rapid responses towards various stimuli (Figure 4.6a) (e.g., thermal, mechanical, pH), which clearly indicates the dynamic non-covalent and self-assembled nature of the gel network. These two hydrogels showed reversible *sol*-to-*gel*

transition in the presence of acid (TFA) and base (ammonia). The gels turns into a clear solution phase in the presence of TFA due to disruption of the H-bonding network (Figure 4.6c). Addition of ammonia quenches the excess acid, which eventually allows the restoration of the H-bonding and consequently the gel phase. Moreover, addition of ammonia could also solubilize the gel owing to the formation of water soluble zinc tetrammine complex. Addition of TFA neutralizes the ammonia from the metal centre liberating the metal ion for complexation, which subsequently leads to the recovery of the gel phase. This phenomenon indicates the presence of the Zn(II)-complex unit, which self-assembles into individual gel fibers (Figure 4.6).

ZNVA hydrogels, could be easily restored as the original hydrogels upon exposition to the same amount of water that the hydrogels ensnared (Figure 4.6b). ZNVA and ZPVA have also been found to be dissolved in excess of water (i.e., 1.5 times of their volume at the CGC; pH = 7) yielding a colloidal solution within 6-7 h at RT. Although it is expected that the dilution of physical gels prepared at the CGC may cause the collapse of the supramolecular network, the *gel*-to-*sol* transition by simple dilution was in this case exceptionally reliable and completely reversible. Thus, the gel phase could be restored upon evaporation of the same amount of water needed to dissolve the gel (Figure 4.6b).

We utilized MALDI-TOF analysis to get insights into the structure of the gelator and the dissolution mechanism of the hydrogels. Detailed study of the obtained spectra suggested that the metal complex (Figure 4.6c) forms due to the replacement of two water molecules of Zn(II) hexaaquo complex (from the precursor metal salts; zinc nitrate hexahydrate and zinc perchlorate hexahydrate) by ligand V during gelation, is probably the fundamental unit of the gel fiber **G** (Figure 4.1 and Figure 4.6c). The water soluble nature of ZPVA and ZNVA can be explained as Zn (II) co-ordinated to 4 water molecules in G. In contrast, the basic unit of our previously reported hydrogel ZAVP (Figure 4.4a) was more hydrophobic in nature (i.e., Zn(II) was connected to two water molecules, one acetate anion and one molecule of ligand V) which makes it more difficult to get dissolved in water by further solvation of the aggregates. Hence, the inherent hydrophilicity and hydrophobicity of the gelator seems to be one of the key factors that govern the solubility of a bulk hydrogel in water. This also illustrates the detoriation of gel strength during the course of transformation of the hydrogels from

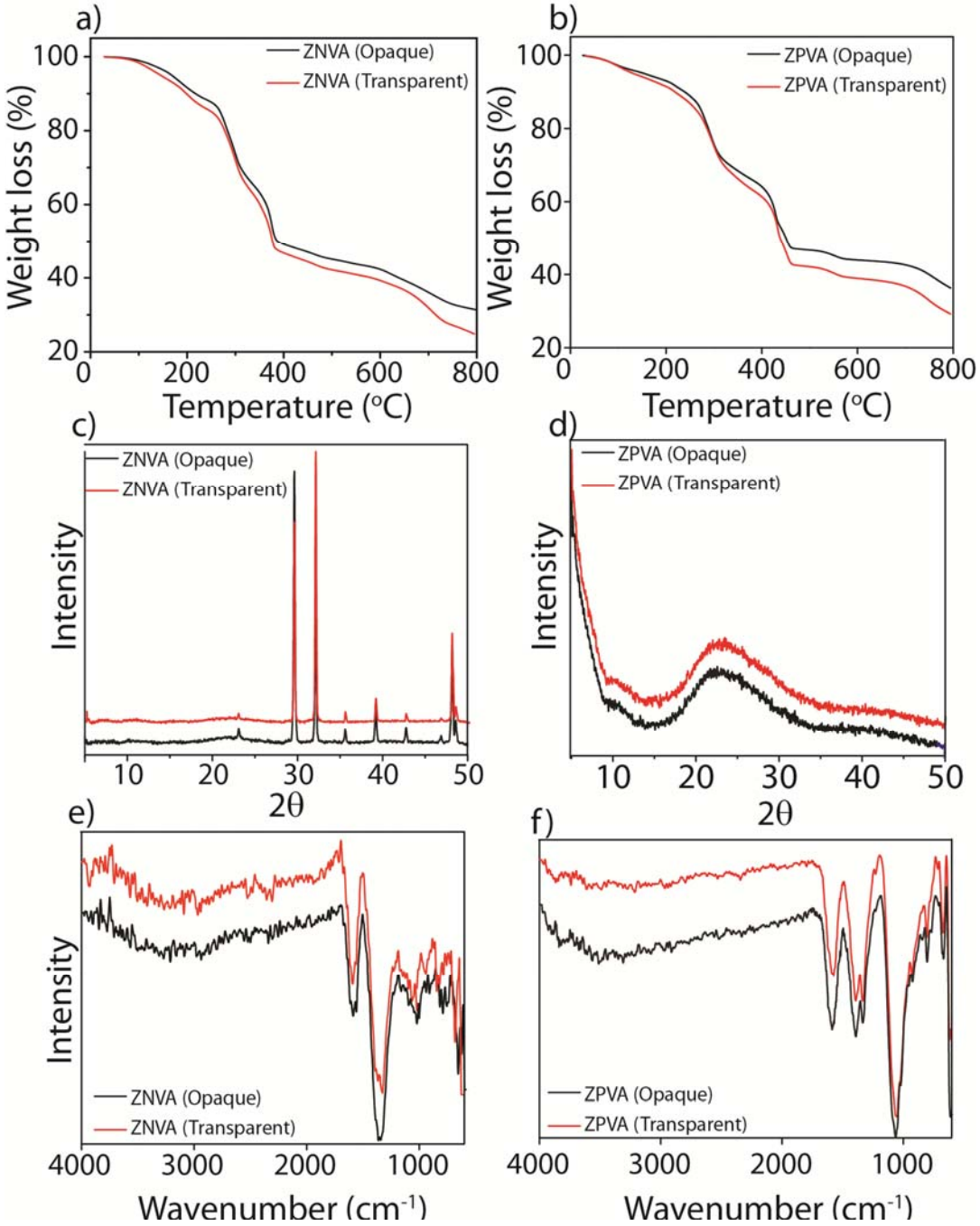

Figure 4.5. Comparison of TGA traces of (a) ZNVA and (b) ZPVA hydrogels, Comparison of PXRD patterns of (c) ZNVA and (d) ZPVA hydrogel and comparison of FTIR patterns of (e) ZNVA and (f) ZPVA hydrogels.

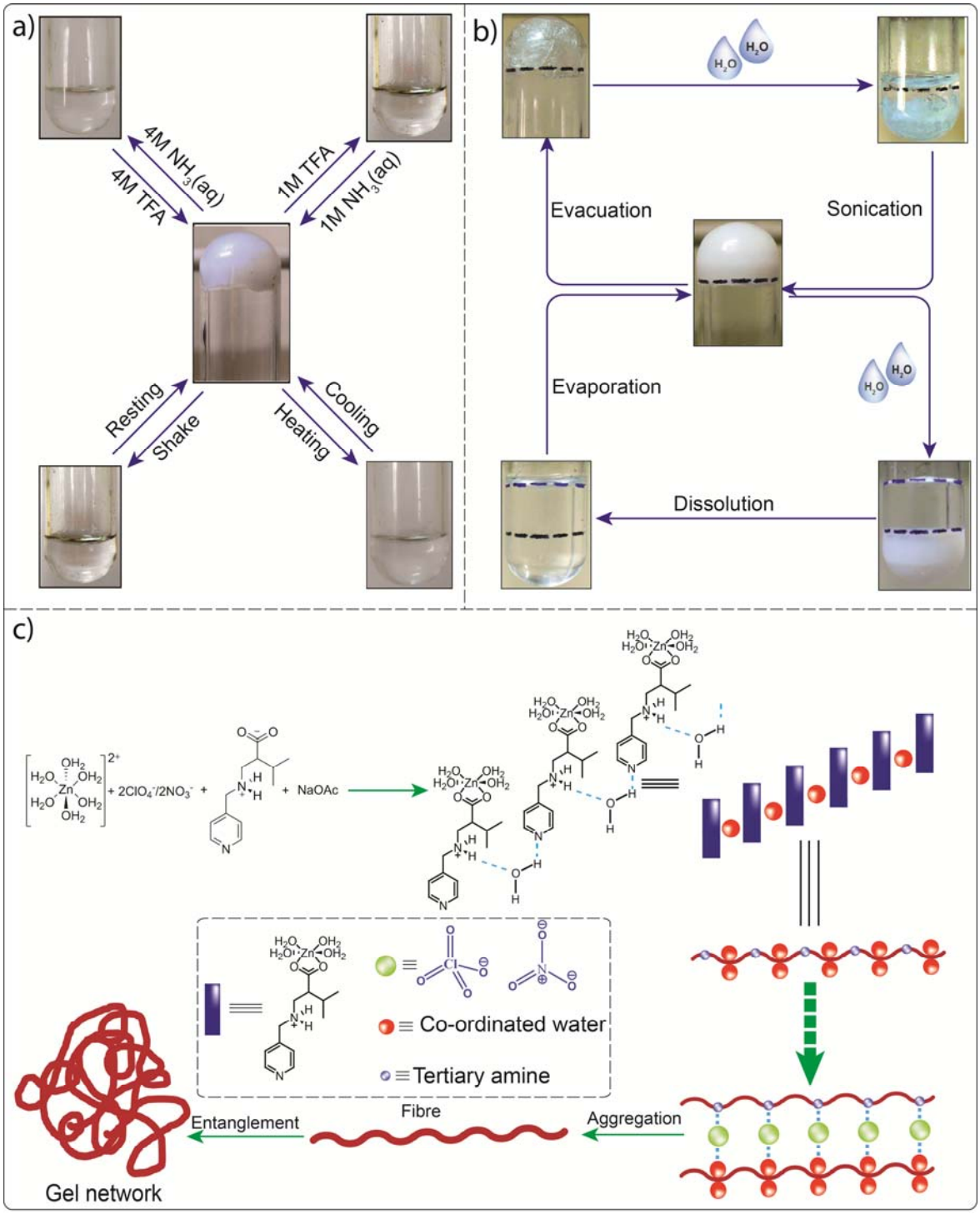

Figure 4.6. a) Multistimuli-responsive nature of ZNVA and ZPVA hydrogels; b) ZNVA and ZPVA hydrogels show *gel*-to-*sol* and *gel*-to-*xerogel* reversible transitions and c) plausible mechanism of formation of the gelator complex and subsequent formation of supramolecular aggregate.

Furthermore, we found that the xerogels derived from the corresponding ZPVA and

opaque to transparent state. The hydrophilic nature of the gelator (G) makes it remain in equilibrium with precursor components (zinc (II) hexaaquo complex and the ligand V) in presence water. Hence, the gradual hydrolysis of the gelator in the self-assembly weakens the fibers and yields to transparent hydrogels of poor mechanical strength. The transparent hydrogels can go back to their orginal opaque state through *sol-gel* transition by heating.

4.2.7. Controlled release of guest molecules.

Time-dependent and efficient solubility of ZNVA and ZPVA hydrogels in neutral as well

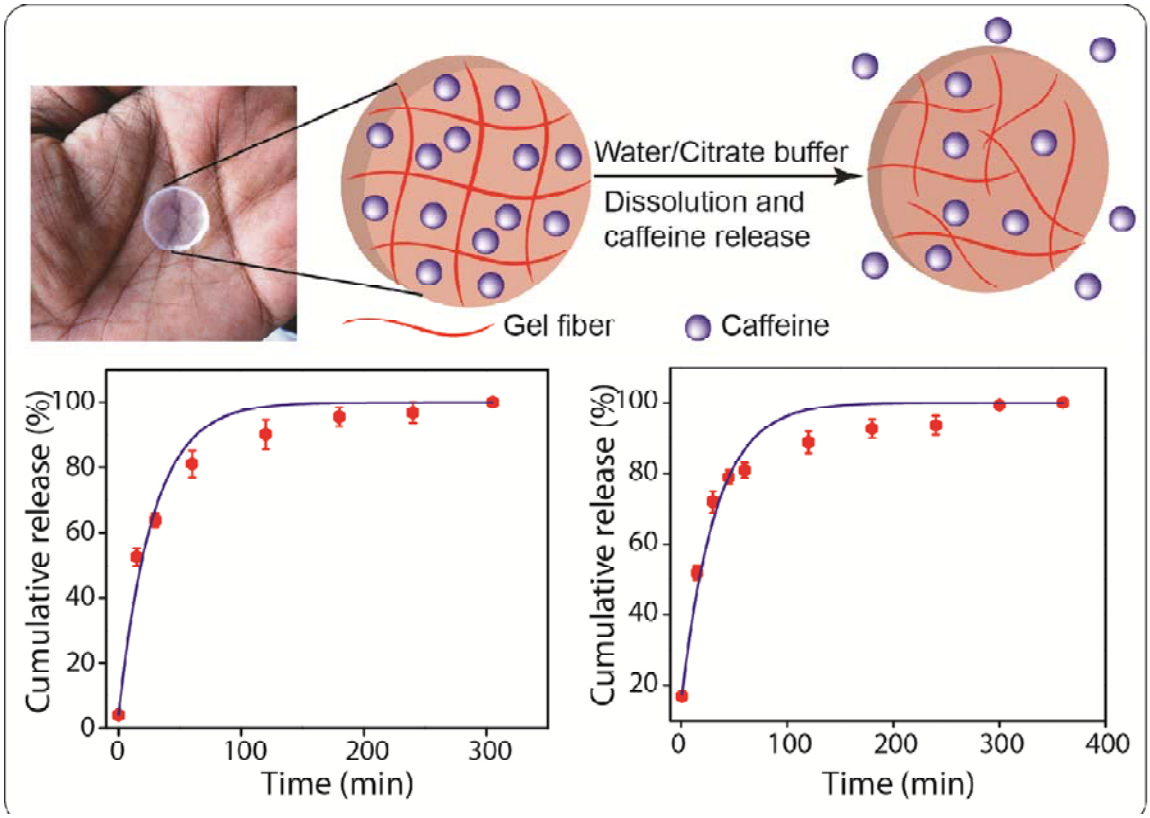

Figure 4.7. a) Self-standing caffeine-loaded hydrogel and caffeine release duirng dissolution of the gel matrix. b)-c) Cumulative release profile in b) citrate buffer and c) water.

as acidic pH motivated us to study the encapsulation and simultaneous degradation-release behavior of these materials using caffeine as a model drug. Although caffeine is a

small polar compound, it is enough hydrophobic to pass through biological membranes. Hence, it has been used in numerous studies as a model compound to examine the ability of hydrogel materials as drug delivery vehicles (4.7). In the present study, we employed 2 mL gel blocks having a caffeine concentration of 0.15 g L^{-1}. These blocks have been immersed in 4 mL citrate buffer (pH = 4.74) and 4 mL deionized water (pH = 7) separately. The dissolution of the gel, as well as the subsequent cumulative drug release has been monitored over time. As shown in Figure 4.7, the caffeine loaded ZNVA exhibits a sustained release of caffeine until it got completely dissolved within 5 h in citrate buffer and 6 h in water (Figure 4.7).

4.3. Conclusion.

We have shown the facile synthesis of two novel non-polymeric supramolecular metallohydrogels by combining an amino acid-based ligand (i.e., L-3-methyl-2-(pyridine-4-yl-methylamino)-butanoic acid) and Zn(II) salts. These hydrogels displayed a unique reversible opaque to transparent phase transition at room temperature, multiresponsive and reversible gel-to-sol and xerogel-to-geltransitions, as well as gradual dissolution in aqueous medium within a wide range of pH at RT. This smooth transition was employed for the *in vitro* release of a model polar drug at both neutral and acidic pH. The unprecedented (opaque gel)-to-(transparent gel) transition evidences the formation of a kinetic supramolecular gel that undergoes self-evolution towards a different gel network of lower energy. The isolation of this intermediate gel phase may have important mechanistic implications on the theory of gelation.

4.4. Experimental section.

4.4.1. Preparation of amino acid based ligands: The ligand system VA was prepared following a modified literature procedure. To an aqueous solution (8 ml) of L-valine (1g, 8.5 mmol) and Na_2CO_3 (0.46 g, 4.25 mmol), 4-pyridinecarboxaldehyde (0.92 g, 8.5 mmol) in MeOH (5 mL) was added slowly. The solution was stirred for 3 h and cooled in an ice bath. $NaBH_4$ (0.38 g, 10.2 mmol) was added to the solution slowly. The mixture was stirred for 12 h, and 50% acteic acid was used to neutralize the basic (pH~12) reaction mixture and adjust the pH to 7.1-7.2. As a result, in the reaction mixture sodium acetate gets generated which eventually plays a very important role in the gelation

process. The solution was stirred further for 1 h and then evaporated to dryness. The solid was extracted in hot and dry EtOH, and the filtrate was evaporated to get a white powder. Yield (L-VA): 1.232g, 74%. The ligand has been crystallized from the aqueous solution of L-VA. Crystals were collected and utilized for its characterization. IR (KBr, cm^{-1}):ν_{OH},3421; ν_{as}(CO2), 1562; ν_s(CO2), 1409.^{1}H NMR (D_2O, ppm): -CH_3(1.21, d, 3H), -CH_3 (1.35, d, 3H), -CH (3.20, m, 1H), -HN-CH (3.65, m, 1H), -CH2 (3.82, dd, 2H), py-H (7.34, d, 2H), py-H (8.38, d, 2H).

NOTE: The results of this chapter have already been published ***Chem Commun., 2014,*** 50 (53), 7032 - 7035. with the title: "*Dissolvable Metallohydrogels for Controlled Release: Evidence of a Kinetic Supramolecular Gel Phase Intermediate".* These publications were the results from the group of Dr. Rahul Banerjee and his student Subhadeep Saha from CSIR National Chemical Laboratory, Pune, India. Majority of the work is contributed by Subhadeep with the help of the instrumental facilities of CSIR National Chemical Laboratory.

CHAPTER 5

Photocatalytic Metal-Organic Framework from CdS Quantum Dot Incubated Luminescent Metallohydrogel

5.1 Introduction:

Gels are comprised of solid gelators and liquid molecules entrapped by surface tension (5.1). The gelators (predominantly polymeric species) form continuous, three dimensional cross-linked fibrillar structure which spans through the matrix allowing copious amount (generally > 90%) of liquid to get immobilized inside the voids (5.2). Apart from the conventional polymeric gelators, low molecular weight gelators (LMWGs) have attracted much attention in past decade owing to their potential applications in nanoelectronics, catalysis and biomedicines (5.3). In addition, LMWGs have garnered recognition as host matrix for various inorganic guests such as noble metal nanoparticles and metal chalcogenide quantum dots (CdS, CdTe) (5.4). The intention behind incorporation of the inorganic nanoparticles in the gels is to make an attempt to organise these nanoparticles on the 3D gelator matrix in a bid to tune the property of the nanoparticles (5.5). However, one finds limited examples of such composite materials with promising property that could be useful for construction of such functional materials (5.6).

In this chapter, we have described a simple one-pot synthetic protocol for uncapped CdS quantum dots in a low-molecular weight metallohydrogel (ZAVA) matrix. This CdS incubated metallohydrogels (CdS@ZAVA gel) exhibits tunable luminescence with time due to size increment of the uncapped quantum dots particles embedded inside the gel matrix. These hydrogels can easily be transformed to dry xerogel form (CdS@ZAVA xerogel) which shows stable luminescence colour under UV light as the sizes of the quantum dots remain unchanged with time inside the solid gelator matrix. Moreover, this metallohydrogel (CdS@ZAVA) can be transformed into luminescent CdS embedded metal-organic framework (ZAVCl MOF) via a unique sodium chloride-mediated room temperature process. Metal-Organic Frameworks

(MOFs) are smart materials which showcase promising applications in the fields of gas storage, catalysis, drug delivery, separation, proton and charge carrier transport (5.7). These crystalline porous materials are mainly synthesized by hydrothermal (5.7a, 5.7c), room temperature (5.7j, 5.7k) or mechanochemical (5.7l) method. However, gel-mediated crystal growth process, which has been well-established as one of the efficient methods to synthesize a large variety of important crystalline materials like metal oxides, zeolites and organic molecules (5.8), has rarely been employed to synthesize MOFs. In this present work we have made an attempt to provide a simple, unprecedented, single step method to obtain high quality MOF single crystals at room temperature via destruction of a low molecular weight metallohydrogel, ZAVA. It is noteworthy that, Yaghi *et al.*, were the first to synthesize a MOF exploiting gel-mediated crystal growth procedure by using inert nonaqueous poly(ethyleneoxide) (PEO) gel as a crystal growth matrix (5.9). Further to that, Steed and co-workers employed low-molecular weight organogels as inert gel matrix for synthesis of single crystals of a range of important organic molecules including APIs (5.10). As mentioned before, we can synthesize uncapped CdS quantum dots in the ZAVA metallohydrogel matrix and subsequently degrade this CdS@ZAVA metallohydrogel to MOF-CdS quantum dot composite single crystals. Synthesis of other MOF-quantum dot composites found in the literature (5.11) requires via multi-step, energy-expensive procedure. To the best of our knowledge, this kind of *in situ* loading of quantum dots in the MOF via self-degradation of CdS-loaded gel is unheard-of. This composite MOF (CdS@ZAVCl) can be used as an efficient photocatalyst for visible light-driven water splitting reaction for production of hydrogen gas (5.12).

5.2 Results and discussion:

5.2.1 Synthesis of quantum dot incubated ZAVA metallohydrogel:

In general, immobilization of quantum dots in a gel (or any host matrix, *e.g.* MOF etc.) requires two steps; i) preparation of quantum dots in presence of capping agent (to avoid agglomeration to bigger particles); ii) entrapment of these quantum dots in the host matrix during its synthesis. On the contrary, synthesis of CdS@ZAVA gel exhibits a unique way for one-pot synthesis of functional composite materials containing CdS quantum dots. This composite material shows tunable luminescence property (white to

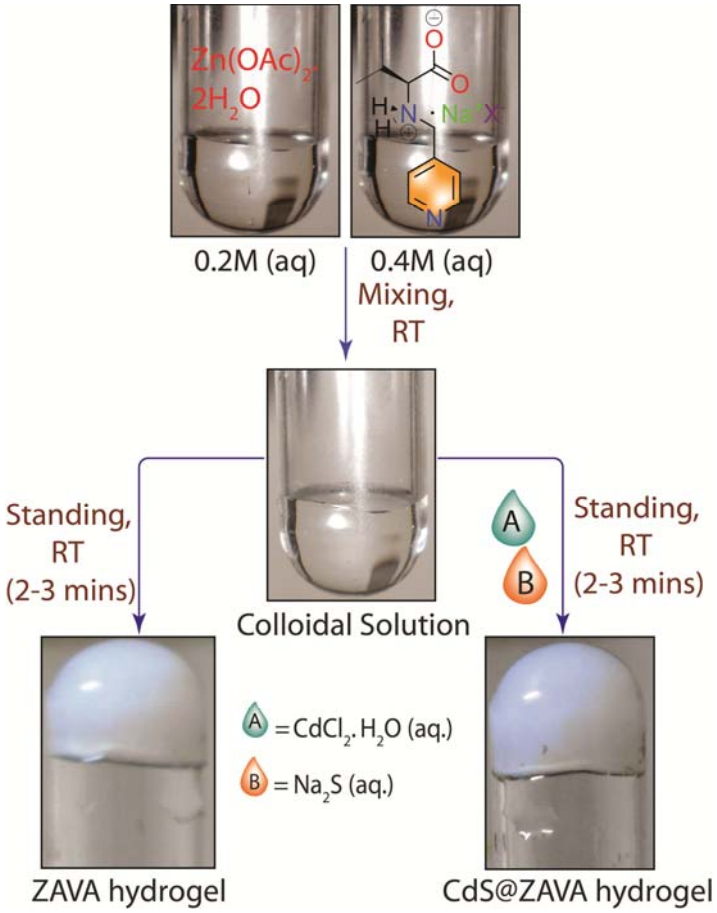

Figure 5.1. Schematic representation of synthesis of the pristine ZAVA gel and CdS incubated ZAVA gel.

yellow to orange) as a consequence of slow aggregation process of the entrapped quantum dots with time (Figure 5.2). However, the augmentation of the quantum dots and the luminescence color of the composite gel can be restricted by transforming this gel to solid xerogel. ZAVA xerogel re-converts to the original gel phase upon addition

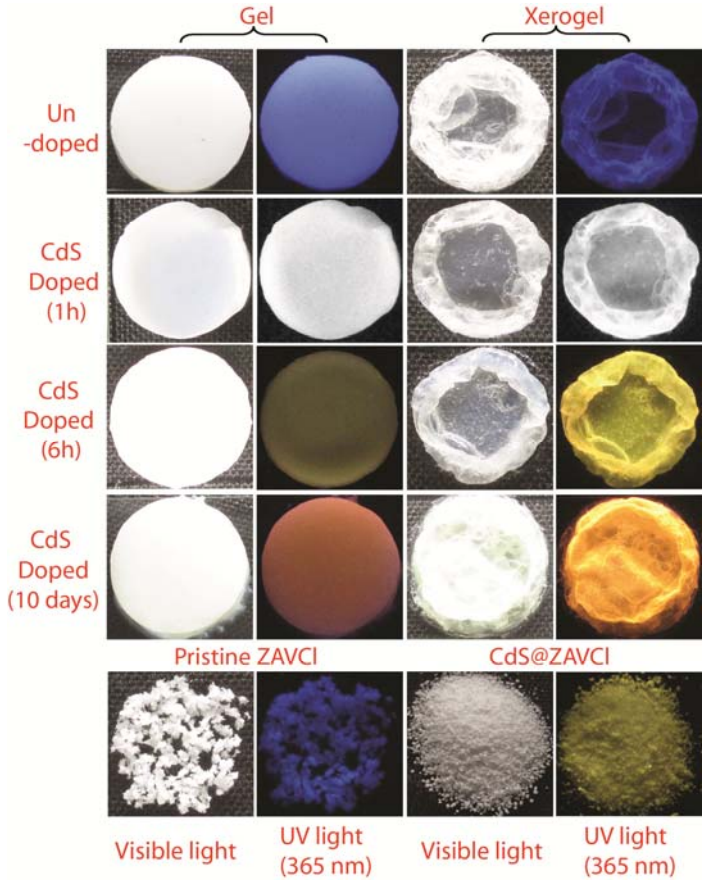

Figure 5.2. Pristine and CdS incubated ZAVA gel and xerogels under visible light and UV light (365 nm).

of equal amount of water extracted during synthesis if the xerogel via vacuum drying. This incident suggests vacuum drying process doesn't destroy the integrity of the material. Figure 5.1 illustrates the rapid formation of ZAVA hydrogel upon mixing of two stock aqueous solutions containing ZA (Zinc acetate dehydrate) and VA [an L-Valine based molecule, i.e., V = L-3-methyl-2-(pyridine-4-yl-methylamino)-butanoic acid and sodium acetate as ligand system], via formation of a transient colloidal suspension phase. The CdS@ZAVA gel can be obtained if aqueous solutions of $CdCl_2 \bullet H_2O$ and $Na_2S \bullet xH_2O$ were added to the aforementioned transient ZAVA colloidal suspension one after another with vigorous shaking.

As mentioned previously, in order to obtain CdS loaded ZAVA gel, first the aqueous solution of $CdCl_2$ and then the aqueous solution of Na_2S have to be added to the colloidal solution one after another. Gelator complex is allowed to form first in this

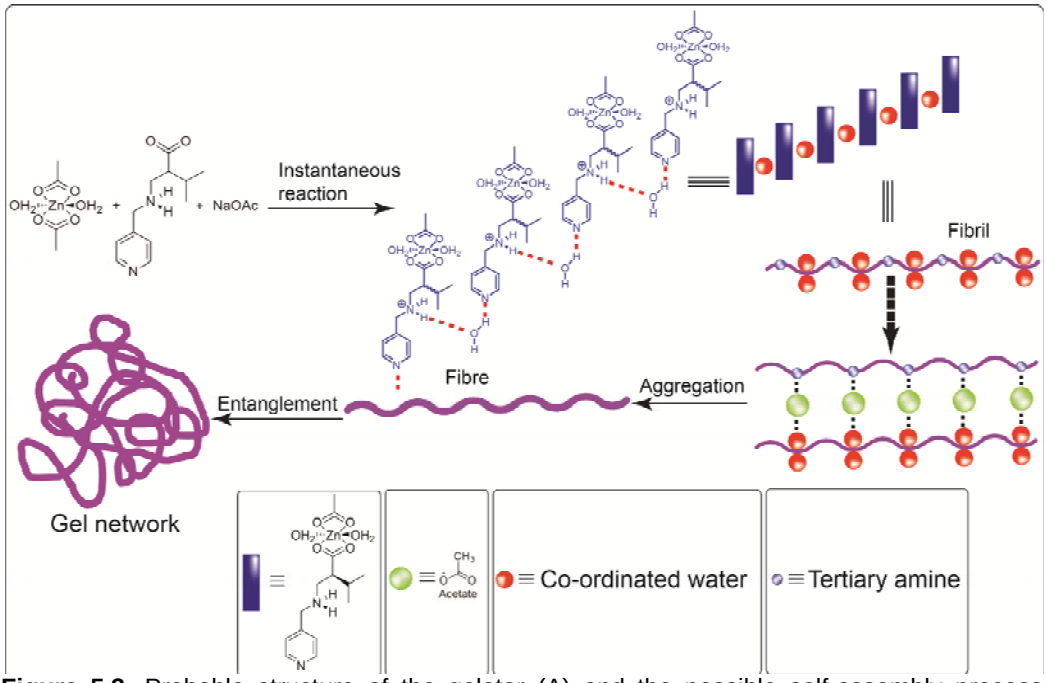

Figure 5.3. Probable structure of the gelator (A) and the possible self-assembly process leading to the formation of gel network.

process. $CdCl_2$ is not recommended to be added in the beginning while mixing of ZA and VA solutions to avoid undesired reaction between Cd^{2+} and VA. After mixing $CdCl_2$ to the colloidal solution, Na_2S has to be added slowly with vigorous shaking as a sudden addition would cause an unwanted formation of ZnS as precipitate. On the other hand, large particles of ZnS (>50 nm) forms (Figure 5.9) if the addition of $CdCl_2$ is skipped and only Na_2S is added directly to the colloidal solution immediately after mixing of ZA and VA solutions. Further studies (*vide infra*) establishes that the incorporated CdS particles are CdS quantum dots (<10 nm in size). To the best of our knowledge, this is a rare single-pot synthesis and immobilization procedure of any semiconductor quantum dot in a gel matrix without any capping agent. There is only one report in the literature related to this phenomenon which describes a complex multistep synthesis of a CdTe nanocrystal doped Cd^{2+} based hydrogel (5.13). The ability of ZAVA gel to immobilize CdS particles of sub-10-nm size can be attributed to the presence of pyridine moiety in the VA ligand. Recent reports (5.14) on nucleotide (*e.g.* ATP, adenosine triphosphate) capped quantum dot nanocrystals unveil that the pyridinic nitrogens of adenine binds to the metal ion of inorganic nanocrystals to restrict

Table 5.1. Solvents tried for gelation:

S.No.	Solvent	Phase	Gelation time	Gel-phase color	Kamlet-Taft solvent pararmeters		
					α	β	γ
1	H_2O	G	~30 s	White	1.17	0.47	1.09
2	DMF	P	–	–	0.00	0.69	0.88
3	DEF	P	–	–	–	–	–
4	DMAC	P	–	–	0.00	0.76	0.88
5	NMF	P	–	–	–	–	–
6	Acetone	S	–	–	0.08	0.43	0.71
7	THF	S	–	–	0.00	0.55	0.58
8	CH_3CN	S	–	–	0.19	0.40	0.75
9	MeOH	S	–	–	0.98	0.66	0.60
10	EtOH	S	–	–	0.86	0.75	0.54
11	*i*-PrOH	S	–	–	0.76	0.84	0.48
12	*n*-Hexane	I	–	–	0.00	0.00	-0.04
13	Et_2O	I	–	–	0.00	0.47	0.27
14	EtOAc	I	–	–	0.00	0.45	0.55
15	CH_2Cl_2	I	–	–	0.13	0.10	0.82
16	$CHCl_3$	I	–	–	0.20	0.10	0.58
17	Benzene	I	–	–	0.00	0.10	0.59
18	Toluene	I	–	–	0.19	0.40	0.75
19	DMF/H_2O	S	–	–	–	–	–

[Solvent abbreviations: DMF = *N*,*N*-dimethylformamide; DEF = *N*,*N*-diethylformamide; DMAC = *N*,*N*-dimethylacetamide; NMP = 1-methyl-2-pyrrolidone; THF = tetrahydrofuran. Abbreviations: S = solution; G = stable gel; I = insoluble; P = precipitates; PG = Partial gel.]

their growth to larger clusters. We assume that, the pyridinic nitrogen of VA ligand (Figure 5.3), which takes part in H-bonding in ZAVA gel network (Figure 5.3) binds to the CdS quantum dots and stabilizes the quantum dots within the gel matrix. However, pyridine moieties are known as labile capping agents for quantum dots hence growth of quantum dots cannot be hindered fully which consequences tunable luminescence of CdS@ZAVA gel with time.

5.2.2 Gelation ability:

Contrary to typical heating-cooling protocol, gelation phenomenon discussed here takes place efficiently at room temperature (25-30 °C). This combination of metal salt

(ZA)

and ligand (VA) cannot afford gelation in most of the protic and aprotic solvents (please see the Table 5.1 for the list of solvents that have been tried for gelation) but water. This feature can be attributed to H-bond donor (5.15) (N_{amine}-H...O_{Water}) and acceptor (O_{Water}-H...$N_{Pyridine}$) nature of the gelator complex (Figure 5.3). The organic part (VA) of the gelator contains amine functionality in protonated form ($–RNH_2^+$) which acts as a H-bond donor by accepting lone pair of electrons from electronegative element (*e.g.* oxygen of water) via its electron deficient proton to form H-bonding. It (VA) also contains a pyridine functionality which can act as H-bond acceptor. Hence, for a efficient gelation to take place, a solvent like water is required which is capable of acting as both H-bond donor (α = 1.17) as well as acceptor (β = 0.47) (5.16). This leads to an assembly of water molecule and the gelator complex which results in the oxygen of water) via its electron deficient proton to form H-bonding. It (VA) also contains a pyridine functionality which can act as H-bond acceptor. Hence, for a efficient gelation to take place, a solvent like water is required which is capable of acting as both H-bond donor (α = 1.17) as well as acceptor (β = 0.47) (5.16). This leads to an assembly of water molecule and the gelator complex which results in the formation of gel network. The ligand VA yields precipitates with most of the other metal salts [*e.g.* common salts of Ca(II), Mg(II), Al(III), Fe(III/II), Co(II/III), Ni(II) etc.], but forms gels in water with zinc nitrate hexahydrate [$Zn(NO_3)_2$•$6H_2O$ = ZN as ZNVA gel] and zinc perchlorate hexahydrate [$Zn(ClO_4)_2$ •$6H_2O$ = ZP as ZPVA gel]. Zn $(NO_3)_2$•$6H_2O$ and Zn $(ClO_4)_2$ •$6H_2O$ fail to form any gel with VA ligand in presence of Na_2S (5.17).

5.2.3 Synthesis of CdS@ZAVCl MOF from CdS@ZAVA gel:

CdS quantum dot is a well known low band gap semiconductor material which has intrinsic ability to absorb light in the visible region. Hence, it is used as a photosensitizer in several composite photocatalyst material used in visible light water splitting reaction (5.18). However, direct use of either of these two composites [CdS@ZAVA gel and its xerogel] as a photocatalyst for water splitting reaction is practically impossible as the gel dissolves in water and the xerogel forms gel in presence of water. This problem provoked us to synthesize water stable CdS loaded material. We have recently reported that, ZAVCl-MOF (5.19c),

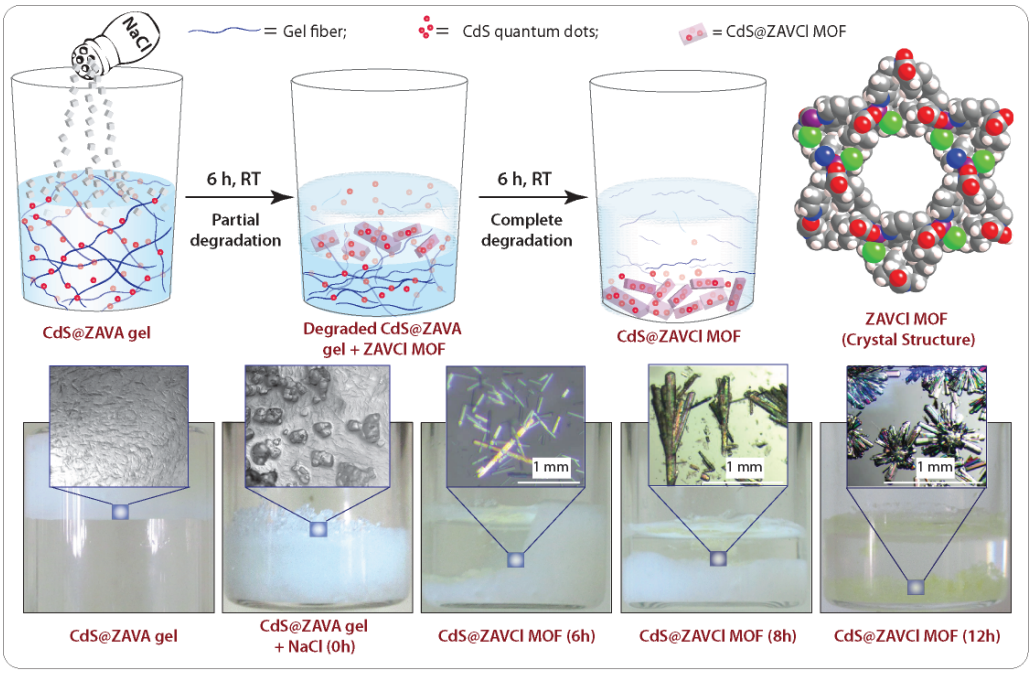

Figure 5.4. (*Top*)Schematic representation of production of CdS loaded ZAVCl MOF (CdS@ZAVCl-MOF) from CdS loaded ZAVA gel (CdS@ZAVA gel) and spacefill representation of crystal structure of ZAVCl (view through c- axis. Color code: carbon= grey, hydrogen= white, zinc= purple, chlorine= green, nitrogen= blue, oxygen=red). (*Below*) Real-time digital photographs of CdS@ZAVA gel to CdS@ZAVCl MOF conversion process. [Reprinted with permission from (5.19d). Copyright 2014 ACS]

which has been synthesized utilizing zinc acetate dihydrate as metal ion precursor and a ligand similar to VA [mixture of (V = L-3-methyl-2-(pyridine-4-yl-methylamino)-butanoic acid and sodium chloride], is stable in water. Crystal structure of ZAVCl- MOF unveils the presence of a chloride ion in the co-ordination environment of Zn^{2+} along with two oxygen (from two carboxylates) and two nitrogens (one from pyridine and one from amine of the ligand) (5.19c). We used this knowledge to synthesize ZAVCl-MOF from ZAVA gel by simple addition of chloride salt (NaCl, KCl, NH_4Cl etc) at room temperature. It is worth mentioning that, this 'room temperature gel-to-crystal' method yields millimetre sized rod-shaped, transparent ZAVCl-MOF crystals (Figure 5.4) contrary to the conventional solvothermal procedure which yields much smaller sized crystals (~50 μm) at high temperature condition (90°C) (5.19c). CdS@ZAVA gel faces a similar fate as ZAVA gel in presence of chloride salts

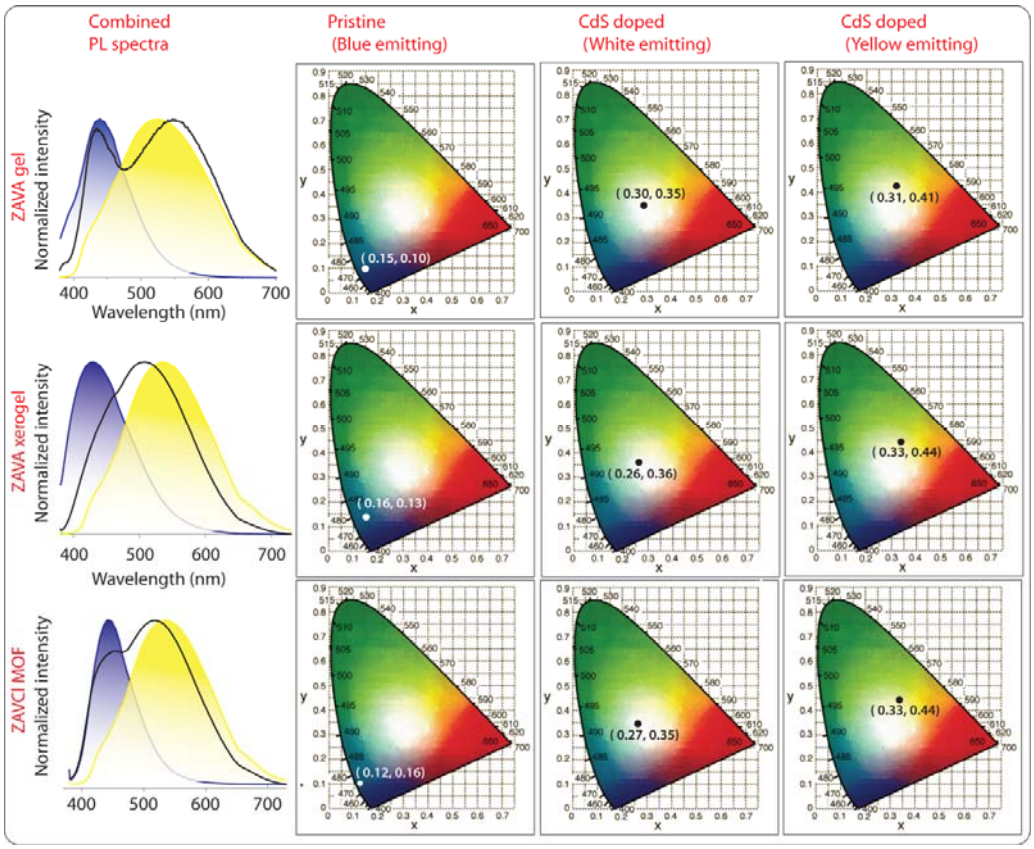

Figure 5.5. PL spectra and CIE chromaticity diagram for pristine and CdS doped ZAVA gel, xerogel and ZAVCl-MOF.

producing CdS quantum dot embedded ZAVCl-MOF crystals (Figure 5.4) at room temperature. To the best of our knowledge, this is the simplest immobilization procedure of any quantum dot nanoparticle in MOF matrix till date (5.11). These CdS quantum dot cannot afford to reside inside the pore of the MOF (pore diameter = 1.2 nm) as they are bigger in size (5-9 nm) than the pore. They don't remain adhered on the outer surface of crystal as their photoluminescence as well as their photocatalytic activity doesn't vary even after several washings in water. Hence, these quantum dots are presumably sandwiched between inter-crystallite surfaces of ZAVCl-MOF (5.11d).

5.2.4 Optical properties:

5.2.4.1 ZAVA gel and xerogel:

All the materials discussed above (pristine and CdS incubated gel, xerogel) looks white under visible light but they exhibit different luminescence colors under UV light (Figure

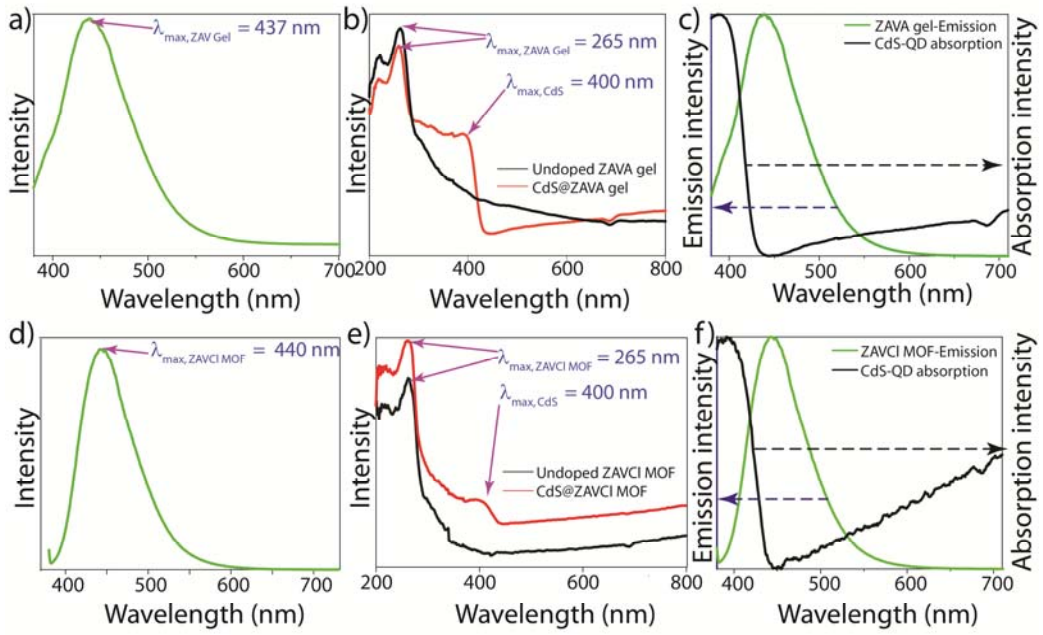

Figure 5.6. a) PL spectra of undoped ZAVA Gel; b) UV-Vis absorbance spectra of undoped and CdS doped ZAVA Gel; c) Overlap of emission spectra of ZAVA gel and absorpion spectra of CdS; d) PL spectra of undoped ZAVCl MOF; e) UV-Vis absorbance spectra of undoped and CdS doped ZAVCl MOF and f) Overlap of emission spectra of ZAVCl MOF and absorpion spectra of CdS.

5.2). The as synthesized ZAVA gel and xerogel exhibit strong blue luminescence (Figure 5.2) under UV light (365 nm) with PL maxima (λ_{em}) of 437 and 429 nm respectively (Figure 5.2 and 5.4). Astonishingly, luminescence color as well as PL maxima of ZAVA gel changes abruptly upon doping of CdS in the ZAVA gel matrix.

The luminescence color of CdS@ZAVA gel transforms to white from blue upon standing at room temperature for ~1h after doping of CdS. PL spectra also changes accordingly and exhibits a broad spectrum, comprising of two humps containing maxima at 434 and 548 nm, spanning the entire visible region (Figure 5.4). This particular stage of CdS@ZAVA gel reveals CIE co-ordinates (0.30, 0.35) (Figure 5.4) which is ideal for white emission in accordance with 1931 CIE coordinate diagram.[20] This transformation can be attributed to the transfer of energy between two chromophoric units (ZAVA gel acts as donor and CdS quantum dots as acceptor chromophore) present in the system (see section S4 in ESI). The optical properties of CdS@ZAVA xerogel composite materials reveal that it has two chromophoric units-ZAVA gel with blue fluorescence ($\lambda_{max,em}$ = 437 nm; λ_{ex} = 365 nm; Figure 5.6b) that

acts as a donor chromophore and CdS quantum dots ($\lambda_{max,abs}$ = 400 nm) incorporated in the ZAVA gel that acts as an acceptor chromophore. The spectral overlap of ZAVA gel emission and CdS absorption (Figure 5.6c) indicates the potential formation of a possible donor-acceptor couple resulting in an excitation energy transfer. The fluorescence lifetime decay profiles of CdS@ZAVA gel (λ_{ex}=370 nm, λ_{em} =430 nm) exhibits a remarkable shortening of the lifetime upon loading of CdS quantum dots, thereby clearly indicating an energy transfer. The corresponding xerogel derived from white-emitting CdS@ZAVA gel also exhibit white luminescence [CIE co-ordinates (0.25, 0.31); Figure 5.2] under 365 nm UV light. PL spectra also shows broad spectrum covering the whole visible region as obtained in the case of CdS@ZAVA gel (Figure 1b). The luminescence colour of CdS@ZAVA gel appears to be transient and gradually turns to yellow (after ~6h) followed by orange (after ~10 days) presumably due to the slow growth process of the CdS quantum dots in the gel matrix. Yellow and orange luminescent gels have also been found to yield xerogels of similar luminescent colour (Figure 5.2).

5.2.4.2 ZAVCl MOF:

Similar to pristine ZAVA gel, pristine ZAVCl-MOF also exhibits blue fluorescence under UV excitation (365 nm, Figure 5.2). Similarly white luminescent CdS@ZAVA gel can be converted to white-luminescent MOF [CIE co-ordinates (0.27, 0.35), Figure 3d] upon reaction with NaCl. Moreover, the CdS@ZAVCl MOF derived from yellow CdS@ZAVA gel also shows yellow fluorescence. This transformation of photoluminescence colour of ZAVCl MOF in presence CdS quantum dots doped inside can be attributed to the possible energy transfer between the donor (ZAVCl MOF) and acceptor chromophore (CdS quantum dots) present in the composite (CdS@ZAVCl MOF; Figure 5.6). Photolominescence spectra as well as the CIE chromaticity diagram of all the materials (pristine and CdS incubated gel, xerogel and MOF materials) has been detailed in Figure 3.

5.2.5 Mechanical properties ZAVA and CdS@ZAVA gel:

The viscoelastic gel nature of ZAVA and its CdS-doped analogues was confirmed from their mechanical properties in dynamic rheological experiments (Figure 5.7).

Both pristine ZAVA gel and CdS@ZAVA gel shows an average storage modulus (*G'*) higher than the loss modulus (*G"*) within linear viscoelastic regime (pulsation ω = 10 rad.s^{-1}; strain=0.1%) as determined by dynamic strain sweep measurements

(range=0.1–100%; Figure 5.7). However, CdS@ZAVA gel was found to be weaker in nature than undoped ZAVA gel (after 1h of doping) as it exhibits one order magnitude lower storage modulus value (*G'*) than the undoped one. It is to be noted that the mechanical properties of CdS@ZAVA changes with time and becomes comparable to the pristine ZAVA gel after 1 week of aging (Figure 5.7). This improvement establishes that incubation of CdS can't affect the mechanical strength of the gel, even though some pyridinic N get involved in capping the CdS quantum dots instead of participating in H-bonding, as the loading of CdS is very low (~1.26 wt%).

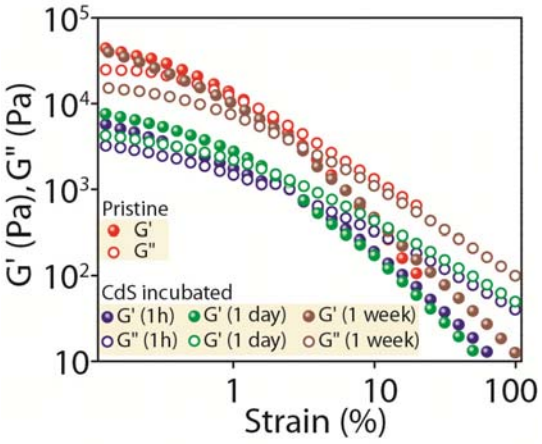

5.2.6. Thermal stability:

5.2.6.1. ZAVA and CdS@ZAVA gel:

In terms of stability, ZAVA remains visually stable upon standing at room temperature in an air-tight container for more than 1 year without any significant change in appearance. It exhibits slow dissolution in water within ~24h (2ml gel in 4 ml water). Regarding thermal stability, thermogravimetric analysis (TGA, under N_2 atmosphere, Figure S6) of the xerogel samples (both pristine and CdS incubated) exhibit initial steady weight loss of ~20% up to 270 °C illustrating loss of water followed by degradation of unreacted ligand [m.p. (VA) = 154 °C]. The sudden weight loss starts at 270-280 °C (~40%) till 470 °C describes destruction of gel network. As expected, the CdS@ZAVA xerogel yields higher amount of leftover mass (~8 wt %) than the pristine one as the former contains CdS along with ZnO which produces due to pyrolysis of xerogel part (up to 800 °C).

5.2.6.2. ZAVCl and CdS@ZAVCl MOF:

As encountered in the case of CdS@ZAVA xerogel, ZAVCl-MOF also shows weight loss in two stages, i) ~3% (loss of water residing in the framework; at 98-100 °C), ii)

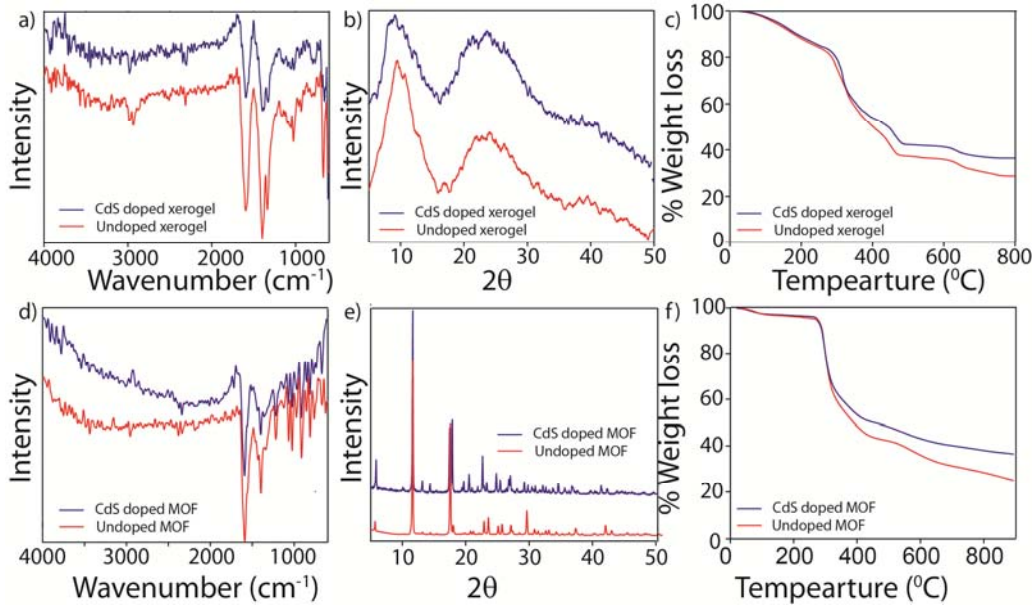

Figure 5.8: FT-IR, PXRD pattern and TGA traces of pristine and CdS loaded ZAVA xerogel a), b), c) and pristine and CdS loaded ZAVCl MOF d), e), f).

~45% (260-270 °C) which can be attributed to the framework collapse, respectively. In this case also the CdS doped material [CdS@ZAVCl MOF] produces more amount of leftover mass (~11wt %) than that of the pristine one owing to the similar reason described in case of CdS@ZAVA xerogel.

5.2.7. PXRD and FTIR spectra:

5.2.7.1. ZAVA and CdS@ZAVA gel:

The FTIR patterns of ZAVA xerogel doesn't differ from its CdS incubated counterpart (Figure 5.8) which indicates that the chemical identity of the xerogel remain intact even after doping of CdS. PXRD pattern of the xerogel samples (undoped as well as CdS doped) reveal their amorphous nature. Presence of crystalline CdS quantum dots does not affect the PXRD patterns of the xerogel samples (Figure 5.8) owing to very small amount of loading (~1.26 wt %) of CdS quantum dot in gel matrix.

5.2.7.2. ZAVCl MOF:

As expected, FTIR spectra of ZAVCl-MOF and CdS@ZAVCl-MOF don't differ much from each other (Figure 5.9). ZAVCl-MOF is highly crystalline in nature and this very nature remains unchanged upon doping of CdS, as amount of loading (~1%) is very less.

5.2.8. Morphological study:

5.2.8.1. CdS@ZAVA gel:

We took transmission electron microscopy (TEM) images to gain insight of the microstructures as well as distribution of CdS quantum dots in CdS@ZAVA xerogel (Figure 5.9). The entangled nanofibrillar morphology of CdS@ZAVA xerogel was visible in the TEM image (Figure 5.9). High resolution TEM images unravel the distribution of sub-10 nm sized CdS quantum dot particles embedded on the gel fibres.

This CdS quantum dot particles shows lattice spacing of 0.336 nm, indicative of the distance between two nearest (111) planes of cubic CdS [JCPDS Card No.-75-1546, (Figure 5.9)].

5.2.8.2. CdS@ZAVCl MOF:

SEM images of the MOF crystals show rod-shaped structure of the ZAVCl-MOF crystals (Figure 5.9). To investigate the distribution and the nature of CdS quantum dots in the MOF matrix, we took HRTEM images of CdS@ZAVCl MOFs. It also a reveals a decent distribution of sub-10 nm sized particles (7-9 nm) engraved in the matrix of the MOF crystals (Figure 5.9) having lattice separation of 0.245nm [d-spacing between two (102) adjacent planes of hexagonal CdS crystals; JCPDS Card No.-41-1049].

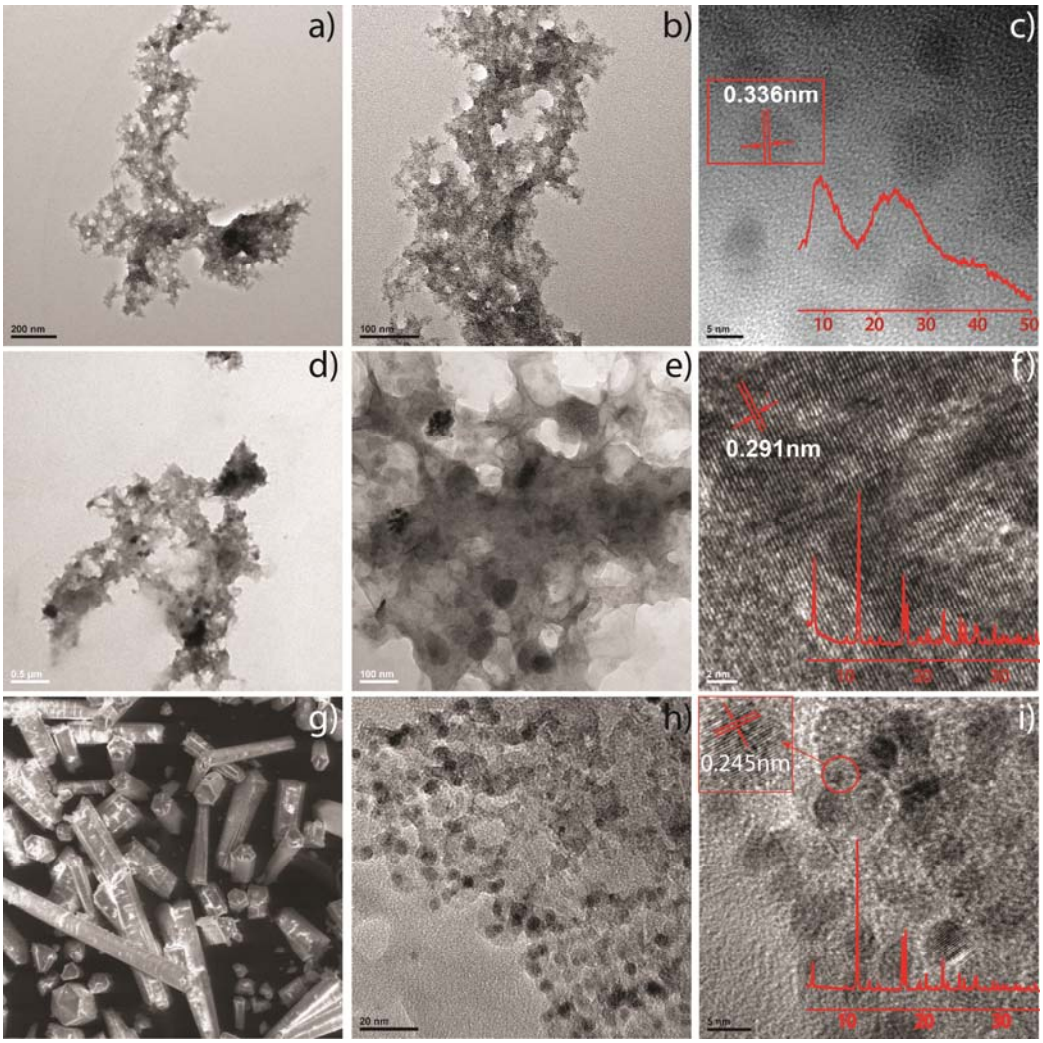

Figure 5.9: HRTEM images of CdS doped xerogel a), b), c); ZnS doped MOF d), e), f); g)SEM images of CdS@ZAVCl h) and i) TEM images of CdS@ZAVCl-MOF.

5.2.9. Photocatalytic activity of CdS@ZAVCl MOF:

Finally, the well-studied photosensitizing ability of visible light active CdS semiconductor quantum dots motivated us to check the photocatalytic activity of such CdS-loaded ZAVCl-MOF. Photocatalytic H_2-production ability of the prepared CdS@ZAVCl MOF was determined under irradiation of visible-light using Pt as a co-catalyst and ethanol as a hole scavanger. The hole scavanger (ethanol) consumes photogenerated holes to prevent the photocatalyst from photocorrosion (5.12a). A blank experiment (in the absence of either irradiation or photocatalyst) indicates no considerable production of hydrogen which establishes that H_2 was produced via

photocatalysis reaction on the photocatalyst. It was observed that the binary composite (CdS@ZAVCl), with CdS having size distribution ranging between 7 to 9

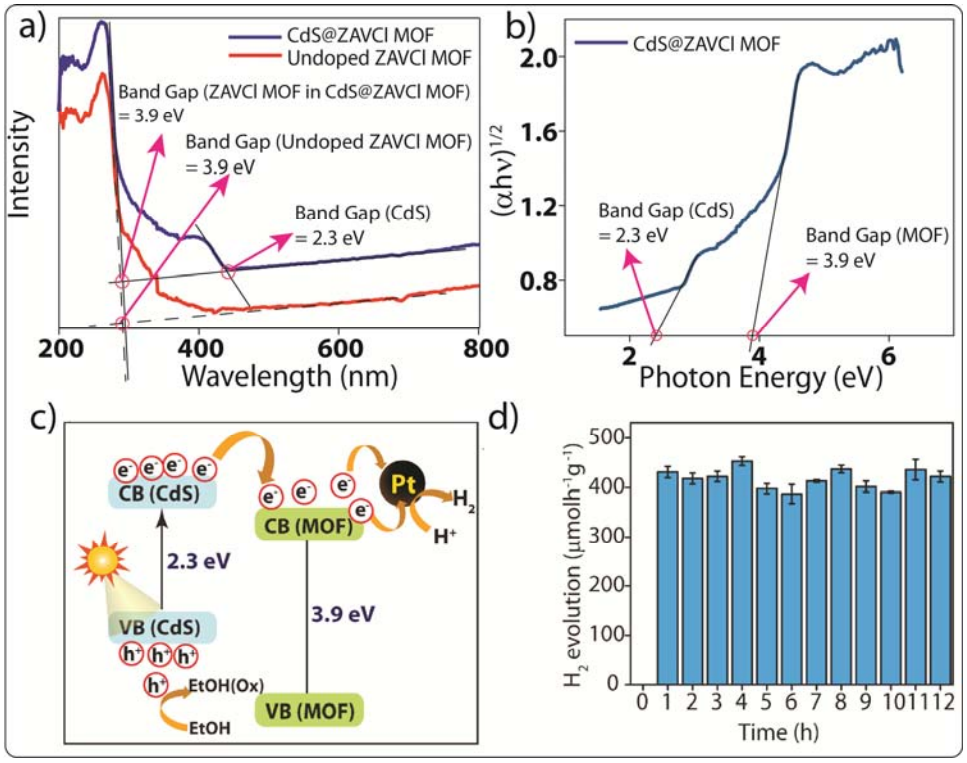

Figure 5.10. a) UV-Vis absorbance spectra of pristine and CdS@ZAVCl MOF; b) Tauc plot (derived from UV-Vis absorbance spectra); c) mechanism of water splitting by CdS@ZAVCl photocatalyst (30 mg), 0.5 wt% co-catalyst Pt and at λ>420 nm and d) stability test of the photocatalyst (CdS@ZAVCl-MOF) in twelve cycles of water splitting reaction. [Reprinted with permission from (5.19d). Copyright 2014 ACS]

nm, showed H_2 production on illumination of visible light (398-418μmolh^{-1}g^{-1} or 39.8- 41.8 mmolh^{-1}g$_{CdS}^{-1}$, considering that the doping of CdS inside MOF is ~1wt%). To determine the influence of MOF on the entrapped CdS quantum dots, thioglycolic acid capped CdS nanoparticles (7-8 nm particle size) were separately synthesized. It is noteworthy that, both pristine ZAVCl (18 μmolh^{-1}g^{-1}) and thioglycolic acid capped CdS quantum dots (100 μmolh^{-1}g^{-1}) showed lower H_2 evolution efficiency than CdS@ZAVCl Quantum Efficiency (Q.E.) of both the material also follow a similar pattern (1.32 % of CdS@ZAVCl MOF *vs.* 0.42 % of thioglycolic acid capped CdS). The inefficiency of ZAVCl-MOF can be attributed to its colourless, transparent nature which doesn't allow it to absorb visible light. Diffuse reflectance spectra of ZAVCl-MOF also support this argument as it shows only one prominent peak in short UV region (265 nm, Figure 5.10a). To ascertain the possible paths for the transfer of

charge carriers in case of CdS@ZAVCl, Mott-Schottky (MS) measurements have been performed on ZAVCl-MOF using electrochemical impedance techniques. A wide band gap of 3.9 eV (5.10a and b) and a positive slope of the MS plot (5.12i) confirm the MOF to be "n-type wide band gap semiconductor"**.** Flat band potential of MOF has been deduced from Mott-Schottky measurement (found to be 0.59 V *vs.* NHE;)**.** It is well known that the flat band potential of an n-type semiconductor equals its Fermi level (5.12j). The conduction band edge of such n-type semiconductors is known to be more negative by about 0.10 V than the flat band potential (5.12k). Hence, the conduction band of ZAVCl MOF can be estimated to be -0.491V *vs.* NHE. Hence**,** the low-lying conduction band-edge of MOF (-0.491 V *vs.* NHE) in comparison to CdS (-0.65 V *vs.* NHE)(5.12b, 5.12c) favors the stabilization of CdS photoelectrons on MOF which thereby results in an efficient charge separation. However, CdS@ZAVCl MOF is unable to split water consequent to well known problem of sluggish reaction kinetics on the surface of photocatalysts (5.12g, 5.12h). Pt (0.5 wt% of the CdS@ZAVCl MOF) co-catalyst conventionally act as electron sink apart from providing effective sites for reduction of hydrogen which thereby decreases the activation energy for the reduction of protons (5.12g, 5.12h). The CdS@ZAVCl MOF exhibits stable photocatalytic activity for multiple cycles (Figure 5.10a).There exist few reports in the literature related to photocatalytic water splitting ability MOF (mainly MOF-CdS composite material) (5.12b, 5.12c). But none of them provide easier synthetic method than that of CdS@ZAVCl MOF as all of them requires high temperature and much longer time for synthesis. Moreover, CdS@ZAVCl MOF exhibit considerably good performance of H_2 production although being loaded with very small amount of CdS (~1 wt %) (5.12b, 5.12c). It is noteworthy that, CdS@ZAVCl MOF performs more efficiently as a photocatalyst (H_2 evolution = 500-510 μmol. h^{-1} g^{-1}) in presence of UV light (i.e., UV+Vis). In absence of a UV filter, the incident radiation now contains photons of all possible wavelengths of visible as well as UV region. Hence, the range of photons that could be now absorbed by CdS quantum dots increases considerably (i.e., 370 nm $<\lambda<$ 440 nm). The increment in the amount of photons absorbed thereby increases the number of photoelectron-hole pairs generated which in turn increases the hydrogen evolution (500-510 μmol. h^{-1} g^{-1}).

5.3. Conclusions:

We have prepared a CdS quantum dot based gel material (CdS@ZAVA gel) in a unique one pot procedure at room temperature. Unlike other methods, this synthesis-cum-entrapment procedure of CdS doesn't require any capping agent to stabilize them in the gel matrix. The gel shows tunable luminescence with time owing to gradual increment in the size of CdS in the gel matrix. But the luminescence colour becomes persistent as we solidified the CdS@ZAVA gel by means of converting it into xerogel. The CdS incubated ZAVA gel can easily be transformed into CdS loaded MOF by simple addition of chloride salt (*e.g.* NaCl, KCl, NH_4Cl etc.). These CdS embedded MOFs can be utilized as photocatalyst in visible light water-splitting reaction. This method not only shows simple way to make high quality single crystals but also immobilization of dopants in the matrix of gel, xerogel and MOF which might lead to construction of functional composite materials.

5.4. Experimental Section:

Unless otherwise noted, zinc acetate dihydrate, L-Valine, sodium borohydrate, acetic acid, cadmium chloride monohydrate, sodium sulfide hydrate ($Na_2S•xH_2O$) were purchased from local suppliers, 4-pyridinecarboxaldehyde was purchased from Sigma-Aldrich and used without further purification. The detailed synthetic procedure for the organic ligand VA [an L-Valine based molecule, i.e., V = L-3-methyl-2-(pyridine-4-yl-methylamino)-butanoic acid and sodium acetate as ligand system] was described in our recent publications.

5.4.1. Preparation of amino acid based ligands:

The ligand system VA was prepared following a modified literature procedure. To an aqueous solution (8 ml) of L-valine (1g, 8.5 mmol) and Na_2CO_3 (0.46 g, 4.25 mmol), 4-pyridinecarboxaldehyde (0.92 g, 8.5 mmol) in MeOH (5 mL) was added slowly. The solution was stirred for 3 h and cooled in an ice bath. $NaBH_4$ (0.38 g, 10.2 mmol) was added to the solution slowly. The mixture was stirred for 12 h, and 50% acetic acid was used to neutralize the basic (pH~12) reaction mixture and adjust the pH to 7.1-7.2. As a result, in the reaction mixture sodium acetate gets generated which eventually plays a very important role in the gelation process. The solution was stirred further for 1 h and then evaporated to dryness. The solid was extracted in hot and dry EtOH, and the filtrate was evaporated to get a white powder. Yield (L-VA): 1.4 g, 70% yield. The ligand has been crystallized from the aqueous solution. Crystals were collected and utilized for its characterization. IR (KBr, cm^{-1}):ν_{OH},3421; ν_{as}(CO2),

1562; ν_s(CO2), 1409.^{1}H NMR (D_2O, ppm): -CH_3(1.21, d, 3H), -CH_3 (1.35, d, 3H), -CH (3.20, m, 1H), -HN-CH (3.65, m, 1H), -CH2 (3.82, dd, 2H), py-H (7.34, d, 2H), py-H (8.38, d, 2H).

5.4.2. Synthesis of ZAVA gel, CdS@ZAVA gel, xerogels, ZAVCl and CdS@ZAVCl MOFs:

Figure 1 illustrates simple preparative procedure of ZAVA gel which forms upon mixing the aqueous solutions (0.5 ml each) of zinc acetate dihydrate (ZA, 0.2 M) and ligand system VA (0.4 M) which turns into a opaque white gel (CGC=57 gL^{-1}) within 30 seconds at room temperature via a transient colloidal solution phase (Scheme 1). 0.025 ml 0.2M cadmium chloride monohydrate ($CdCl_2$•H_2O) solution rapidly added to this colloidal solution. To this mixture, 0.25 ml of 0.05M aqueous solution of sodium sulfide (Na_2S•xH_2O) was added drop wise with vigorous shaking. The resulting gelatinous colloidal suspension transforms into an opaque white gel upon 5-10 minutes standing at room temperature. Pristine ZAVA gel and CdS@ZAVA gel was dried under vacuum to obtain the xerogel. This gel-to-xerogel conversion is a unique reversible process. The xerogel can easily be converted to ZAVA gel upon addition of equivalent amount of water extracted during the course of conversion from gel-to-xerogel. In order to make ZAVCl-MOF, 0.012 gm (0.2 mmol) solid sodium chloride (NaCl) was added to 1ml of ZAVA gel. The gel starts degrading immediately after addition of NaCl and completely converts into MOF crystals within 12 hrs. The colourless ZAVCl-MOF crystals can be washed with water after separation and dried under vacuum. CdS@ZAVCl-MOF was obtained from CdS incubated ZAVA gel following the same procedure.

5.4.3. Photocatalytic reaction:

In a typical photocatalytic water splitting reaction, a 300 W xenon light source with an AM 1.5G filter (Newport) and a UV cut-off filter (λ> 420 nm) was used as a source of visible light. The glass reactor was ensured to be clean and 9.25 mL of deionized water was used each time. A known amount of photocatalyst (CdS@ZAVCl MOF, 30 mg) was added along with 0.75 mL of ethanol as a sacrificial donor. A certain amount of $H_2PtCl_6.6H_2O$ aqueous solution was added to this system in order to load 0.5 wt % Pt onto the surface of the photocatalyst by a photochemical reduction deposition method. Before irradiation, the solution was bubbled with N_2 gas for 15 minutes to remove the dissolved oxygen. Then the system was stirred in the

dark for 30 min to establish the adsorption−desorption equilibrium between the sample and reactant. The reaction solution was continuously stirred to keep the entire mixture homogeneous. The whole assembly was evacuated before exposing it to Xenon light source. The reaction was carried out for 1 h. Then the gases generated were collected and analyzed using a GC (Agilent technologies 7890A gas chromatograph) equipped with molecular sieve 5A column and a TCD detector.

5.4.4. Mott-Schottky experiment:

Mott–Schottky analysis of ZAVCl-MOF (coated on FTO as working electrode, Pt as counter electrode and Na_2SO_4 as electrolyte) was measured at frequencies of 1 KHz and 10 KHz using *BioLogic* VPM3 electrochemical workstation. As shown in Fig. S6c, the positive slope of the plot indicates the MOF to be a typical n-type semiconductor. The flat band position (V_{fb}) determined is approximately -0.591 V vs. NHE for ZAVCl-MOF. Since it is generally believed that the bottom of the conduction band in many n-type semiconductors is more negative by about 0.10 V than the flat band potential, the conduction band of ZAVCl-MOF can be estimated to be -0.49 V vs. NHE, which is more negative than the redox potential of H^+/H_2(-0.41 V vs. NHE, pH = 7).

5.4.5. Calculation of quantum efficiency:

The apparent quantum efficiency (QE) was determined under the similar photocatalytic reaction condition except that four 420 nm-LEDs (3 W) were used as light sources to trigger the photocatalytic reaction, instead of the xenon arc lamp. The LEDs were positioned 1 cm away from the reactor in four different directions, and the focused intensity on the flask for each of them was ca. 39.0 $mW.cm^{-2}$ over an area of 1 cm^2**.** The QE was calculated according to the equation given below**:**[1]

$$\text{Q. E. (\%)} = \frac{\text{number of reacted electrons}}{\text{number of incident photons}} \times 100$$

$$= \frac{\text{number of evolved H2 molecules} \times 2}{\text{number of incident photons}} \times 100$$

NOTE: The results of this chapter have already been published ***J. Am. Chem. Soc., 2014, 136, 14845–14851*** with the title: "*Photocatalytic Metal-Organic Framework from CdS Quantum Dot Incubated Luminescent Metallohydrogel"*. These publications were the results from the group of Dr. Rahul Banerjee and his student Subhadeep Saha from CSIR National Chemical Laboratory, Pune, India. Majority of the work is contributed by Subhadeep with the help of the instrumental facilities of CSIR National Chemical Laboratory.

CHAPTER 6

Conclusion of All Chapters and Future Directives

6.1. Conclusion:

In this dissertation, electrochemical and photocatalytic aspect of metallogels has been described. A series of metallogels have been synthesized for such applications.

In chapter 2, we have synthesized new modular, stimuli-responsive, and multifunctional metallogels (i.e., CuA-Ox and CuP-Ox gels) based on the combination of two commercially available and inexpensive components: A Cu(II) salt and oxalic acid as the only bridging ligand. The gelation process occurs at RT upon mixing stock solutions of each component prepared under optimized concentrations, while the facile and economic procedure allows the preparation of the metallogels at multigram scale. The overall stability of this type of materials represents a complex equilibrium between thermal stability of the coordination aggregates, electrostatic interactions involving also the counteranions, degree of crosslinking and solvation-related interactions. Major novelties of this investigation include (a) introduction of oxalic acid as the lowest molecular weight organic ligand that is able to form stable metallogels, (b) growth of different Cu(II) oxalate non-aquo polymorphs from one metallogel and its corresponding xerogel, which illustrates an unprecedented xerogel-to-crystal phase transition and (c) first demonstration of proton conductivity in molecular gels with lowest activation energy among metal-organic materials and. The described results open new perspectives on bootom-up approach of high temperature proton conducting metal-organic material and inorganic crystal engineering.

In chapter 3, We have described the facile preparation of new non-polymeric supramolecular metallohydrogels by combining two stock solutions of an amino acid-based ligand (i.e.,L-3-methyl-2-(pyridine-4-yl-methylamino)-butanoic acid) and a

Zn(II)salt. These hydrogels displayed unique multiresponsive gel-to-sol and sol-to-gel transitions, as well as remarkable moldable, load-bearing, andautonomic self-healing behavior at room temperature**.**

In chapter 4, we have shown the facile synthesis of two novel non-polymeric supramolecular metallohydrogels by combining an amino acid-based ligand (i.e., L-3-methyl-2-(pyridine-4-yl-methylamino)-butanoic acid) and Zn(II) salts. These hydrogels displayed a unique reversible opaque to transparent phase transition at room temperature, multiresponsive and reversible gel-to-sol and xerogel-to-geltransitions, as well as gradual dissolution in aqueous medium within a wide range of pH at RT. This smooth transition was employed for the *in vitro* release of a model polar drug at both neutral and acidic pH. The unprecedented (opaque gel)-to-(transparent gel) transition evidences the formation of a kinetic supramolecular gel that undergoes self-evolution towards a different gel network of lower energy. The isolation of this intermediate gel phase may have important mechanistic implications on the theory of gelation.

In chapter 5, we have prepared a CdS quantum dot based gel material (CdS@ZAVA gel) in a unique one pot procedure at room temperature. Unlike other methods, this synthesis-cum-entrapment procedure of CdS doesn't require any capping agent to stabilize them in the gel matrix. The gel shows tunable luminescence with time owing to gradual increment in the size of CdS in the gel matrix. But the luminescence colour becomes persistent as we solidified the CdS@ZAVA gel by means of converting it into xerogel. The CdS incubated ZAVA gel can easily be transformed into CdS loaded MOF by simple addition of chloride salt (*e.g.* NaCl, KCl, NH_4Cl etc.). These CdS embedded MOFs can be utilized as photocatalyst in visible light water-splitting reaction. This method not only shows simple way to make high quality single crystals but also immobilization of dopants in the matrix of gel, xerogel and MOF which might lead to construction of functional composite materials.

6.2. Future directive:

Plan-I: Synthesis of thiolated metal-organic gels for efficient CdS capping and heavy metal binding:

The aim of our future plan implies synthesis of metallohydrogels composing of ligand containing thiol (-SH) moiety. Thiol is known functionality which helps in capping

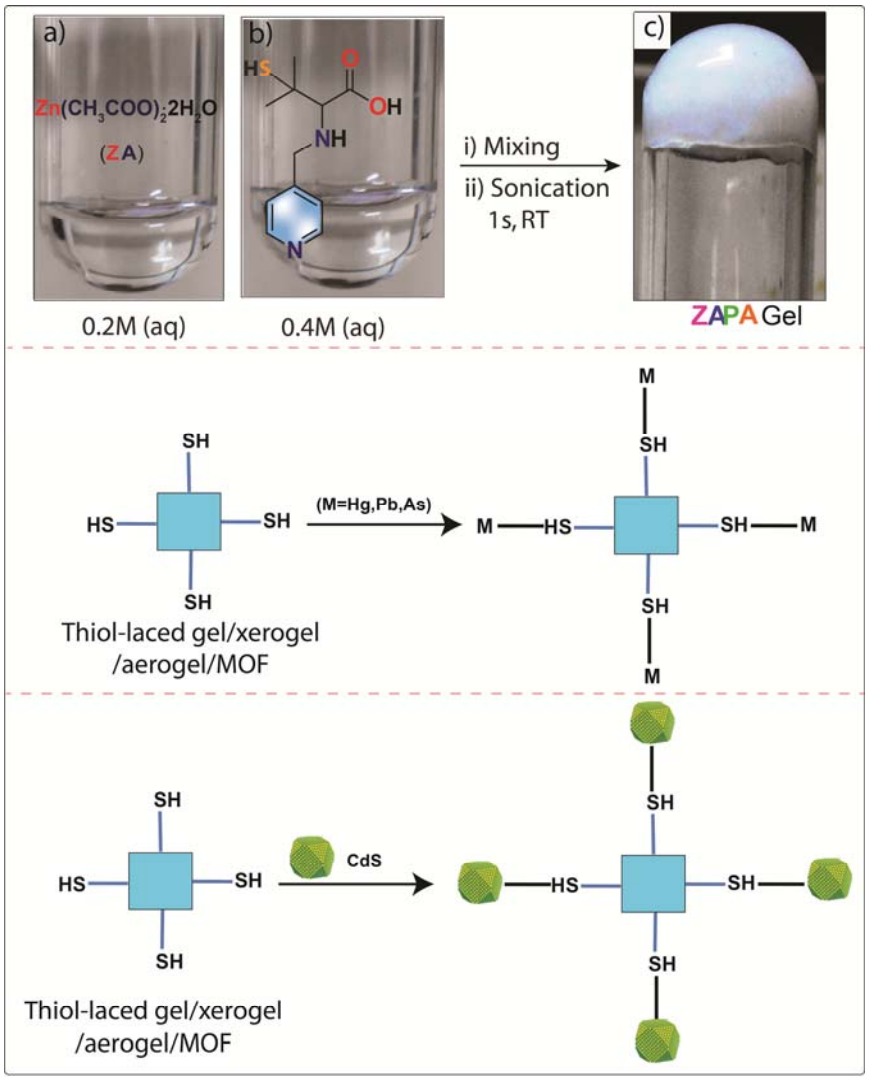

Figure 6.1. *(top)* Scheme of synthesis of thiolated analogue of ZAVA; *(middle)* heavy metal trapping by the gel/xerogel or derived MOF; (bottom) *in-situ* synthesis/capping of CdS quantum dots by the gel.

inorganic nanoparticles. The target material of this proposal would be an analogue of ZAVA, named ZAPA, where the valine will be replaced by penicilamine (Figure 6.1). Due to presence of this thiol moiety this gelator will be able cap CdSquantum dots more efficiently than ZAVA (chapter 5) hence color will not change with time. Moreover, the blue fluorescent ZAPA gel is expected to change its fluorescent colour upon binding (*via* –SH moiety) with heavy metal [e.g. Hg(II)] .

References

Chapter 1

1.1. D. J. Lloyd, In *Colloid Chemstry*, Alexander, J., Ed. Chemical Catalogue Company: New York, 1926; Vol. 1.

1.2. a) P. J. Flory, Molecular Size Distribution in Three Dimensional Polymers. I. Gelation *The Journal American Chemical Society* 1941**, 63**, 3083; b) P. J. Flory, Constitution of Three-dimensional Polymers and the Theory of Gelation. *Journal of Physical Chemistry* 1942**, 46**, 132; c) W. H.Stockmayer, Theory of Molecular Size Distribution and Gel Formation in Branched Polymers II. General Cross Linking. *Journal of Chemcial Physics* 1944**, 12**, 125.

1.3. Burchard, W. R.-M., S. B., Burchard, W. R.-M., B., Ed. Elsevier: London, 1990.

1.4. Almdal K, D. J., Hvidt S, and Kramer O., 1993**, 1**, 5.

1.5. A. Keller, Introductory lecture. Aspects of polymer gels. *Faraday Discussions* 1995**, 101**, 1.

1.6. Q. Wang and M. Y. J. L. Mynar, E. Lee, M. Lee, K. Okuro, K. Kinbara, T. Aida, *Nature*, 2010, **463**, 339.

1.7. S. Dong, B. Zheng, D. Xu, X. Yan, M. Zhang and F. Huang, *Adv. Mater.*, 2012, **24**, 3191.

1.8. B. L. Feringa, Molecular Switches; Wiley-VCH Verlag GmbH: Weinheim, Germany, 2001.

1.9. M. Irie, Diarylethenes for Memories and Switches. *Chem. Rev.* 2000, **100**, 1685.

1.10. A. Hashidzume, F. Ito, I. Tomatsu, A. Harada, *Macromol. Rapid Commun.*2005, **26**, 1151.

1.11. Y. Takashima, T. Nakayama, M. Miyauchi, Y. Kawaguchi, H. Yamaguchi, A. Harada, *Chem. Lett.* 2004, **33**, 890.

1.12. I. Tomatsu, A. Hashidzume, A. Harada, *Macromol. Rapid Commun.* 2006, **27**, 238.

1.13. N. M. Sangeetha and U. Maitra, *Chem. Soc. Rev.*, 2005, **34**, 821.

1.14. P. Terech and R. G. Weiss, *Chem. Rev.*, 1997, **97**, 3133.

1.15. T. Aida, E. W. Meijer and S. I. Stupp, *Science*, 2012, **335**, 813.

1.16. J. M. Lehn, *Chem. Soc. Rev.*, 2007, **36**, 151.

1.17. F. Fages, Low Molecular Mass Gelators, *Top. Curr. Chem.*, 2005, **256**, 283.

1.18. Han. S.; Wei, Y.; Valente, C.; Forgan, R. S.; Gassensmith, J. J.; Smaldone, R. A.; Nakanishi, H.; Coskun, A.; Stoddart, J. F.; Grzybowski, B. A. *Angew. Chem. Int. Ed.* 2011, **50**, 276.

1.19. K. Kuroiwa, T. Shibata, A. Takada, N. Nemoto and N. Kimizuka, *J. Am. Chem. Soc.*, 2004, **126**, 2016.

1.20. X. Zhang, Z.-K. Chen and K. P. Loh, *J. Am. Chem. Soc.*, 2009, **131**, 7210.

1.21. J. W. Steed and J. L. Atwood, Supramolecular Chemistry, J. Siley & sons, 2nd edn, Chichester, 2009.

1.22. D.-S. Guo and Y. Liu, *Chem. Soc. Rev.*, 2012, **41**, 5907.

1.23. B. Xing, M.-F. Choi and B. Xu, *Chem.–Eur. J.*, 2002, **8**, 5028.

1.24. T. Nishimura, T. Onoue, K. Ohe and S. Uemura,*Tetrahedron Lett.*, 1998,**39**, 6011.

1.25. J. H. Lee, H. Lee, S. Seo, J. Jaworski, M. L. Seo, S. Kang, J. Y. Lee and J. H.

Jung, *New J. Chem.*, 2011, **35**, 1054.
1.26. H. Lee, S. Kang, J. Y. Lee and J. H. Jung, *Soft Matter*, 2012, **8**, 2950.
1.27. A. Kuhnle, T. R. Linderoth, B. Hammer and F. Besenbacher, *Nature*, 2002,**415**, 891.
1.28. H. Lee, S. H. Jung, W. S. Han, J. H. Moon, S. Kang, J. Y. Lee, J. H. Jung and S. Shinkai, *Chem.–Eur. J.*, 2011, **17**, 2823.
1.29. A. K. Geim, *Science*, 2009, **324**, 1530.
1.30. D. Li and R. B. Kaner, *Science*, 2008, **320**, 1170.
1.31. H. Bai, C. Li, X. L. Wang and G. Q. Shi, *Chem. Commun.*, 2010, **46**, 2376.
1.32. G. Eda and M. Chhowalla, *Adv. Mater.*, 2010, **22**, 2392.
1.33. J. K. Lee, K. B. Smith, C. M. Hayner and H. H. Kung, *Chem. Commun.*, 2010, **46**, 2025.
1.34. J. H. Lee, S. Kang, J. Jaworski, K.-Y. Kwon, M. L. Seo, J. Y. Lee and J. H. Jung, *Chem.–Eur. J.*, 2012, **18**, 765.
1.35. J. A. Foster, M.-O. M. Piepenbrock, G. O. Lloyd, N. Clarke, J. A. K. Howard and J. W. Steed, *Nat. Chem.*, 2010, **12**, 1037.
1.36. Z. Yang, G. Liang, L. Wang and B. Xu, *J. Am. Chem. Soc.*, 2006, **128**, 3038.
1.37. B. Joddar and Y. Ito, *J. Mater. Chem.*, 2011, **21**, 13737.
1.38. C. Y. Goh, T. Becker, D. H. Brwon, B. W. Skelton, F. Jones, M. Mocerino and M. I. Ogden, *Chem. Commun.*, 2011, **47**, 6057.
1.39. M.-O. M. Piepenbrock, N. Clarke and J. W. Steed, *Soft Matter*, 2011, **7**, 2412.
1.40. H. Lee, J. H. Lee, S. Kang, J. Y. Lee, G. John, J. H. Jung, *Chem. Commun.*, 2011, **47**, 2937.
1.41. Tamesue, S.; Takashima, Y.; Yamaguchi, H.; Shinkai, S.; Harada,A. *Angew. Chem., Int. Ed.* 2010, **49** , 7461.
1.42. M. Nakahata, Y. Takashima, H. Yamaguchi, A. Harada, *Nat. Commun.* 2011, *2*, 511.
1.43. S. R. Jadhav, P. K. Vemula, R. Kumar, S. R. Raghavan, G. John, *Angew. Chem. Int. Ed.* 2010, **49**, 7695.
1.44. Z. Yang, P.-L. Ho, G. Liang, K. H. Chow, Q. Wang, Y. Cao, Z. Guo, B. Xu, *J. Am. Chem. Soc.*, 2007,**129**, 266.

Chapter 2

2.1. K. Murata, M. Aoki, T. Nishi, A. Ikeda and S. Shinkai, *J. Chem. Soc., Chem. Commun.*, 1991, 1715.
2.2. K. Murata, M. Aoki, T. Suzuki, T. Harada, H. Kawabata, T. Komori, F. Ohseto, K. Ueda and S. Shinkai, *J. Am. Chem. Soc.*, 1994, **116**, 6664.
2.3. J. E. S. Sohna and F. Fages, *Chem. Commun.*, 1997, 327.
2.4. J. H. Jung, J. H. Lee, J. R. Silverman and G. John, *Chem. Soc. Rev.*, 2013, **42**, 924.
2.5. S. Saha, E.-M. Schön, C. Cativiela, D. D. Díaz and R. Banerjee Chem. Eur. J. 2013, 19, 9562 – 9568.
2.6. M. George, G. Tan, V. T. John and R. G. Weiss *Chem. Eur. J.* 2005, **11**, 3243-3254.

2.7. (a) Boyle, Godfrey. Renewable energy. OXFORD university press, 2004; (b) Johansson, Thomas B., and Laurie Burnham, eds. Renewable energy: sources for fuels and electricity. Island Press, 1993.

2.8. (a) G. W. Crabtree, M. S. Dresselhaus, *MRS Bull*. 2008, **33**, 421; (b) S. Hamrock and M. Yandrasits, *Polym. Rev.*, 2006, **46**, 219.

2.9. (a) H. Steininger, M. Schuster, K. D. Kreuer, A. Kaltbeitzel, B. Bingol, W. H. Meyer, S. Schauff, G. Brunklaus, J. Maier and H. W. Spiess, *Phys. Chem. Chem. Phys.* 2007, **9**, 1764.b) M. F. H. Schuster, W. H. Meyer, M. Schuster and K. D. Kreuer, *Chem. Mater*. 2004**, 16**, 329.

2.10. a) P. Ramaswamy, N. E. Wong and G. K. H. Shimizu, *Chem.Soc.Rev*. 2014, **43**, 5913. b) V. G. Ponomareva, K. A. Kovalenko, A. P. Chupakhin, D. N. Dybtsev, E. S. Shutova and V. P. Fedin, *J. Am. Chem. Soc.* 2012, **134**, 15640.c) S. Bureekaew, S. Horike, M. Higuchi, M. Mizuno, T. Kawamura, D. Tanaka, N. Yanai and S. Kitagawa, *Nature Mater*.,2009, **8**,831.

2.11. A. Gavezzotti; G. Filippini, Chem. Commun. 1998, 287-294.

2.12. a) P. Byrne, G. O. Lloyd, L. Applegarth, K. M. Anderson, N. Clarke, J. W. Steed, *New J. Chem.* 2010, **34**, 2261; b) C. D. Jones, J. C. Tan, G. O. Lloyd, *Chem. Commun.* 2012, **48**, 2110.

2.13. Dimethylammonium cation originates from the decomposition of DMF in the presence of metal ions. See, a) M. Tsuchimoto, N. Yoshioka, S. Ohba, *Eur. J. Inorg. Chem.* 2001, 1045-1049; b) G. S. Papaefstathiou, S. Manessi, C. P. Raptopoulou, E. J. Behrman, T. F. Zafiropoulos, *Inorg. Chem. Commun.* 2004, **7**, 69.

2.14. a) G. R. Desiraju, D. Y. Curtin, I. C. Paul, *J. Am. Chem. Soc.* 1977, **99**, 6148; b) H. K. Henisch, J. M. Garcia-Ruiz, *J. Cryst. Growth* 1986, 75, 203; c) C. Daiguebonne, A. Deluzet, M. Camara, K. Boubekeur, N. Audebrand, Y. Gérault, C. Baux, O. Guillou, *Cryst. Growth Des.* 2003, **3**, 1015; d) R. I. Petrova, J. A. Swift, *J. Am. Chem. Soc.* 2004, **126**, 1168; e) R. I. Petrova, R. Patel, J. A. Swift, *Cryst. Growth Des.* 2006, **6**, 2709; f) H. Li, Y. Fujiki, K. Sada, L. A. Estroff, *CrystEngComm* 2011, **13**, 1060; g) D. Braga, S. d'Agostino, E. D'Amen, F. Grepioni, *Chem. Commun.* 2011, **47**, 5154-5156; h) J. A. Foster, M.-O. M. Piepenbrock, G. O. Lloyd, N. Clarke, J. A. K. Howard, J. W. Steed, *Nat. Chem.* 2010, **2**, 1037.

2.15. a) A. Sannigrahi, S. Ghosh, S. Maity, T. Jana, *Polymer* 2011, **52**, 4319; b) S. Ghosh , S. Maity, T. Jana, *J. Mater. Chem.* 2011, **21**, 14897.

2.16. a) S. Bureekaew, S. Horike, M. Higuchi, M. Mizuno, T. Kawamura, D. Tanaka, N. Yanai, S. Kitagawa, *Nat. Mater.*, 2009, **8**, 831. b) B. M. Wiers, M.-L. Foo, N. P. Balsara, J. R. Long, *J. Am. Chem. Soc.* 2011, **133**, 14522. c) M. Sadakiyo, T. Yamada, H. Kitagawa, *J. Am. Chem. Soc.* 2009, **131**, 9906.

2.17. CrysAlisPro, Version 1.171.33.66; Oxford Diffraction Ltd.: Abingdon, U.K., 2010.

2.18. G. M. Sheldrick, (1997). SHELXS '97 and SHELXL '97. University of Göttingen, Germany.

2.19. A. L. Spek (2005) PLATON, A Multipurpose Crystallographic Tool, Utrecht University, Utrecht, The Netherlands.

Chapter 3

3.1. Self-healing materials: An Alternative Approach to 20 Centuries of Materials Science (Ed. : S. Van der Zwaag), Springer, Dordrecht, 2007.

3.2. (a) J. M. Lehn, *Prog. Polym. Sci.* 2005, **30**, 814; (d) A. Phadke, C. Zhang, B. Arman, C.-C. Hsu, R. A. Mashelkar, A. K. Lele, M. J. Tauber, G. Arya and S. Varghese, *Proc. Natl. Acad. Sci. U.S.A.* 2012, **109**, 4383.

3.3. (a) D. J. Abdallah and R. G. Weiss, *Adv. Mater.* 2000, **12**, 1237; (b) N. Yan, Z. Xu, K. K. Diehn, S. R. Raghavan, Y. Fang and R. G. Weiss, *J. Am. Chem. Soc.* 2013, **135**, 8989; (c) P. Dastidar, *Chem. Soc. Rev.*, 2008,**37**, 2699; (d) J. Nanda, A. Biswas, B. Adhikari, A. Banerjee, *Angew. Chem. Int. Ed.* 2013, **52**, 5041. (e) S. Roy, A. Baral and A. Banerjee, *Chem. Eur. J.*, 2013, **19**, 14950. (f) G. O. Lloyd and J. W. Steed, *Nature Chemistry*, 2009, **1**, 437; (g) R. C. T. Howe, A. P. Smalley, A. P. M. Guttenplan, M. W. R. Doggett, M. D. Eddleston, J. C. Tan and G. O. Lloyd, *Chem. Commun.*, 2013, **49**, 4268.

3.4. M. Nakahata, Y. Takashima, H. Yamaguchi and A. Harada, *Nat. Commun.*, 2011, **2**, 511.

3.5. A. Vidyasagar, K. Handore and K. M. Sureshan, *Angew. Chem., Int. Ed.*, 2011, **50**, 8021.

3.6. S. Saha, J. Bachl, T. Kundu, D. D. Dı ´az and R. Banerjee, *Chem. Commun.*, 2014, **50**, 3004.

3.7. G.R. Desiraju, T. Steiner, The Weak Hydrogen Bond in Structural Chemistry and Biology, Oxford University Press, Oxford, 1999.

3.8. M. J. Kamlet, J. L. M. Abboud, M. H. Abraham, R. W. J. Taft, *Org. Chem.*1983, **48**, 2877.

3.9. J.-S. Shen, G.-J. Mao, Y.-Hua Zhou, Y.-B. Jiang an*d* H.-W. Zhang, *Dalton Trans.* 2010, **39**, 7054.

3.10. P. Sahoo, R. Sankolli, H.-Y. Lee, S. R. Raghavan and P. Dastidar, *Chem. Eur. J.* 2012, **18**, 7965.

3.11. P. Terech, M. Yan, M. Mare´chal, G. Royal, J. Galvez and S. K. P. Velu, *Phys. Chem. Chem. Phys.*2013,**15**, 7338.

3.12. J. Yuan, X. Fang, L. Zhang, G. Hong, Y. Lin, Q. Zheng, Y. Xu, Y. Ruan, W. Weng, H. Xia and G. Chen, *J. Mater. Chem.*, 2012, **22**, 11515.

3.13. M. Zhang, D. Xu, X. Yan, J. Chen, S. Dong, B. Zheng and F. Huang, *Angew. Chem. Int. Ed.*, 2012, **124**, 7117.

3.14. S. Basak, J. Nanda and A. Banerjee, *Chem. Commun.*, DOI: 10.1039/C3CC48896A.

3.15. S. Samai, K. Biradha, *Chem. Mater.* 2012, **24**, 1165.

Chapter 4

4.1. (a) T. Vermonden, R. Censi, and W. E. Hennink, *Chem. Rev.*, 2012, **112**, 2853; (b) E. A. Appel, J. del Barrio, X. J. Loh, and O. A. Scherman, *Chem. Soc. Rev.*, 2012, **41**, 6195; c) D. D. Díaz, D. Kühbeck, and R. J. Koopmans, *Chem. Soc. Rev.*, 2011, **40**, 427; (d) S. Banerjee, R. K. Das, and U. Maitra, *J. Mater. Chem.*, 2009, **19**, 6649; (e) L. A. Estroff, and A. D. Hamilton, *Chem. Rev.*, 2004, **104**, 1201.

4.2. (a) L. A. Estroff and A. D. Hamilton, *Chem. Rev.*, 2004, **104**, 1201; (b) M-O M. Piepenbrock, G. O. Lloyd, N. Clarke, and J. W. Steed, *Chem. Rev.*, 2010, **110,** 1960; (c) G. O. Lloyd and J. W. Steed, *Nat. Chem.*, 2009, **1**, 437; (d) R. C. T. Howe, A. P. Smalley, A. P. M. Guttenplan, M. W. R. Doggett, M. D. Eddleston, J. C. Tan and G. O. Lloyd, *Chem. Commun.*, 2013, **49**, 4268; (e) D. J. Abdallah and R. G. Weiss, *Adv. Mater.* 2000, **12**, 1237; (f) N. Yan, Z. Xu, K. K. Diehn, S. R. Raghavan, Y. Fang and R. G. Weiss, *J. Am. Chem. Soc.*, 2013, **135**, 8989; (g) P. Dastidar, *Chem. Soc. Rev.*, 2008, **37**, 2699; (h) J. Nanda, A. Biswas, B. Adhikari, A. Banerjee, *Angew. Chem. Int. Ed.*, 2013, **52**, 5041; (i) S. Roy, A. Baral and A. Banerjee, *Chem. Eur. J.*, 2013, **19**, 14950; (j) D. K. Kumar, D. A. Jose, A. Das and P. Dastidar. *Chem. Commun.* 2005, 4059; (k) J. Zhou, X. Du, Y. Gao, J. Shi, and B. Xu, *J. Am. Chem. Soc.*, 2014, **136**, 2970.

4.3. a) A. Yiu-Tam, and V. W.-W. Yam, *Chem. Soc. Rev.*, 2013, **42**, 1540; (b) J. Zhang, and C.-Y. Su, *Coord. Chem. Rev.*, 2013, **257**, 1373; (c) J. H. Jung, J. H. Lee, J. R. Silverman, and G. John, *Chem. Soc. Rev.*, 2013, **42**, 924; (d) Y. Zhang, B. Zhang, Y. Kuang, Y. Gao, J. Shi, X. X. Zhang, and B. Xu, *J. Am. Chem. Soc.*, 2013, **135**, 5008.

4.4. a) S. Saha, J. Bachl, T. Kundu, D.D. Díaz and R. Banerjee, *Chem. Commun.*, 2014, **50**, 3004. b) L. L. Koh, J. O. Ranford, W. T. Robinson, J. O. Svensson, A. L. C. Tan and D. Wu, *Inorg. Chem.* **1996**, *35*, 6466. c) S. C. Sahoo, T. Kundu and R. Banerjee, *J. Am. Chem. Soc.* **2011**, *133*, 17950. d) T. Kundu, S. C. Sahoo, S.Saha and R. Banerjee, *Chem. Commun.*, 2013, **49**, 5262.

4.5. (a) V. A. Mallia, P. D. Butler, B. Sarkar, K. T. Holman, and R. G. Weiss, *J. Am. Chem. Soc.* 2011, **133**, 15045. (b) A.Kotlewski, B. Norder, W. F. Jager, S. J. Pickenand, and E. Mendes, *Soft Matter*, 2009, **5**, 4905. (c) J. Li, X. Gong, X. Yi, P. Sheng, and W. Wen, *Smart Mater. Struct.*, 2011, **20,** 075005.

4.6. S. Saha, J. Bachl, T. Kundu, D.D. Díaz and R. Banerjee, *Chem. Commun.*, 2014, **50**, 7032.

4.7. (a) A. Mallick, B. Garai, D. D. Díaz and R.Banerjee, *Angew. Chem. Int. Ed.*, 2013, **125**, 14000. (b) L. Baumann, Katrin Schöller, D. de Courten, D. Marti, M. Frenz, M. Wolf, R. M. Rossi, and L. J. Scherer, *RSC Adv.*, 2013, **3**, 23317.

Chapter 5

5.1. (a) D. D. Díaz, D. Kühbeck; R. J. Koopmans *Chem. Soc. Rev.*2011,**40**, 427. (b) P. Fatás, J. Bachl, S. Oehm, A. I. Jiménez, C. Cativiela, D. D. Díaz, *Chem. Eur. J.* 2013, **19**, 8861. (c) R. G. Weiss, D. J. Abdallah, *Adv. Mater.*2000, **12**, 1237. (d) P. Terech, R. G. Weiss, *Chem. Rev.* 1997, 97, 3133. (e) R. G. Weiss, *J. Am. Chem. Soc.*, 2014, **136**, 7519. (f) J. W. Steed *Chem. Soc. Rev.* 2010, **39**, 3686. (g) D. K. Kumar, J. W. Steed, *Chem. Soc. Rev.*2014,**43**, 2080. (h) L. Meazza, J. A. Foster, K. Fucke, P. Metrangolo, Resnati, G. J. W. Steed, *Nat. Chem.*2013, **5**,42.

5.2. (a) J. Zhou, X. W. Du, Y. Gao, J. F. Shi, B. Xu, *J. Am. Chem. Soc.* 2014, **136**, 2970. (b) Y. Zhang, B. Zhang, Y. Kuang, Y. Gao, J. Shi, X. X. Zhang, B. Xu, *J. Am. Chem. Soc.*2013, **135**, 5008. (c) Q. Wang, J. L. Maynar, M. Yoshida, E. Lee, M. Lee, K. Okuro, K. Kinbara, T. Aida, *Nature*, 2010,**463**, 339. (d) S. Tamesue, M. Ohtani, K. Yamada, Y. Ishida, J. M. Spruell, N. A. Lynd, C. J. Hawker, T. Aida, *J. Am. Chem. Soc.*2013,**135,** 15650. (e) A. Harada, R. Kobayashi, Y. Takashima, A. Hashidzume, H. Yamaguchi, *Nat. Chem.* 2011, **3**, 34. (f) H. Yamaguchi, Y. Kobayashi, R. Kobayashi, Y. Takashima, A. Hashidzume, A. Harada, *Nat. Commun.* 2012, **3**, 603. (g) P. Dastidar, *Chem. Soc. Rev.* 2008, **37**, 2699.

5.3. (a) T. Vermonden, R. Censi, W. E. Hennink, *Chem. Rev.*, 2012, **112**, 2853. (b) E. A. Appel, J. del. Barrio, X. J. Loh, O. A. Scherman, *Chem. Soc. Rev.*2012, **41**, 6195. (c) S. Banerjee, R. K. Das, U. Maitra, *J. Mater. Chem.*, 2009, 19, 6649. (d) L. A. Estroff , A. D. Hamilton, *Chem. Rev.* 2004, **104**, 1201.

5.4. (a) G. Palui, J. Nanda, S. Ray, A. Banerjee, *Chem. Eur. J.* 2009, **15**, 6902. (b) P. D. Wadhavane, R. E. Galian, M. A. Izquierdo, S. J. Aguilera, F. Galindo, L. Schmidt, M. I. Burguete, J. Perez-Prieto, S. V. Luis, *J. Am. Chem. Soc.*2012,**134**, 20554. (c) A. Chakrabarty, U. Maitra, A. D. Das *J. Mater. Chem.* 2012, **22**, 18268.

5.5. M. Cametti, Z. Džolić, *Chem. Commun.*, 2014, **50**, 8273.

5.6. J. Yuan, D. Wen, N. Gaponik, A. Eychmüller, *Angew. Chem. Int. Ed.* 2013, **52**, 976.

5.7. (a) H. K. Chae, D. Y. Siberio-Perez, J. Kim, Y. Go, M. Eddaoudi, A. J. Matzger, M. O'Keeffe, O. M. Yaghi, *Nature* 2004, **427**, 523. (b) H. Furukawa, K. E. Cordova, M. O'Keeffe, O. M. Yaghi, *Science*, 2013, **341**, 1230444. (c) H. Furukawa, F. Gándara, Y.-B. Zhang, J. Jiang, W. L. Queen, M. R. Hudson, O. M. Yaghi *J. Am. Chem. Soc.* 2014, **136**, 4369. (d) J. Y. Lee, O. K. Farha, J. Roberts, K. A. Scheidt, S. T. Nguyen, J. T. Hupp, *Chem. Soc. Rev.* 2009, **38**, 1450. (e) V. Guillerm, Ł. J. Weseliński, Y. Belmabkhout, A. J. Cairns, V. D'Elia, Ł. Wojtas, K. Adil, M. Eddaoudi, *Nat. Chem.,* 2014, **6**, 673. (f) M. H. Alkordi, J. A. Brant, L. Wojtas, V. C. Kravtsov, A. J. Cairns, M. Eddaoudi, *J. Am. Chem. Soc.*, 2009, **131**, 17753. (g) P. Li, Y. He, J. Guang, L. Weng, J.C.-G. Zhao, S. Xiang, B. Chen, *J. Am. Chem. Soc.*2014**, 136**, 547. (h) A. Schoedel, C. Scherb, T. Bein, *Angew. Chem. Int. Ed.* 2010, **49**, 7225. (i) C. Scherb, A. Schoedel, T. Bein, *Angew. Chem. Int. Ed.* 2008, **47**, 5777. (j) I. Senkovska, S. Kaskel, *Chem. Commun.* 2014, **50**, 7089. (k) A. Schneemann, V. Bon, I. Schwedler, I. Senkovska, S. Kaskel R. A. Fischer, *Chem. Soc. Rev.*, 2014, **43,** 6062. (l) S. Yang, J. Sun, A.J. Ramirez-

Cuesta, S.K. Callear, W.I.F. David, D.P. Anderson, R. Newby, A.J. Blake, J.E. Parker, C.C. Tang, M. Schröder, *Nat. Chem.*2012, **4**, 887. (m) J. Cravillon, S. Munzer, S. J. Lohmeier, A. Feldhoff, K. Huber, M. Wiebcke, *Chem. Mater.*2009, **21**, 1410. (n) J. L. Zhuang, D. Ceglarek, S. Pethuraj, A. Terfort, *Adv. Funct. Mater.* 2011, **21**, 1442. (o) T. Friščić, I. Halasz, P. J. Beldon, A. M. Belenguer, F. Adams, S. A. J. Kimber, V. Honkimaki, R. E. Dinnebier, *Nat. Chem.* 2013, **5**, 66. (p) C. Dey, T. Kundu, B. P. Biswal, A. Mallick, R. Banerjee, *Acta Cryst. B* 2014,**70**, 3.

5.8. Y. Yan, T. Bein, *J. Am. Chem. Soc.*1995, **117**, 9990; (b) T. Bein, Brown, K *J. Am. Chem. Soc.*1989, **111**, 7640. (c) G. R. Desiraju, D. Y. Curtin, I. C. Paul, *J. Am. Chem. Soc.*1977, **99**, 6148.

5.9. O. M. Yaghi, G. Li, H. Li, *Chem. Mater.*1997, **9**, 1074.

5.10. J. A. Foster, M.O.M. Piepenbrock, G. O. Lloyd, N. Clarke, J. A. K. Howard, J. W. Steed, *Nature Chem*. 2010, **2**,1037.

5.11. (a) G. Lu, S. Z. Li, Z. Guo, O. K. Farha, B. G. Hauser, X. Y. Qi, Y. Wang, X. Wang, S. Y. Han, X. G. Liu, J. S. DuChene, H. Zhang, Q. C. Zhang, X. D. Chen, J. Ma, S. C. J. Loo, W. D. Wei, Y. H. Yang, J. T. Hupp, F. W. Huo, *Nat. Chem.*2012, **4**, 310. (b) S. Jin, H.-J. Son, O. K. Farha, G. P. Wiederrecht, J. T. Hupp, *J. Am. Chem. Soc.* 2013, **135**, 955. (c) D. Buso, J. Jasieniak, M. D. H. Lay, P. Schiavuta, P. Scopece, J. Laird, H. Amenitsch, A. J. Hill, P. Falcaro, *Small*, 2012, **8**, 80.

5.12. (a) Q. Li, B. D. Guo, J. G. Yu, J. R. Ran, B. H. Zhang, H. J. Yan, J.R. Gong, *J. Am. Chem. Soc.* 2011, **133**, 10878. (b) R. Lin, L. Shen, Z. Ren, W. Wu, Y. Tan, H. Fu, J. Zhang, L. Wu, *Chem. Commun*. 2014, **50**, 8533. (c) J. He, Z. Yan, J. Wang, J. Xie, L. Jiang, Y. Shi, F. Yuan, F. Yu, Y. Sun, *Chem. Commun.* 2013, **49**, 6761 (d) Y. Kataoka, K. Sato, Y. Miyazaki, K. Masuda, H. Tanaka, S. Naito, W. Mori *Energ. Env. Sci.* 2009, **2**, 397. (e) C. Wang, K. E. deKrafft, W. Lin, *J. Am. Chem. Soc.* 2012*,* **134***,* 7211. (f) M. A. Nasalevich, M. van der Veen, F. Kapteijn, J. Gascon, *CrystEngComm* 2014, **16,** 4919. (g) J. Yang, D. Wang, H. Han, C. Li, *Acc. Chem. Res.*, 2013, **46**, 1900. (h) J. Ran, J. Zhang, J. Yu, M. Jaroniecc, S.Z. Qiao, *Chem. Soc. Rev.*, DOI: 10.1039/c3cs60425j. (i) K. Gelderman, L. Lee, S. W. Donne, *J. Chem. Ed.*, 2007, **84**, 685. (j) X. An, X. Yu, J. C. Yu, G. Zhang, *J. Mater. Chem. A*, **2013**,1, 5158 (k) J. He, J. Wang, Y. Chen, J. Zhang, D. Duan, Y. Wangand, Z. Yan *Chem. Commun.,* 2014, **50**, 7063.

5.13. V. Lesnyak, S. V. Voitekhovich, P. N. Gaponik, N. Gaponik, A. Eychmüller, *ACS Nano.*2010, **4**, 4090.

5.14. L. Berti, G. A. Burley *Nat. Nanotech.*, 2008, **3**, 81.

5.15. (a) G.R. Desiraju, T. Steiner, The Weak Hydrogen Bond in Structural Chemistry and Biology, Oxford University Press, Oxford, 1999.

5.16. M. J. Kamlet, J. L. M. Abboud, M. H. Abraham, R. W. Taft, *J. Org. Chem.*1983, **48**, 2877.

5.17. This phenomenon can be attributed to the co-ordination environment of probable gelator complex. ZNVA and ZPVA contain four water molecules in its co-ordination environment (rest two are occupied by the carboxylate of ligand VA) whereas ZAVA accommodates only two water molecules (rest four are

occupied by two carboxylates from acetate and VA ligand). Now, according to HSAB principle, Zn^{2+} is a soft-to-borderline acid and prefers acetate (medium field ligand) over H_2O (stronger than acetate). Hence, ZNPA/ZPVA becomes more vulnerable than ZAVA in presence of sulfide which leads to quick precipitation of ZnS.

5.18. (a) Q. Li, B. D. Guo, J. G. Yu, J. R. Ran, B. H. Zhang, H. J. Yan, J.R. Gong *J. Am. Chem. Soc.* 2011, **133**, 10878. (b) R. Lin, L. Shen, Z. Ren, W. Wu, Y. Tan, H. Fu, Zhang, J.; Wu, L. *Chem. Commun*. 2014, **50**, 8533. (c) J. He, Z. Yan, J. Wang, J. Xie, L. Jiang, Y. Shi, F. Yuan, F. Yu, Y. Sun, *Chem. Commun.* 2013, **49**, 6761. ; (d) Y. Kataoka, K. Sato, Y. Miyazaki, K. Masuda, H. Tanaka, S. Naito; and W. Mori; *Energ. Env. Sci.* 2009, **2**, 397. (e) C. Wang, K. E. deKrafft, W. Lin, *J. Am. Chem. Soc.* 2012, **134**, 7211. (f) M. A. Nasalevich, M. van der Veen, F. Kapteijn, J. Gascon, *CrystEngComm* 2014, **16**, 4919. (g) J. Yang, D. Wang, H. Han, C. Li, *Acc. Chem. Res.*, 2013, **46**, 1900. (h) J. Ran, J. Zhang, J. Yu, M. Jaroniecc, S.Z. Qiao, *Chem. Soc. Rev.*, DOI: 10.1039/c3cs60425j. (i) K. Gelderman, L. Lee, S. W. Donne, *J. Chem. Ed.*, 2007, **84**, 685. (j) X. An, X. Yu, J. C. Yu, G. Zhang, *J. Mater. Chem. A*, 2013,**1**, 5158 (k) J. He, J. Wang, Y. Chen, J. Zhang, D. Duan, Y. Wangand, Z. Yan, *Chem. Commun.,* 2014, **50**, 7063.

5.19. (a) S. Saha, J. Bachl, T. Kundu, D.D. Díaz, R. Banerjee, *Chem. Commun.* 2014, **50,** 3004. (b) S. Saha, J. Bachl, T. Kundu, D.D. Díaz, R. Banerjee, *Chem. Commun.*, 2014, **50**, 7032. (c) S. C. Sahoo, T. Kundu, R. Banerjee, *J. Am. Chem. Soc.* 2011, **133**, 17950. (d) S. Saha, G. Das, J.Thote, R. Banerjee, *J. Am. Chem. Soc.* 2014, **136**, 14845.

5.20. http://hyperphysics.phy-astr.gsu.edu/hbase/vision/cie.html.

About The Author

Subhadeep Saha, son of Samir Ranjan Saha and Kabita Saha, was born in Burdwan, West Bengal, India, in 1984. He has received his higher secondary degree from Burdwan Municipal High School, Burdwan. He completed his B.Sc. from University of Calcutta (Ramakrishna Mission Residential College, Narendrapur), Kolkata in 2006. After the completion of his B.Sc. he joined Department of Chemistry, University of Delhi to pursue his M.Sc. Afterwards, he joined Department of Physical chemistry, NCL, Pune to pursue his Ph.D. Degree in July 2009 under the guidance of Dr. Rahul Banerjee. He was awarded research fellowship by Council of Scientific and I ndustrial Research (JRF and SRF) for 2009-2014.

List of Publications

1. Harshitha Barike Aiyappa, **Subhadeep Saha**, (equal contribution) Pritish Wadge, Rahul Banerjee* and Sreekumar Kurungot* *"Fe (III) Phytate Metallogel as a Prototype Anhydrous, Intermediate Temperature Proton Conductor"* ***Chem. Sci.***, 2014, **DOI:** 10.1039/C4SC02294G

2. **Subhadeep Saha**, Gobinda Das, Jayshri Thote and Rahul Banerjee* *"Photocatalytic Metal-organic Framework from the CdS Quantum Dot Incubated Luminescent Metallohydrogel"* ***J. Am. Chem. Soc.***, 2014, 136, 14845–14851.

3. Harshitha Barike Aiyappa, **Subhadeep Saha**, Bikash Garai, Jayshri Thote, Sreekumar Kurungot* and Rahul Banerjee* *"A Distinctive $PdCl_2$ Mediated Transformation of Fe-based Metallogels into Metal Organic Frameworks"* ***, Cryst. Growth and Des.,*** 2014, 14 , 3434–3437.

4. **Subhadeep Saha**, Jürgen Bachl, Tanay Kundu, David Díaz Díaz* and Rahul Banerjee* *"Dissolvable Metallohydrogels for Controlled Release: Evidence of a Kinetic Supramolecular Gel Phase Intermediate"* ***Chem. Commun.,*** 2014, 2014, **50**, 7032-7035**.**

5. **Subhadeep Saha**, Jürgen Bachl, Tanay Kundu, David Díaz Díaz* and Rahul Banerjee* *"Amino Acid-based Multiresponsive Low-Molecular-Weight Metallohydrogels with Load-bearing and Rapid Self-healing Ability"* ***Chem Commun.,*** 2014**,** 50**,** 3004-3006**.** [*Recommended as one of the 'hot' articles of March '14 by the editor,* http://blogs.rsc.org/cc/2014/03/19/chemcomm-hot-articles-for-march/#more-6236]

6. Tanay Kundu, Subash C. Sahoo, **Subhadeep Saha,** Rahul Banerjee* *"Salt Metathesis in Three Dimensional Metal Organic Frameworks (MOFs) with Unprecedented Hydrolytic Regenerability"* ***Chem. Commun.,*** 2013, 49, 5262−5264**.**

7. Subhadeep Saha, Eva-Maria Schön, Carlos Cativiela, David Díaz Díaz* and Rahul Banerjee*. *"Proton-Conducting Supramolecular Metallogels from Lowest Molecular Weight Assembler Ligand: A Quote for Simplicity"* ***Chem. Eur. J.,*** 2013, 19, 9562 – 9568**.**

8. Subhadeep Saha, Suman Chandra, Bikash Garai and Rahul Banerjee* *"Carbon dioxide capture by metal organic frameworks"* ***Indian Journal of Chemistry,*** 2012, 51,

1223-1230**.** [*Published as part of a Special Issue on Carbon Dioxide Capture, Sequestration & Utilization*]

9. Iti Kapoor, Eva-Maria Schön, Jürgen Bachl, Dennis Kühbeck, Carlos Cativiela, **Subhadeep Saha**, Rahul Banerjee, Stefano Roelens, José Juan Marrero-Tellado* and David Díaz Díaz* *"Competition between gelation and crystallisation of a peculiar multicomponent liquid system based on ammonium salts"* ***Soft Matter,*** 2012, 8, 3446−3456.

10. Arijit Mallick, **Subhadeep Saha**, Pradip Pachfule, Sudip Roy and Rahul Banerjee* *"Structure and Gas Sorption Behavior of a New Three Dimensional Porous Magnesium Formate."* ***Inorg. Chem.,*** 2011, 50, 1392-1401**.**

11. Arijit Mallick, **Subhadeep Saha**, Pradip Pachfule, Sudip Roy and Rahul Banerjee*, *"Selective CO_2 and H_2 Adsorption in a Chiral Magnesium based Metal Organic Framework (Mg-MOF) with Open Metal Sites."* ***J. Mater. Chem.***, 2010, 20, 9073–9080.